The Thesis Committee for Kyle Michael McKenzie
Certifies that this is the approved version of the following thesis:

Outcrop-Derived Facies Model and Cycle Architecture of the Tansill G27 – G28 High-Frequency Sequences, Rattlesnake Canyon, New Mexico

APPROVED BY
SUPERVISING COMMITTEE:

Co-Supervisor: _____
Charles Kerans

Co-Supervisor: _____
Robert G. Loucks

_____
William L. Fisher

Outcrop-Derived Facies Model and Cycle Architecture of the Tansill G27 – G28 High-Frequency Sequences, Rattlesnake Canyon, New Mexico

by

Kyle Michael McKenzie, B.S.

Thesis

Presented to the Faculty of the Graduate School of

The University of Texas at Austin

in Partial Fulfillment

of the Requirements

for the Degree of

Master of Science in Geological Sciences

The University of Texas at Austin

May, 2016

Dedication

To Greg and Crystal for your encouragement and support.

To Stephanie for your love, support, and understanding, without which, accomplishing this would have seemed impossible.

Acknowledgements

First and foremost, I would like to thank Project STARR at the Bureau of Economic Geology, with William Ambrose as the primary investigator, for funding my research and providing financial support during my time at the Jackson School, as well as the Reservoir Characterization and Research Laboratory for aiding with this project.

This thesis would not have been possible without the patience and guidance of Dr. Charles Kerans and Dr. Robert Loucks while working with me through multiple thesis topics. My path to this project was somewhat of an unconventional route involving a series of thesis topics and restarts. Finally, after pushing for an outcrop study, Dr. Kerans helped come up with the project I conducted in the Guadalupe Mountains. He rescued me from thesis limbo, and for that I am grateful. This study benefited tremendously from the insights and knowledge of committee members Dr. Charles Kerans, Dr. Robert Loucks, and Dr. William Fisher whose comments and edits helped to significantly reshape this manuscript. Thanks to Steve Bachtel and Chevron for scanning thin sections used in this project. Also, thank you to Andrew Parker for insightful discussions about the Gulf PDB-04 core and subsurface datasets within the Central Basin Platform. Thanks to the Reservoir Characterization and Research lab research scientist and staff members Dr. Chris Zahm, Josh Lambert, and Stephaine Lane who helped make this research possible.

Finally, I would like to thank my fellow graduates and the RCRL research group students who helped make my experience here at the Jackson School one I will cherish for the rest of my life. Long hours spent on assignments and research would not have been the same without you by my side. In particular, I would like to thank Kris Voorhees and Ben Smith for in depth discussions pertaining to my research with a special thanks to Kris for his help with field work.

Abstract

Outcrop-Derived Facies Model and Cycle Architecture of the Tansill G27 – G28 High-Frequency Sequences, Rattlesnake Canyon, New Mexico

Kyle Michael McKenzie, M.S. Geo. Sci.

The University of Texas at Austin, 2016

Co-Supervisor: Charles Kerans

Co-Supervisor: Robert G. Loucks

High-relief, steep-rimmed carbonate margins are significant geologic features documented in a variety of locations throughout the geologic record. The Tansill Formation, the shallow-water platform equivalent of the steep-rimmed Capitan Reef, is the end member of a depositional system that progressively narrowed through time and has the most compressed outer-shelf-facies tract of Permian strata on the Northwest Shelf. Extensive precipitation of in-situ marine cements allowed for early lithification and oversteepening of the narrow outer-shelf and resulted in the most extensive network of syndepositional fractures and the best margin collapse features documented in the Late Guadalupian. Tansill shelfal strata is well constrained and served as part of the the archetype high-frequency cycle (HFC)/sequence (HFS) stratigraphic framework developed and modified over decades of extensive outcrop studies (Tyrrell, 1969),

making it one of the type locations to study depositinal processes of a structurally dynamic platform. This study provides the opportunity to examine the terminal phase of carbonate deposition of a dynamically restrictive basin and better understand the associated platform geometries and facies architecture of a steep-rimmed platform leading up to the extreme reorganization of basin fill as evaporite precipitation took over during the Wuchiapingian Stage, Ochoan Series.

The stratigraphic framework at Rattlesnake Canyon for the lower and middle Tansill was built from eight detailed measured sections within the Guadalupian HFS G27-G28 interval, totaling 467 m. Sections were described on the northern wall of Rattlesnake Canyon where detailed characterization of the G25 and G26 (Hairpin and Triplet) HFSs had been resolved. Distinct bedding planes within each measured sections were correlated using photomosaic panels of the canyon walls and airborne LIDAR-based digital outcrop models, creating a high degree of certainty when correlating and interpreting cycle architecture along a palinspastically reconstructed dip-oriented cross section. The spacing between sections ranges between 58 m – 232 m, and when projected onto a true dip profile they span a distance of 1.1 km, beginning 300 m inland of the G28 platform margin. The close spacing of measured sections was mandated by the abrupt lateral facies tract changes within the narrow Tansill shelf.

A more extensive record of the G27 and G28 HFSs were documented in Rattlesnake Canyon than in adjacent canyons where exposure is incomplete because of covered intervals (Dark Canyon) or the collapse of the time-equivalent platform margin and removal of outer-shelf strata (Walnut Canyon). The framework of the G27-G28

HFSs further constrains the maximum flooding surface (MFS) of the CS13 and indicates a rocky shoreline juxtaposed against the windward side of shelf-crest tepee-pisolite barrier-island complexes. Previous studies have emphasized the stacking patterns comprising the outer few kilometers of the platform but have given little to no recognition to the breccia prone high-energy shorelines deposits and have not incorporated this distinct facies into depositional models. Comparison of data from this study with the proximal Walnut and Dark Canyon profiles help to further delineate the G27 – G28 platform geometries and facies tract widths and can be incorporated into the larger scale stratigraphic framework of Permian strata exposed in the Guadalupe Mountains.

Table of Contents

List of Tables

List of Figures

INTRODUCTION

The development of a well-constrained high-resolution stratigraphic framework built upon a record of small order, meter-scale, cyclicity is the foundation for gaining insights into the sedimentological processes of platform-top carbonates. Shallow-water carbonates are sensitive environmental proxies that respond in a predictable manner to eustatic oscillations and climatic and tectonic variations, and grant the possibility of discerning the regional and global history of a carbonate shelf. Decades of extensive outcrop studies have constrained the nested hierarchy of cyclicity e.g., (Kerans et al. 1992; Kerans and Fitchen 1995; Tinker 1998; Kerans and Tinker 1999, Kerans and Kempter 2002; Rush and Kerans 2010, Kerans et al. 2013) in Late Permian strata of the Delaware Basin. The Tansill Formation is the youngest Late Guadalupian platform equivalent of the Capitan Reef and represents the last phase of Permian carbonate deposition on the Northwest Shelf of the Delaware Basin (Fig. 1). This study provides a high-resolution sequence stratigraphic framework for the G27 and G28 high-frequency sequences (HFS) in the, late Guadalupian, Permian Composite Sequence (CS) 13 exposed in Rattlesnake Canyon, Guadalupe Mountains, New Mexico (Fig. 2). Previous studies of this stratigraphic interval in nearby canyons (Rush and Kerans 2010; Frost et al. 2012) contain insufficient outcrop exposure of the Tansill to adequately document the complete stratigraphic framework of the G27 and G28 high-frequency sequences and constrain facies tract dimensions. The focus of this study is on developing a 2-dimensional cycle architecture, with a series vertical measured sections, across the shelf profile. Upon developing the framework, it is possible to delineate the stratigraphic

context of facies tract widths, platform geometries, and shoreline patterns of a structurally dynamic steep-rimmed carbonate platform during a time of increasing basin-wide restriction.

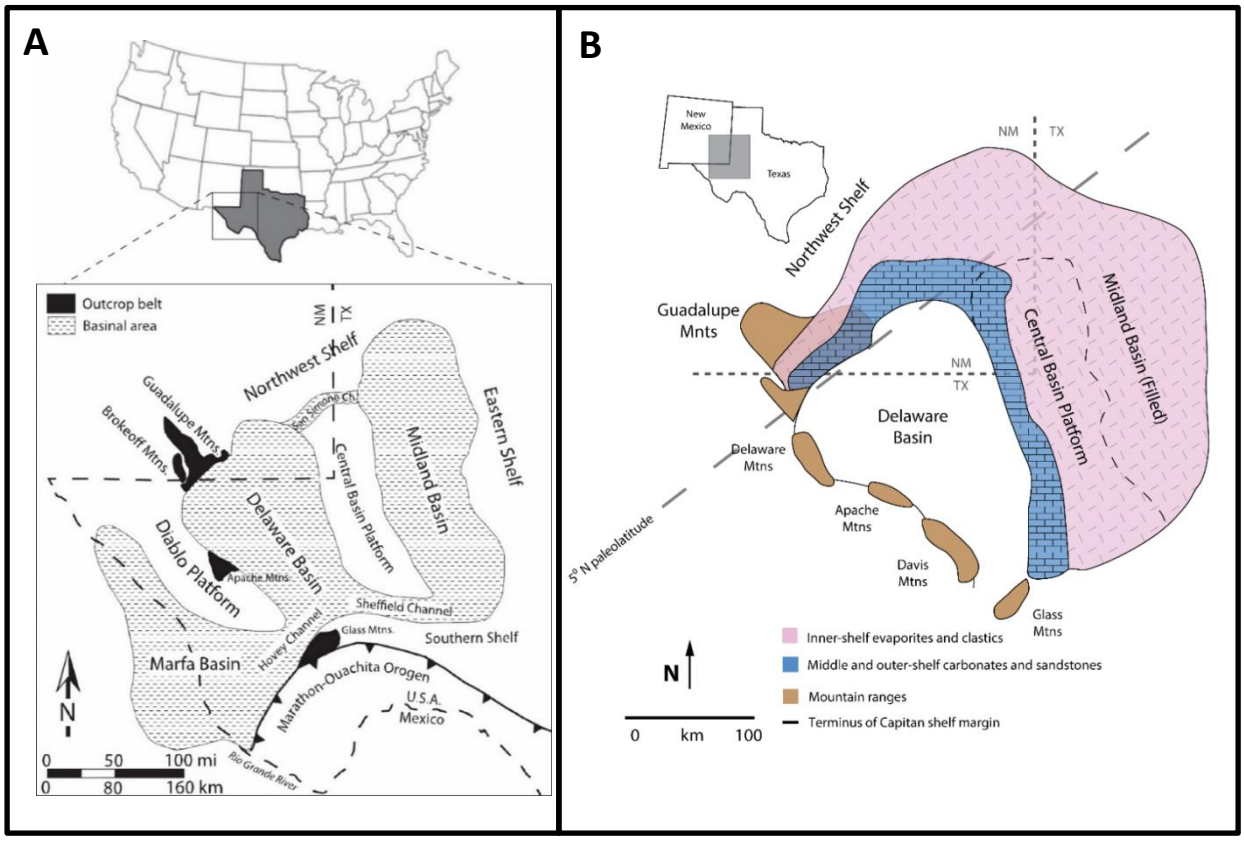

Figure 1: Location of study area**. A)** Geographic map and regional geologic setting of the Permian Basin showing structural components in the study area. After Ward et al. (1986). **B)** Geologic map of the Delaware Basin during the Late Guadalupian with the approximated paleolatitude (Hill 1972). Modified after Ward et al. (1986), Tinker (1998), and Harman (2011).

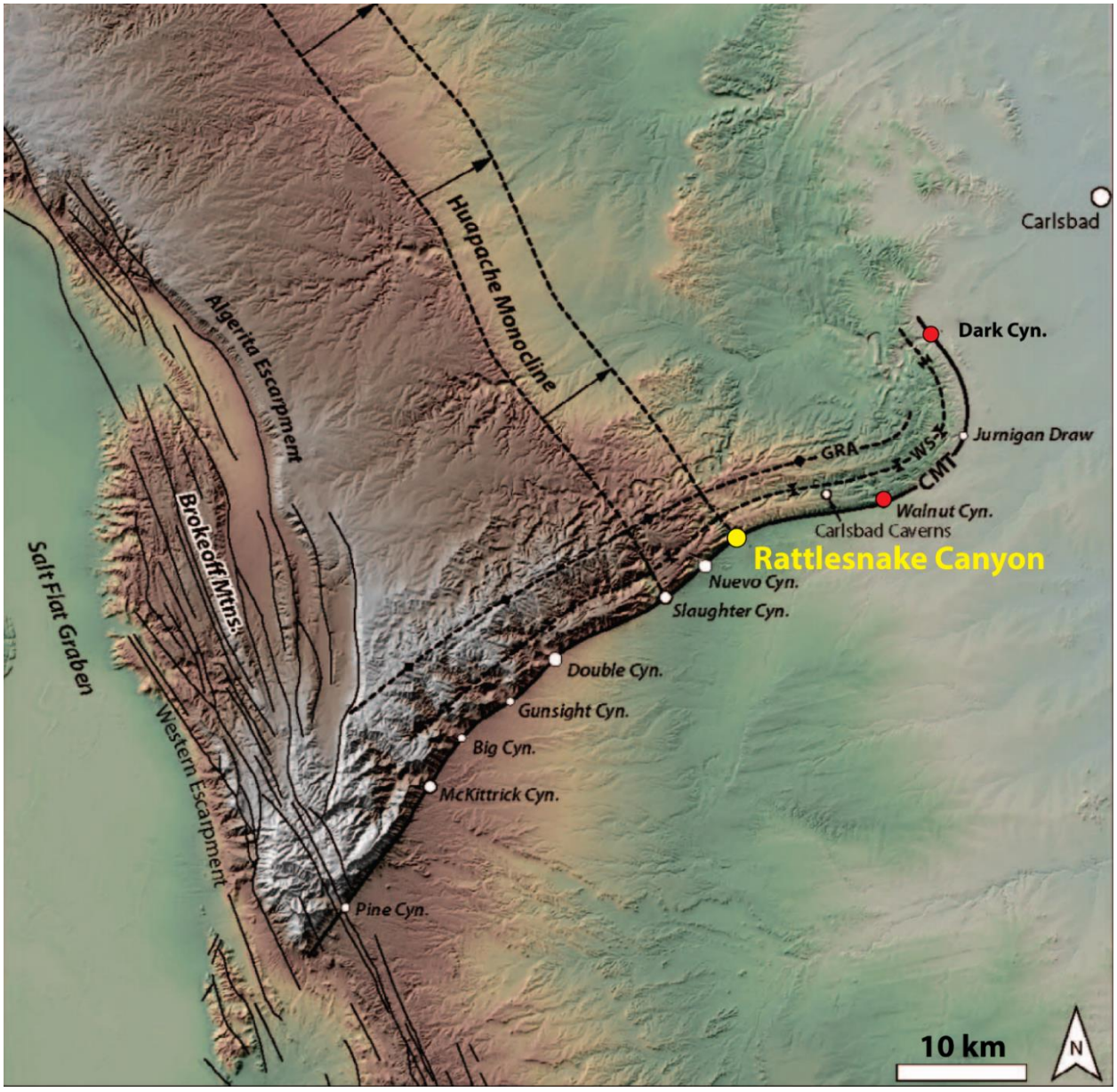

Figure 2: Shaded digital elevation model of the Guadalupe Mountains showing major basin and range structural trends and canyons (Cyn.) along the Capitan Reef Escarpment on the eastern border of the mountain range. The general trend of shelf progradation was east to southeast into the Delaware Basin. CMT = Capitan Margin Trend, GRA = Guadalupe Ridge Anticline, WS = Walnut Canyon Syncline, Yellow Circle = Locality of this study, Red Circle = Location of other Tansill studies. Modified After Frost et al. (2012).

GEOLOGIC BACKGROUND AND PLATFORM EVOLUTION

BACKGROUND

Permian mixed carbonate-siliciclastic-evaporite systems are relatively undeformed and well exposed in extensive outcrops along dip-parallel canyon walls in the Guadalupe Mountains, West Texas and New Mexico (King 1948, Newell et al 1953). Deposition occurred approximately 5º north of the paleoequator, in an arid subequatorial environment with predominantly northeasterly winds (Ross 1978; Hills 1972) (Fig. 1). In this setting along the Northwest Shelf of the Delaware Basin, shelf-to-margin strata is highly cyclic and exhibit lateral facies changes over relatively short distances (Bebout and Kerans 1993; Rush and Kerans 2010; Frost et al 2012). The broad slowly subsiding ancestral, Early Paleozoic, Toobosa basin underwent a period if intense deformation caused by the collision Laurasia with Gondwana in the Late Mississippian through Early Permian. The associated southwest-to-northeast compresion of the Ouichita-Marathon fold belt gave rise to the Central Basin Platform which subsequently divided the Toobosa basin into two seperate foreland sub-basins, the Midland Basin to the east and the Delaware Basin to the west (Hoark 1985; Yang and Dorobek 1995; Ye et al 1996). By the Late Permian, the Midland Basin was filled and had coalesced with the Central Basin Platform focusing sedimentation on the tectonically stable shelf margin rimming the Delaware Basin (King 1948; Tyrrel 1962; Kerans and Fitchen, 1995). The asymmetrical Delaware Basin subsided more rapidly to the east making its shallow western rim a prime environment for platform/reef growth (Ye et al 1996). Aggrading shelfal carbonates and siliciclastics prograded towards the basin center until the end of the Late Guadalupian

(end Tansill) by which time sedimentation had ceased and the Delaware Basin was filled by evaporites of the Castile and Salado formations (Bebout et al. 1993).

Following Permo-Triassic burial, the compresional regime associated with the Laramide Orogeny partially exhumed the western side of the Guadalupe Mountains. Later, during extension of the Basin and Range Province in the Oligocene-Pliocene, the Northwest Shelf and Capitan Reef complex were partially exhumed along the Capitan Reef Escarpment, which represent the most eastern expression of NNW – SSE oriented Basin and Range high-angle normal fualts (Hayes, 1964; Garber et al 1989). The gentle structural dip of the Guadalupe Mountains (east 1 – 2 º) (King 1948; Koša and Hunt 2006) creates a scenario in which topographically lower canyons to the northeast expose stratigrapically younger strata. For this reason, Rattlesnake Canyon and other proximal canyons (Walnut and Dark Canyon) have good outcrop exposure of the Tansill Formation, despite having less topographic relief than many of the canyons to the southwest, and are the type locations for studying the G27 and G28 HFSs.

EVOLUTION OF THE PLATFORM

Through time, the Northwest Shelf has progressively evolved from a low-angle carbonate ramp system to a steep-rimmed shelf platform (Fig. 3) with an over-steepened sponge-microbial boundstone reefal margin. It is a well-established depositional pattern for carbonate platforms to undergo a ramp-rim evolution at the second-order supersequence scale (10-100 my), (Read 1985, Kerans et al 2013), but a thorough understanding of the sedimentilogical elements involved in this process are still being developed. The driving mechanism behind the transition from a ramp to rimmed platform

in the Guadalupian resulted from a combination of factors including siliciclastic influx and dampening of fine-grained carbonate production, preexisting topography, and differential subsidence according to Kerans et al (2013).

The G14 HFS, Upper Queen Formation and equivalent Goat Seep Margin, is the first preserved reef-rimmed platform in the Guadalupe Mountains. After becoming established, this platform morphology persisted for the remaining sixteen HFSs (G15 – G30) until the shutdown of the carbonate factory at the end of Tansill deposition. Once the ramp-to-rim transition occurred, small-scale dynamics continued to modify the reef-rimmed depositional profile. High-frequency sequence-scale transgressions can have subtle effects on the platform geometry that constructively form noticeable trends through time (Tinker, 1998). Careful documentation of the G27 and G28 cycle architecture and facies tract dimensions affords the opportunity to study the platform geometries and facies distributions at-or-near the extreme end member of the steep-rimmed profile approaching the cessation of carbonate deposition on the shelf at the end of the Guadalupian.

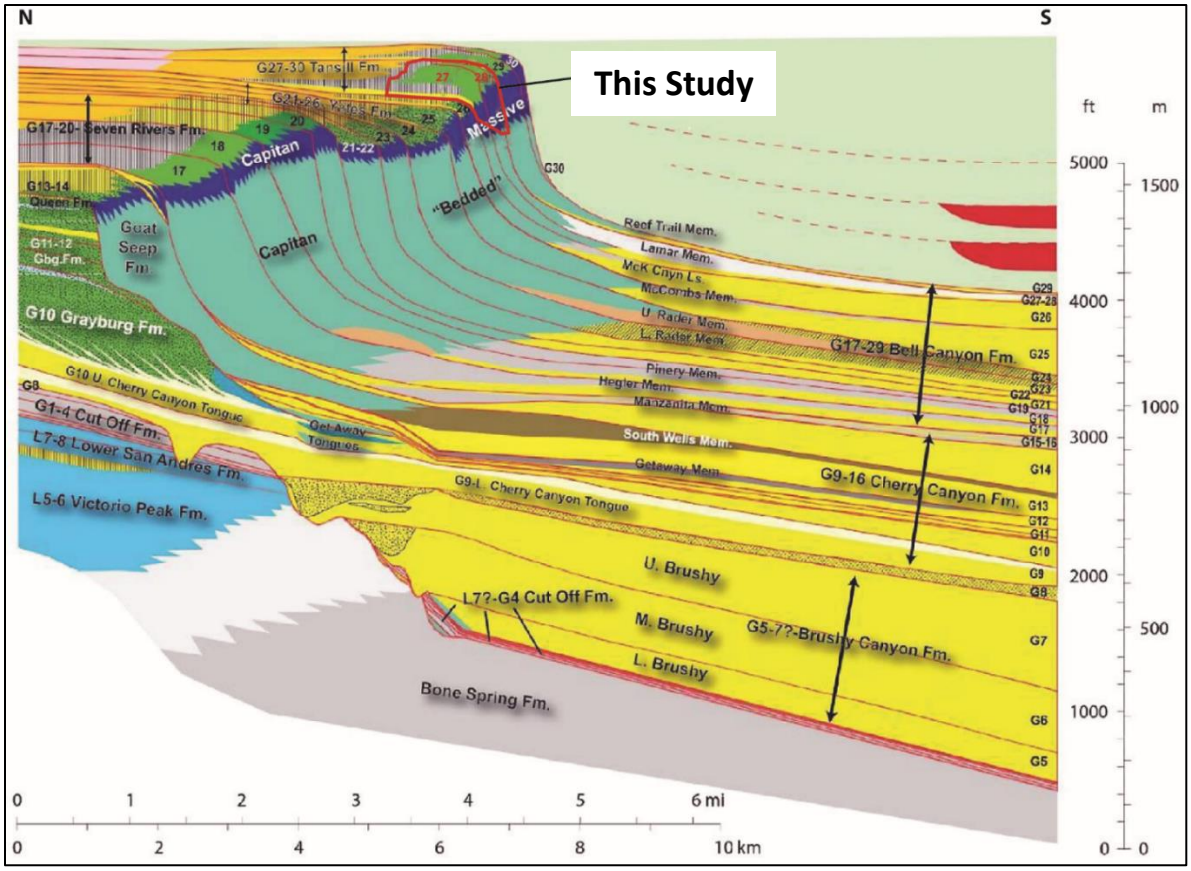

Figure 3: Study interval within the sequence stratigraphic framework of the Guadalupe Mountains showing the evolution of late Leonardian – Guadalupian systems from a ramp to reef-rimmed margin. Kerans and Kempter (2002).

SEQUENCE STRATIGRAPHIC FRAMEWORK

The stratigraphic framework used herein is modeled after modifications made to the hierarchy of sequences in Mitchum and Van Wagoner (1991) by Kerans and Fitchen (1995) to better align with carbonate systems. High-frequency cycles (HFC), HFSs, CSs, and supersequences, in order from shortest to longest time duration, are the main genetic units upon which stacking pattern analysis are built. High-frequency sequences, analogous to parasequences of Osleger and Read (1991), are allocyclic "meter-scale" cycles (1-10 m) of genetically related strata that can be mapped across multiple facies tracts (Kerans and Fitchen, 1995). Multiple HFCs stack to build retrogradational to progradational HFC sets, a set of cycles bound above and below by a marine flooding surface (Harris et al 1993; Kerans et al 1994), that together represent a full base-level transit cycle of an unconformity bound HFS. High-frequency sequences are analogous to the third-order depositional sequences of Vail (1987), and are grouped according to stacking patterns into lowstand sequence set (LSS), transgressive sequence sets (TSS), and highstand sequence sets (HSS) within a larger order CS (Kerans and Tinker 1999) according to the ratio of progradation to aggradation (P/A) and degree of exposure at the HFS boundary. The evolution of stratal relationships within a CS are from a LSS characterized by extensive subaerial exposure with the potential for sediment bypass and karstification to a TSS with backstepping HFSs and minor exposure to a HSS with increasingly higher P/A ratios and progressively extended durations of exposure atop HFSs.

Through time, shallow-water carbonates act as sensitive proxies to minor fluctuations in sea level and frequently exhibit multiple levels of ordered cyclical deposition (Grotzinger 1986, Goldhammer et al 1993 Lehrmann and Goldhammer 1999). Early work on Permian stratigraphy around the Delaware Basin recognized this same depositional pattern in outcrop (e.g., Kerans et al 1992, Kerans and Fitchen 1995, Tinker 1998, Kerans and Tinker 1999) and in the subsurface (Borer and Harris 1991, Andreason 1992; Garber and Harris 1993). The framework within this study uses a modified form of this framework from (Kerans et al 2013) (Fig. 4).

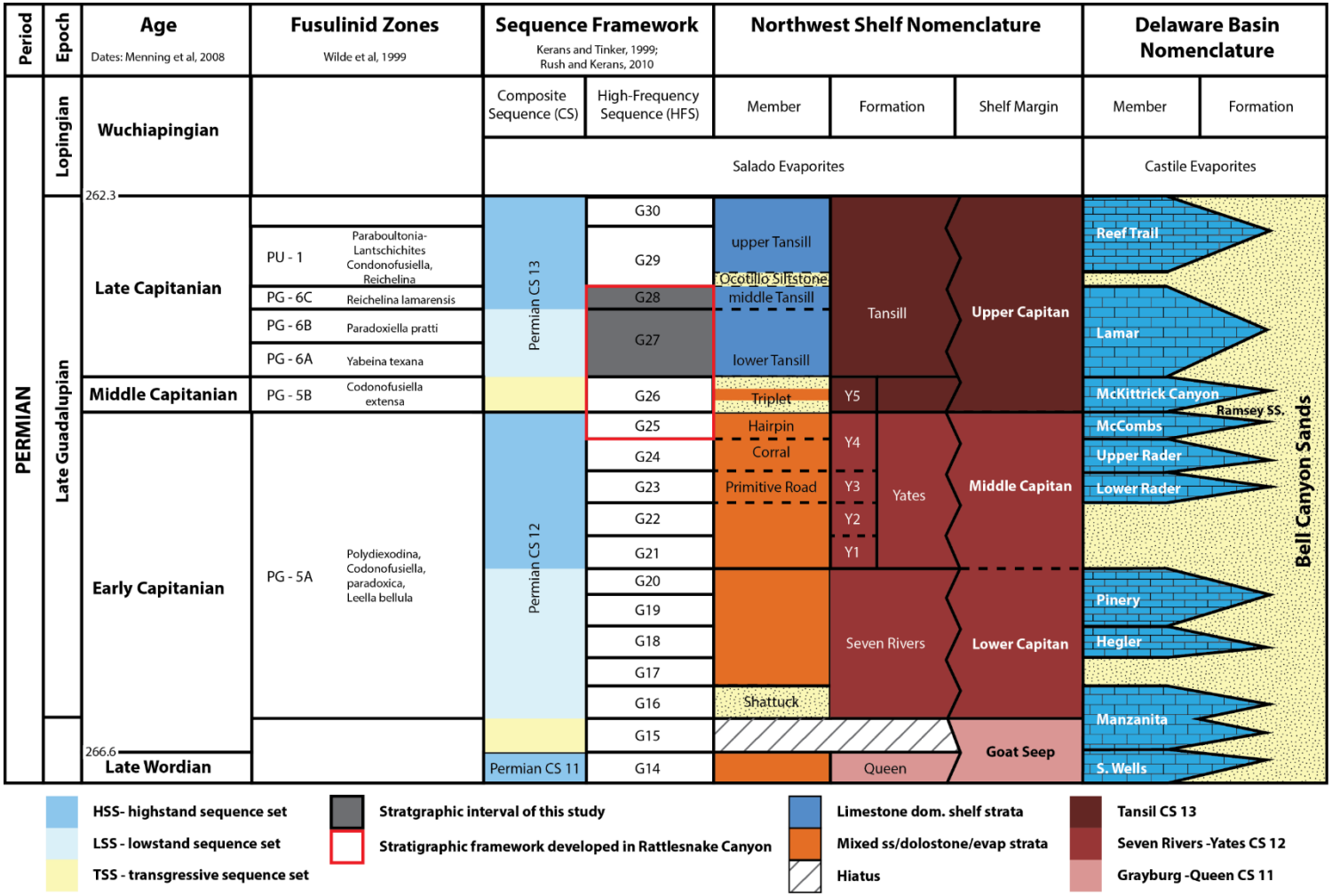

Figure 4: High-frequency and composite-sequence-scale framework of the Late Guadalupian section of the Guadalupe Mountains. CS = composite sequence, TSS = transgressive sequence set, LSS = lowstand sequence set, and HSS = highstand sequence set. Modified from Rush and Kerans (2010) and Kerans et al. (2013).

The Late Guadalupian, Capitanian, section includes two CSs (CS12 – CS13)and sixteen HFSs (G15 – G30) . The Tansill Formation, composed of four HFSs (G27 – G30), is Late Guadalupian in age and comprises the TSS and early HSS of the CS13 (Kerans et al. 2013). The specific focus of this study is on the HFC architecture of the G27 – G28 HFSs and their broader context within CS13 and the evolving steep-rimmed flat-top platform. After the cardinal study of the Tansill in an area northeast of Carlsbad, NM, (DeFord and Riggs 1941), it has been the focal point of many subsequent works across the Guadalupe Mountains. Numerous projects that followed with a component of stratigraphy to them include (Kerans and Harris 1993) McKittrick Canyon, (Neese and Schwartz 1977; Schwartz 1981) Rattlesnake Canyon, (Neese and Schwartz 1997; Rush and Kerans 2012) Walnut Canyon, and (Parsley 1988; Mazzullo 1999; Frost et al 2012) Dark Canyon, and this study will further build upon these existing works (Fig. 5). A particular emphasis will be place on making comparisons to recent the work of Rush and Kerans (2010) and Frost et al. (2012). Both studies were conducted within close proximity to Rattlesnake Canyon, used the same stratigraphic nomenclature as this study, and had a significant impact on the current understanding of the G27 and G28 HFSs, margin failure in the G27 HFS Rush and Kerans (2010), and structural and mechanical behavior of the high-relief steep-rimmed Tansill platform Frost et al. (2012). The G27 – 28 HFSs upper and lower boundaries are well defined by distinctive sandstone marker beds of the Triplet (G26) and Ocotillo (base G29). The Ocotillo Siltstone member at the base of the G29 is laterally correlatable for over 100 km (DeFord and Riggs, 1941) and subdivides the lower and middle Tansill from the upper Tansill. These two marker beds

proved useful in determining the proper location of the G27 and G28 HFSs in Rattlesnake Canyon.

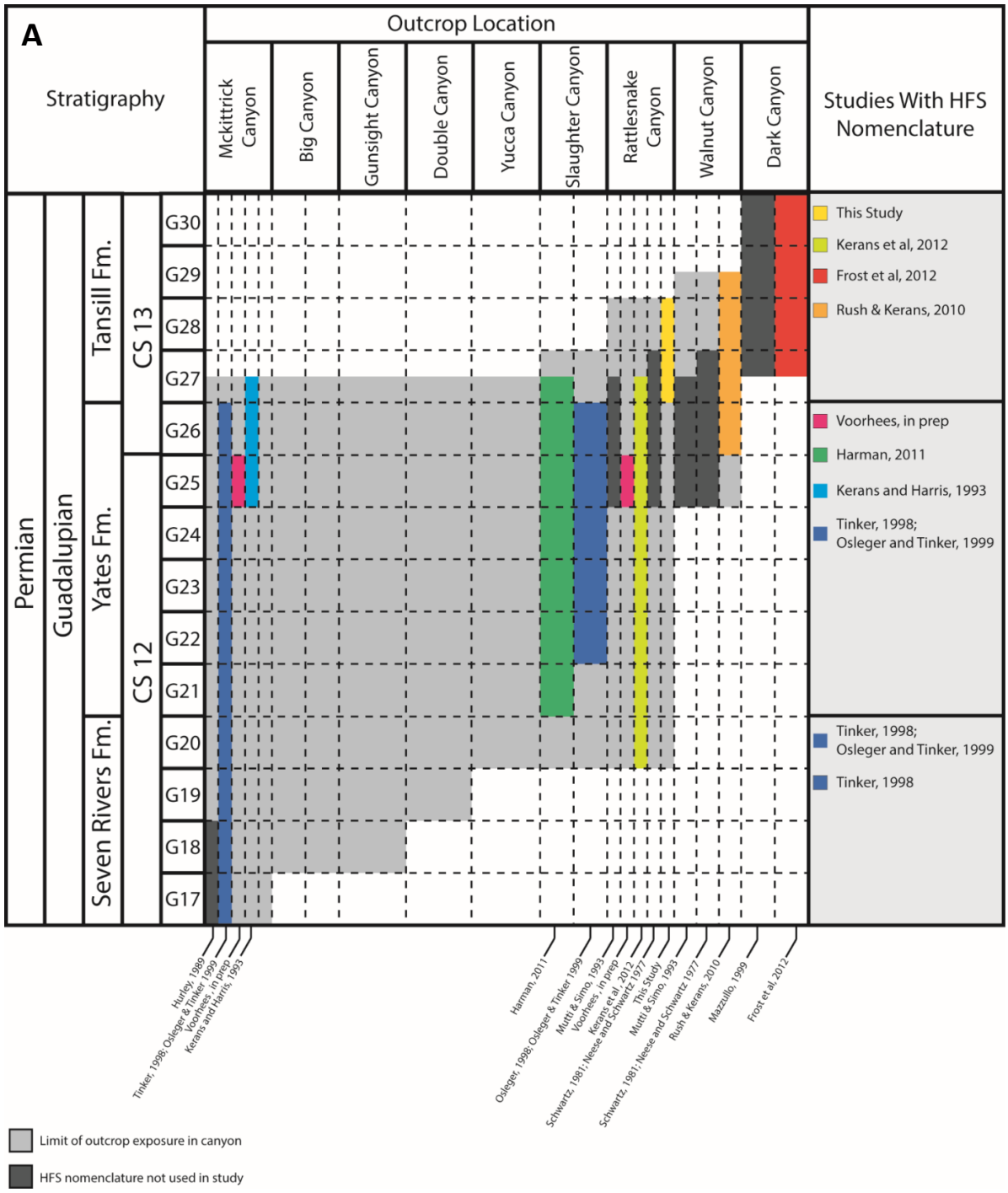

Figure 5: Compilation of studies in the Guadalupe Mountains with a component of Late Guadalupian stratigraphic analysis. **A)** Studies organized by the stratigraphic intervals of Kerans et al. (2013) and location within the Guadalupe Mountains. Continued on next page.

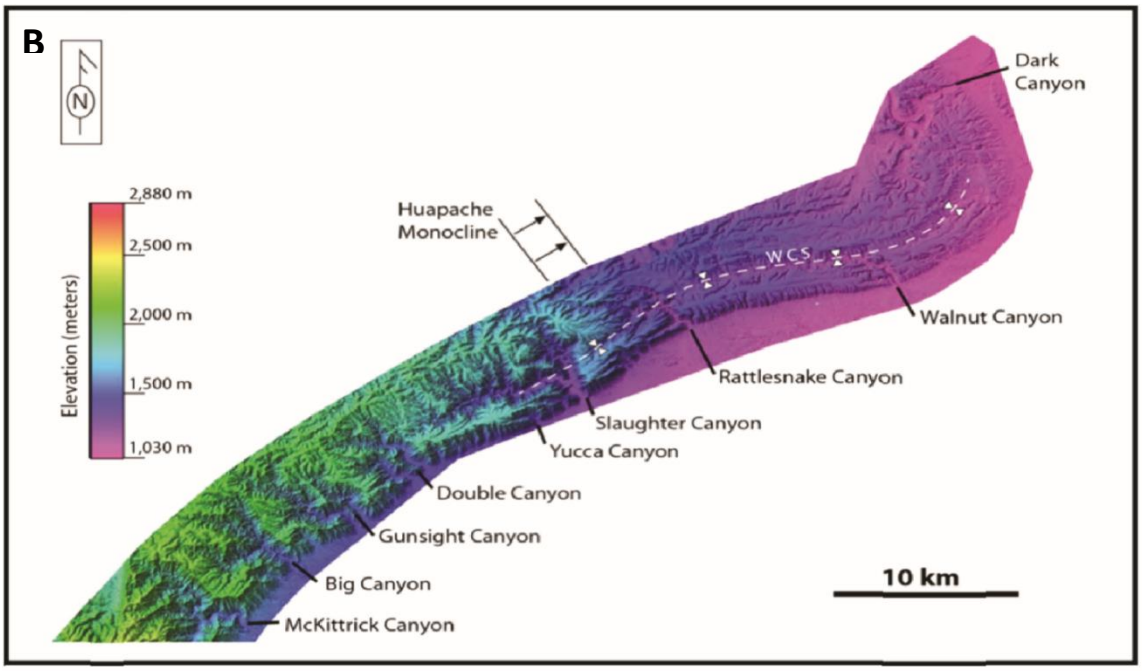

Figure 5: Continued. B) Shaded digital elevation model from Harman (2011) showing the position of relevant canyon in the Guadalupe Mountains.

DEPOSITIONAL MODELS

Different platform morphologies have been proposed for the Capitanian system and continual field-test of depositional models have aided in constraining the paleobathymetric profile of the platform. Models developed from the pioneering field studies in the Guadalupe Mountains by King, (1942, 1948) proposed an uninterrupted sloping shelf to margin profile. However, this model failed to explain the tepee-pisolite island-complexes that developed landward of the reef or the restrictive lagoonal muds and evaporites landward of the shelf crest. Later work by Newell et al. (1953) proposed a barrier-reef morphology with a framework reef that grew up to sea level. A lack of exposure surfaces and deposition of fine grained sediments within the reef cannot be explained by this model (Garber et al. 1989), and like the uninterrupted slope model, the barrier-reef model fails to explain the pisolite shoals in back of the reef. This distinct shelf crest facies tract contains abundant desiccation features and pisolith fabrics indicative of a vadose marine hypersaline peritidal environment (Esteban and Pray, 1988). Dunham (1969, 1972) proposed a marginal mound profile with a paleobathymetric high positioned at the peritidal to supratidal shelf crest, with the reef located in 10 – 30 m of water. A modified version of this profile is the foundation upon which the model developed from outcrop studies of the G27 and G28 HFSs in Rattlesnake Canyon were built (Fig. 6).

Late Guadalupian depositional models are subdivided into distinct facies tracts, or genetically linked associations of facies defined by discrete changes in depositional energy, water depth, grain type and sorting, sedimentary structures (Kerans and Tinker,

1997). Osleger and Tinker (1999) used four facies tracts (reef margin, outer-shelf, shelf-crest, and continental siliciclastic interior) when working in McKittrick and Slaughter Canyons. To accurately reflect dip-related changes in sediment source and depositional energy, the model herein uses the facies tracts defined by these works with the addition of a further subdivision of the outer-shelf facies from (Kerans et al 1993) in which the outer-shelf profile was modified by the addition of a shelf-crest shoreface tract. Additionally, the model incorporates an oversteepend reef margin (Tinker 1998; Kerans and Tinker 1999), syndepositional fracturing and shelf parallel deformation above antecedent shelf margins (Hunt et al 2002; Koša and Hunt 2005; Frost et al 2012; Jones 2013; and Mathisen 2014), and platform margin collapse (Rush and Kerans 2010) (Fig. 7).

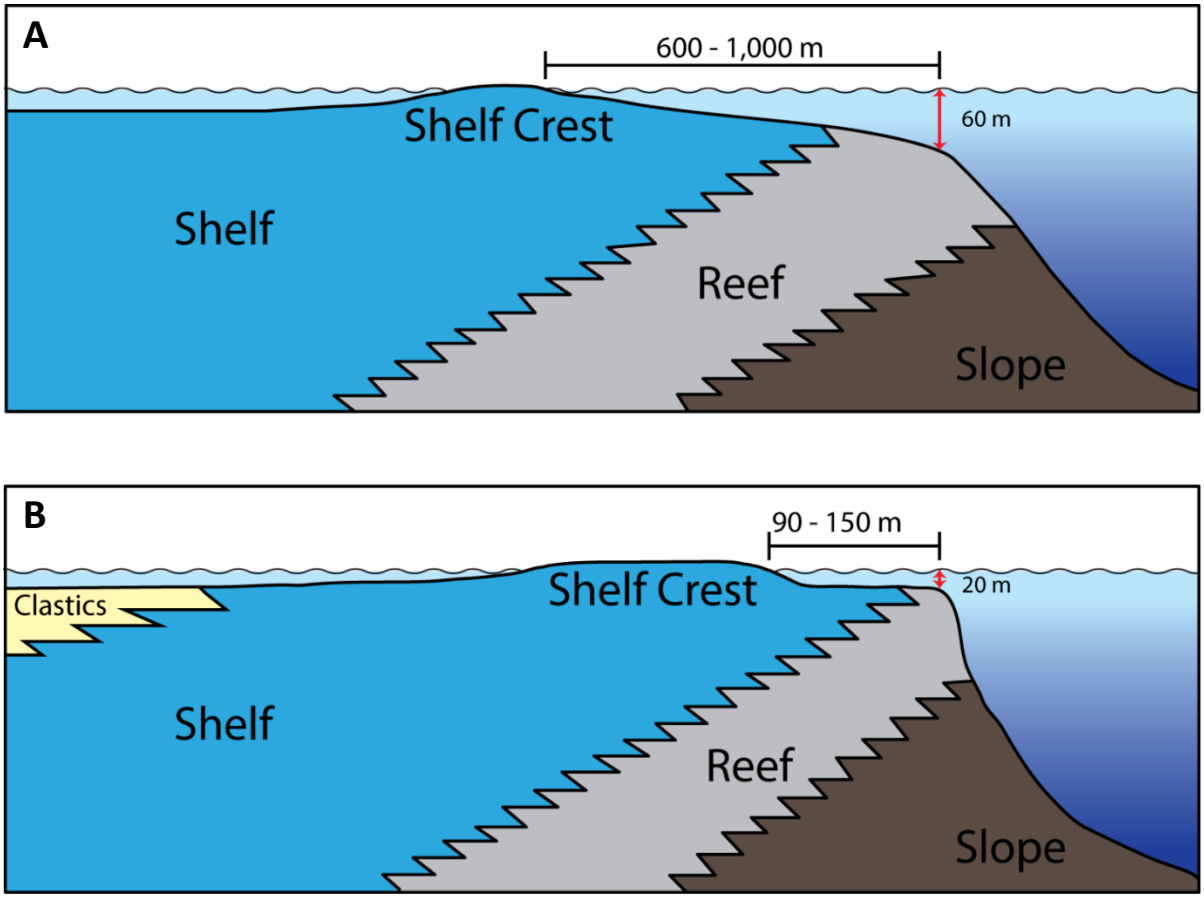

Figure 6: Schematic cross sections depicting alternative depositional profiles. A) Marginal mound profile of the Dunham (1972). B) Modified version of the marginal mound profile to reflect geometries observed in Rattlesnake Canyon. Modified after Gaber and Harris (1989).

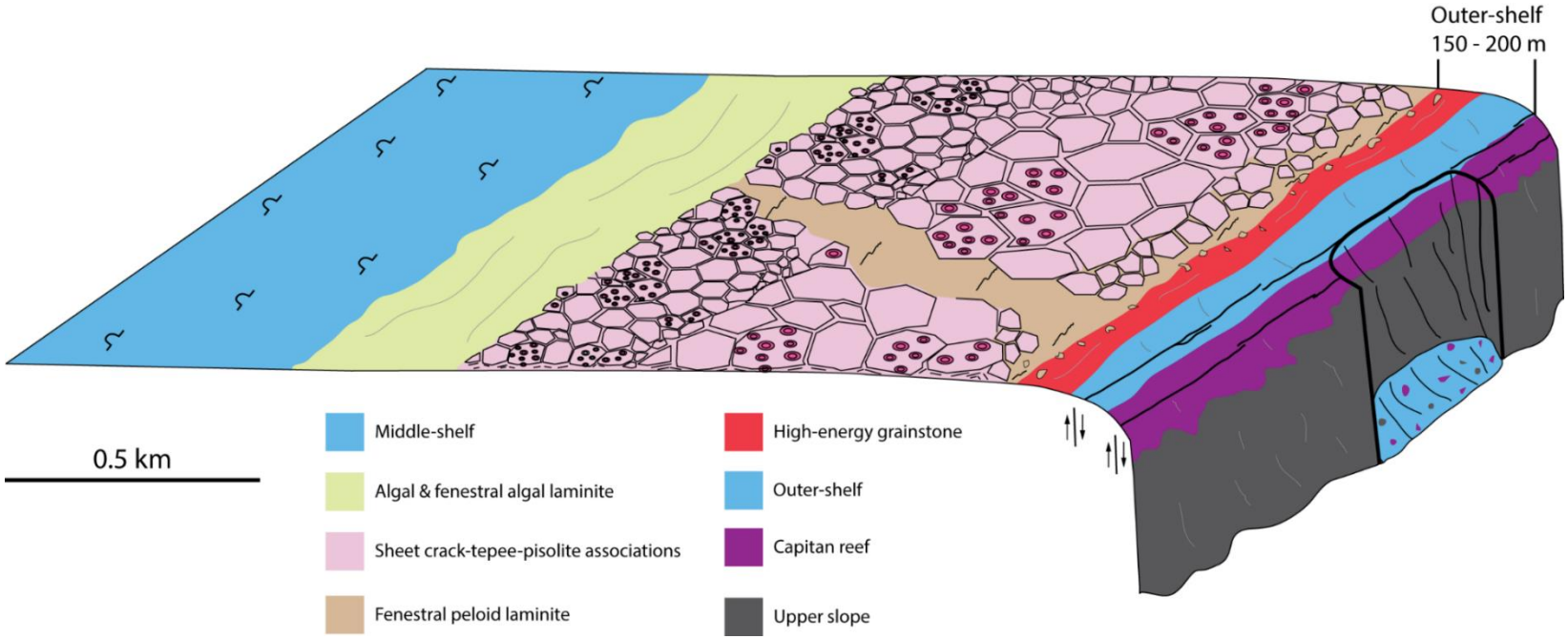

Figure 7: Depositional model of the G27 – G28 HFSs. This depositional model is drawn to scale and incorporates features from field observations and studies in nearby canyons including an expansive shelf crest, conglomerate beachrock deposits, a compressed outer shelf (150 – 200 m), syndepositional fracturing and faulting in the outer shelf, and a scalloped margin with collapsed scars and onlapping debris wedges.

DATA AND METHODS

FIELD AND DIGITAL-BASED

To characterize the stratigraphic framework, cycle architecture, and depositional facies belts of the late TSS and early HSS of CS 13 (Kerans et al. 2013), data were collected from the lower and middle Tansill Formation in Rattlesnake Canyon (Fig. 8). The outcrop exposure in Rattlesnake Canyon, located 6 km southwest of the Carlsbad Caverns National Park Center, provides an opportunity to study a more complete interval of shelf-to-margin platform stratigraphy than previously documented. Rattlesnake Canyon preserves the record of the G27 – G28 HFSs along a 1.4 km, roughly dip-oriented, cross-sectional exposure along the northern canyon wall, of the lower and middle Tansill shelf crest to reef-margin profile. Field data includes mapping and measured sections that were enhanced through integration with airborne LIDAR-based digital outcrop models, high-resolution satellite imagery, centimeter-scale resolution gigapan photomosaics, and other digital photos. Ancillary data includes the detailed work of Rush and Kerans (2010) from Walnut Canyon, used to gain a comparative stratigraphic framework for Rattlesnake Canyon.

Eight vertical measured sections were collected, totaling 467 m, documenting Dunham classification, grain size, major allochems, and sedimentary structures at a 10 cm scale of resolution. Sections were described on the northern wall of Rattlesnake Canyon where detailed characterization of the G25 and G26 (Hairpin and Triplet) (Kerans et al 2012) sequences had been resolved. Measured sections to the west of the canyon mouth, inland of the shelf margin, were vertically limited by the modern-day

erosional profile of the Guadalupe Mountains. Additional data is available from Walnut Canyon for more interior sections and studies by Schwartz (1981) and Kerans et al. (2012) contain an additional five measured section of up to 18 m above G26 sequence boundary, positioned 1.8 – 3.1 km inland if the G27/28 shelf margin. When projected onto a true-dip profile (Fig. 9), the spacing of sections in this study ranges between 58 m - 232 m, spans a distance of 1.1 km, beginning 300 m inland of the G28 platform margin. The close spacing of measured sections was mandated by the abrupt lateral facies tract changes observed.

Distinct bedding planes and key stratigraphic surfaces within each measured sections were plotted manually on photographs in the field. If possible, cycle and sequence-scale horizons identified within a measured section were followed laterally in the field or were traced on photomosaic panels. Correlations made using photomosaic panels of the canyon walls were aided by airborne LIDAR-based digital outcrop models developed from part of a LIDAR survey covering the entire southeast edge of the Guadalupe Mountains as well as the Delaware Mountains conducted in 2008. Using these techniques in tandem creates a high degree of confidence when correlating and interpreting cycle architecture along a palinspastically reconstructed dip-oriented regional cross section, shelf-profile dimensions, and when determining facies tract widths.

CORE BASED

In 1984, the Gulf PDB-04 stratigraphic research well was drilled in the Golden Lane field in Eddy County, New Mexico by Gulf Research and Development Company. From this well, approximately 1500 m of continuous core was recovered and became the

focal point of extensive studies carried out thereafter. A new look at the classic PDB-04 core provides a key subsurface tie-point and illustrates how outcrop-based high-frequency sequence framework from outcrop patterns can be brought into the subsurface. Procedures for logging and recovering the PDB-04 core are outlined in Garber et al. (1989). This study focuses on an approximately 35 m thick interval of the core covering the G27 and G28 HFSs. The slabbed and etched core was described in detail, at a centimeter-scale of resolution, and photomicrographs were used to aid in identifying allochems and lithofacies. From these descriptions, the 1-dimensional sequence and cycle architecture for the PDB-04 core was developed.

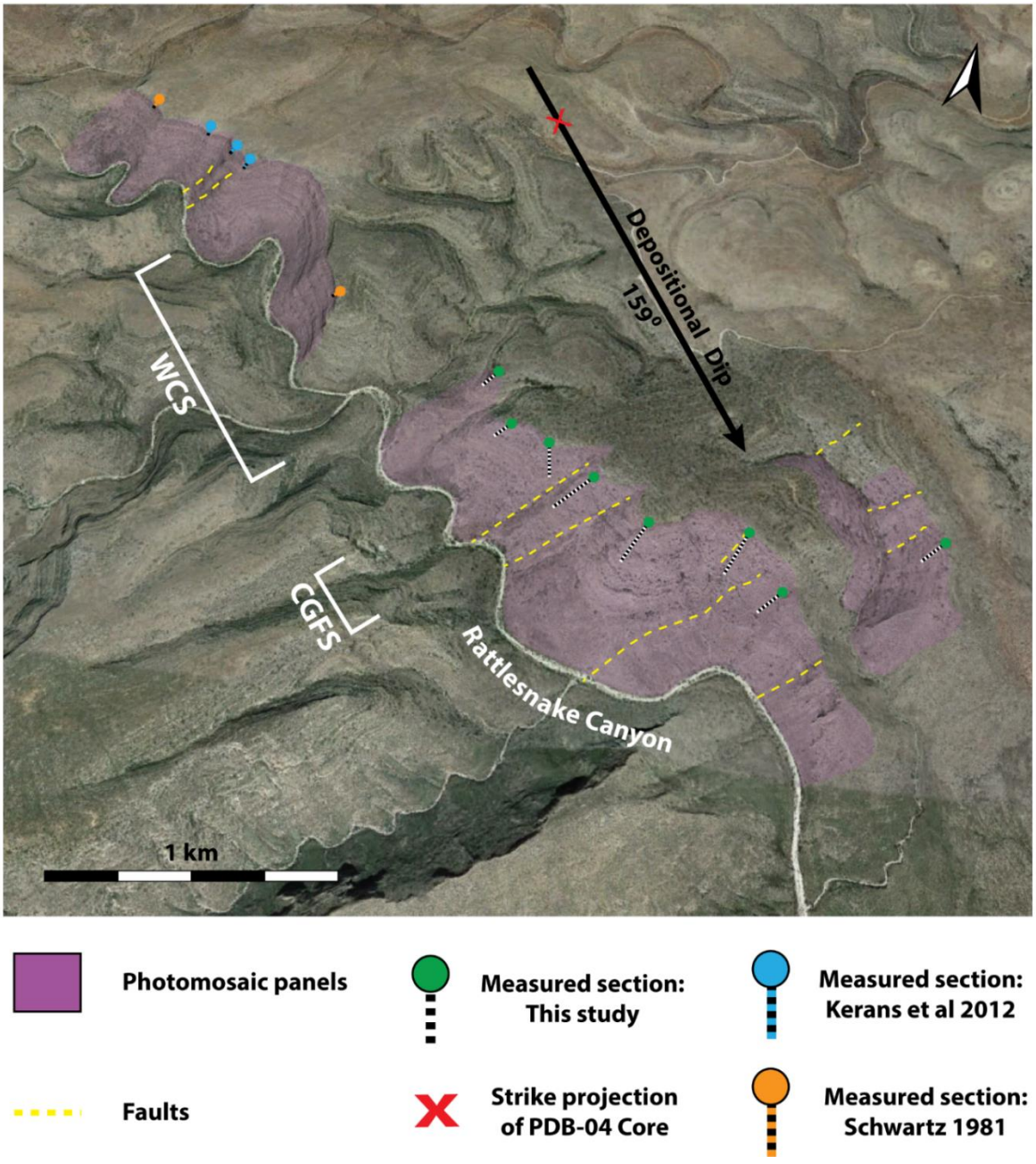

Figure 8: Slightly oblique satellite image of Rattlesnake Canyon from Google Earth Pro showing the position of measured sections and photomosaic panels used in this study. Faults include many interpreted in Jones (2012) and Kerans et al (2012). CGFS = Cave Graben Fault System, WCS = Walnut Canyon Syncline.

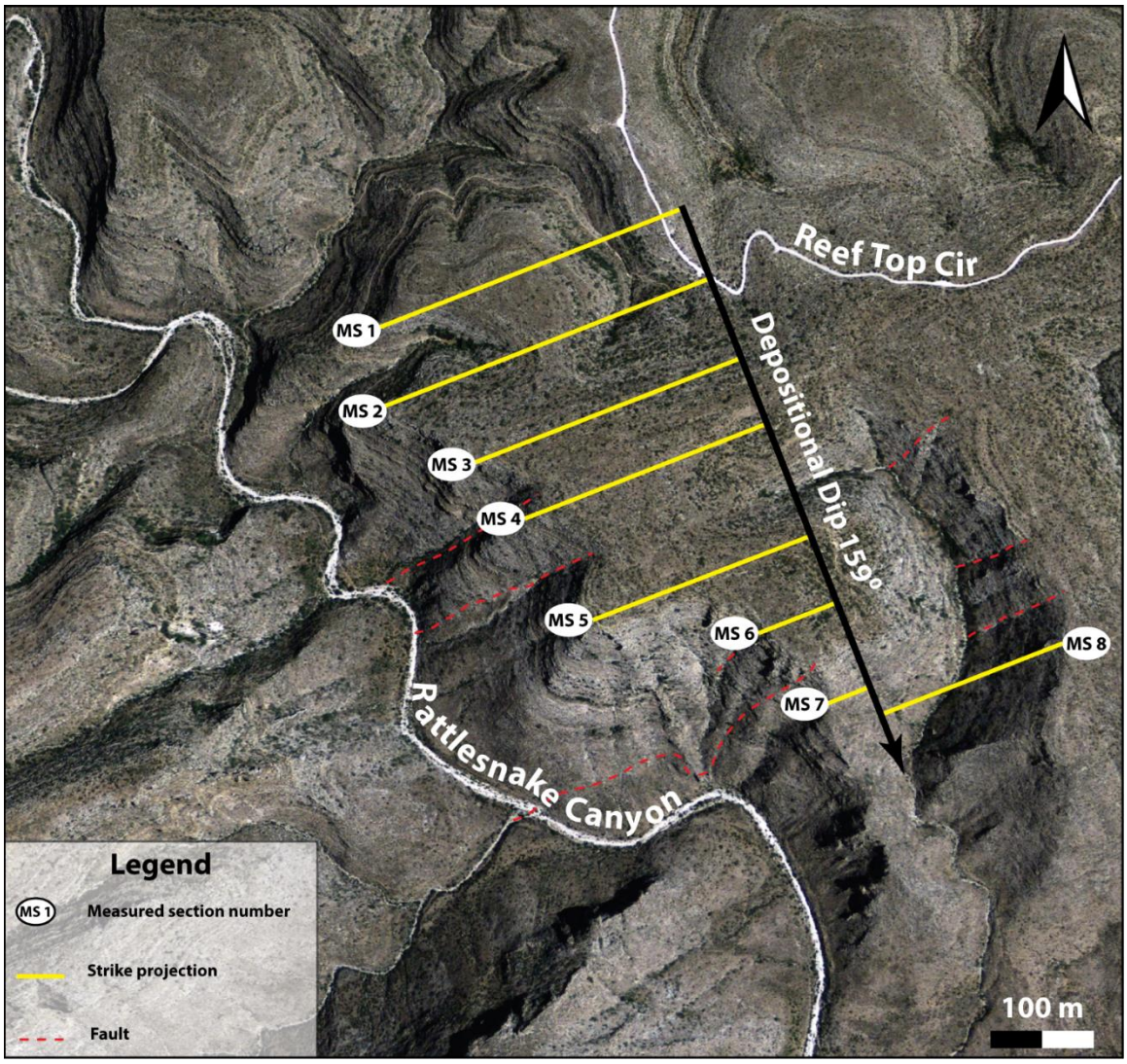

Figure 9: Satellite image of Rattlesnake Canyon from Google Earth Pro showing the strike projection of the vertical measured sections onto a dip line used in constructing the regional dip-oriented cross section.

OUTCROP LITHOFACIES

Seventeen different facies were define in the field, identified according to diagnostic sedimentary structures, grain types, and rock fabric, and then binned into similar facies tracts (Table 1).

RESTRICTED MIDDLE SHELF (FIG. 10)

1. Marine reworked dolomitic siltstone/sandstone:

Dolomitic siltstones to sandstones are thin, centimeter-scale, recessive slope forming units with sedimentary structures that include planar thin beds, ripple laminations, and rare fenestrae. These units can also be bioturbated to massive or interbedded with thin algal laminite units. Dolomitic siltstones and sandstones on the northwest shelf are composed predominantly of quartz and feldspar grains with minor amounts of peloids and rare skeletal fragments. These siliciclastics deposits are interpreted to have initially formed as blankets of aeolian dunes that prograded out onto the shelf during lowstands and were then subsequently reworked by the initial transgression of the following cycle (Kendal 1969; Gardner 1992; Mazzullo et al 1995). These siltstones and sandstones have sharp to erosional bases and pass gradationally upwards into carbonates.

2. Peloid wackestone – mud-dominated packstone:

Peloid wackestone to mud-dominated packstone units are composed of planar, submeter scale bedding with a flaggy to recessive weathering profile. The planar thin beds of this unit are commonly laminated, or bioturbated with small millimeter to

centimeter diameter vertical burrowing structures that are infilled with coarse-grained sediment including peloids, incipient pisoids, and *Mizzia*, or are occluded by cements in the case of millimeter-scale burrows. The dominant allochems in the peloid wackestone to mud-dominated packstone lithofacies are peloids and rare skeletal fragments and minor amounts of silt-sized quartz grains. Minor amounts of peloidal mud-dominated packstones were also interpreted in the outer-shelf area of the platform but are not genetically related to this lithofacies and were grouped with the peloidal grain-dominated packstones.

SHELF CREST (FIGS. 11 AND 12)

The shelf crest is arguably the most important facies tract on the deposition profile and was a prominent platform top feature during the G27 and G28 HFSs. Topographically, it was the highest position on the shelf, 15 m above the equivalent Capitan Reef (Bebout and Kerans, 1993), and was dominated by low to moderate depositional energy facies including fenestral and microbial laminites, pisoids, tepees, and sheet cracks. The shelf crest is an effective indicator of the arid paleoshoreline, and displays an acute sensitivity to minor relative sea-level fluctuations. This depositional setting is characterized by subtle facies variations and a somewhat random facies mosaic of discontinuous interfingering environments formed by isolated hypersaline ponds. These developed in response to periodic wetting of the subaerially exposed supratidal shelf crest causing pooling in localized depressions and creating a microenvironment favorable for the deposition of fenestral to microbial laminites and pisoids. High-

frequency cycles and HFC sets are easily correlated through the shelf-crest environment where teepees serve as a proxy for shoreline migration (Rush and Kerans, 2010).

1. Tepee/sheet crack/fenestral laminite associations:

The tepee-associated facies are dominated by buckled and upwards arching irregular laminar fenestral crusts that commonly form cliffs. Tepees are generally onlapped by pisoid-composite-grain-ooid rudstones and intraclastic grainstones indicating syndepositional relief. In more landward measured sections, tepee voids are filled with red peloidal siltstones, and in more seaward settings on the shelf, the voids become progressively filled with more marine paleoaragonite botryoids, as well as skeletal grains. Tepees act as a repository for whatever grains are forming in the adjacent offshore environment. The large voids beneath tepees can also be filled by peritidal fenestral blocks formed by autobrecciation related to expansion and collapse of buckled strata.

2. Sheet crack complex:

Sheet crack associated units consist of a network of early formed tepees with horizontal sheet cracks that develop in irregularly laminated fenestral laminites and can be filled with siliciclastics, marine cements, or marine sediment. Sheet crack lithofacies most commonly form within a matrix of peritidal facies consisting of pisoids, composite grains, coated grains, peloids, and ooids, but closer to the shelf edge, sheet cracks were observed in subtidal facies matrix and were filled predominantly with marine cements. Much like tepees, the more proximal they are positioned to the inner shelf, the higher their affinity will be to be filled with siliciclastics as opposed to marine cements.

3. Pisoid rudstone:

Pisoid rudstone units form planar, submeter-scale beds that commonly have poor lateral continuity and generally lap out against tepees, fill the voids beneath buckled strata, and form weakly resistant to recessive weathering profiles. Pisoids are large (> 2 mm) coated grains with regularly spaced concentric laminae of alternating thin micrite layers and microspars are intermixed with composite grains, superficial ooids, ooids, and peloids. Pisoid rudstones exhibit a variety of sorting from well-sorted unimodal grain sizes to chaotic poorly sorted grain sizes, to inverse or normally graded beds. The origin of pisoids has been disputed for years. Newell et al. (1953) and Kendall (1969) argued that pisolites form by means of algal mediation, Thomas (1968) and Dunham (1969) claimed that they formed though the precipitation of cements in the vadose zone in caliches or as concretions, Scholle and Kinsman (1974), made use of Quaternary deposits in Abu Dhabi to build his argument that pisolites form in sabkha-type caliches, and most recently, and currently the most accepted interpretation, is from Esteban (1976; Esteban and Pray 1977) whom interpreted the origins of pisoids to be subaqueous hypersaline waters based on stratigraphic constraints, and the morphology and geometries of the pisoids.

4. Peloid-intraclastic grain-dominated packstones to grainstone:

Peloid-intraclastic grain-dominated packstones to grainstone consist of planar submeter-scale bedding with planar and low-angle stratification. The dominant allochems are small angular intraclasts of mud and peloids with minor amounts of skeletal fragments. This lithofacies is positioned on the inner flank of the shelf crest and intersects

with the restricted middle shelf lagoon, and commonly onlaps tepees (Rush and Kerans 2010).

5. Algal laminite:

Algal laminite units developed planar submeter-scale bedding with crenulated and crinkly irregular microbial laminations. The dominant allochems of the algal laminite lithofacies are peloids and coated grains, and rare skeletal fragments. The algal laminite commonly contain fine to very fine silt sized quartz grains, especially when capping cycles and when positioned proximal to the middle shelf. Algal laminites were most commonly observed developing in an intermediary position between the landward flank of the shelf crest and the middle shelf.

6. Fenestral algal laminite:

Fenestral algal laminite units form planar, submeter-scale bedding with irregular microbial laminations and well-developed fenestrae. Fenestrae develop as planar parallel elongate to ovoid millimeter-scale gaps in the rock framework. Fenestral fabrics are useful criterion for recognizing peritidal environments with periodic wetting and drying cycles and they are reported to form through multiple processes including developing as molds within algal mats, as planar shrinking cavities formed by alternating wetting and drying sediments, or from trapped air or gas bubbles within unlithified sediments (Boyd, 1975). Major allochems include peloids and small incipient pisoids intermixed with carbonate mud, and similar to the algal laminites, Fenestral algal laminites were most commonly observed developing in an intermediary position between the landward flank of the shelf crest and the middle shelf.

7. Fenestral peloid laminite:

Fenestral peloid laminite units form planar submeter-scale bedding characterized by poor to moderately well-developed fenestrae with planar laminations and common faint irregular microbial laminations. The dominant allochems in fenestral peloid laminites are peloids, coated grains, incipient pisoids, superficial ooids, *Mizzia*, and skeletal fragments. Compared to fenestral algal laminites, fenestral peloid laminites are significantly more grain-rich, have a less well-developed fenestral fabric, and are more widespread and deposited across the shelf crest.

HIGH ENERGY OUTER-SHELF: (FIG. 13)

1. Conglomeratic beachrock

Conglomeratic beachrock units form planar-to-seaward-dipping meter-scale beds. Beachrock conglomerates are deposited in shingled seaward-dipping cross beds of ooid grainstones and skeletal-coated-grain-*Mizzia* grain-dominated packstones to grainstones that generally contain irregular undulose laminations. The clasts are tens of centimeters in diameter and composed of the same lithology as the matrix in which they are deposited. Also, associated with the clasts of beachrock are large (tens of centimeters) blocks of fenestral laminites forming by way of autobrecciation processes within tepees complexes that are then shed off the shelf crest and reworked into the shallow foreshore and upper shoreface environments. In places, the beachrock conglomerate can be seen lapping onto the seaward side of a tepee structure. The dominate allochems of the matrix are *Mizzia*, ooids, coated grains, peloids, incipient pisoids, and minor amounts gastropod and bivalve fragments.

2. Ooid grainstone:

Ooid grainstone units form planar meter-scale bedding with a resistant weathering profile and smooth surface. Grains are well sorted in the high-energy environment associated with this lithofacies and sedimentary structures include low-to-high-angle current-stratified cross beds, hummocky cross beds and, and low-angle seaward-dipping wedge-set cross stratification. The dominant allochems in the ooid grainstone lithofacies are ooids, incipient pisoids, and minor skeletal fragments.

3. Ooid-peloid grain-dominated packstone – grainstone:

Ooid-peloid grain-dominated packstone to grainstone units form a resistant weathering profile with planar-to-seaward-dipping submeter-scale bedding planes. Common sedimentary structures associated with ooid-peloid grain-dominated packstone to grainstone are low-angle, seaward-dipping current and planar stratification. The dominant allochems of this lithofacies are ooids and peloids with some bivalve and gastropod fragments.

4. Skeletal-coated-grain-*Mizzia* grain-dominated packstone – grainstone:

Skeletal-coated-grain-*Mizzia* grain-dominated packstones to grainstones form planar-to-seaward-dipping meter-scale beds that have shingled seaward-dipping to low-angle, wedge-set cross stratification and irregular undulose/hummocky cross stratification with skeletal grains concentrated in the planes of laminations. Dominant allochems consist of a mixed assemblage of subtidal skeletal grains including fragments of *Mizzia*, bivalves, and gastropods, that generally have coatings, and nonskeletal coated grains

composed of ooids and peloids. At times this facies has a nearly monospecific faunal assemblage and is composed almost entirely of coated *Mizzia* grains (Fig. 13-D).

5. Peloid grain-dominated packstone to mud-dominated packstone:

Peloid grain-dominated packstone to mud-dominated packstone units consist of planar-to-seaward-dipping meter-scale bedding, but can also generally be massive and structureless. The dominant allochems are peloids with rare small skeletal fragments. The general lack of sedimentary structures and indicator faunal assemblages can make peloid grain-dominated packstone to mud-dominated packstone difficult to constrain to a single depositional environment.

LOW ENERGY OUTER-SHELF (FIG. 14)

1. Peloid-gastropod-bivalve-skeletal packstone to rudstone:

Peloid-gastropod-bivalve-skeletal packstone to rudstone units form seaward-dipping meter to submeter-scale beds that are planar stratified to structureless. In the most distal section of the outer-shelf profile, this lithofacies is composed of large skeletal fragments of Bellerophotid gastropods, scaphapods, brachiopods, and minor fragments of frame-building reef fauna in a peloid-skeletal back-reef matrix. Transitioning landwards the size of skeletal fragments decrease and gastropods, bivalves, and *Mizzia* are the dominant allochem present in a more grain-rich peloid grain-dominated packstone matrix. Burrowing, particularly single vertical burrow tubes of 1 cm diameter are common.

2. Skeletal-fusulinid packstone to fusulinid-coated-grain rudstone:

Skeletal-fusulinid packstone to fusulinid-coated-grain rudstone units form massive to faintly horizontally stratified meter-scale beds. The dominant allochems are fusulinids, bivalves, gastropods, *Mizzia*, forams, coated grains, oncoids, and peloids, but this lithofacies can be devoid of many of the allochems and consist primarily of fusulinids and large coated grains that form rudstone in a grain-dominated packstone matrix.

3. Skeletal-oncoid rudstone/grain-dominated packstone:

Skeletal-oncoid rudstone/grain-dominated packstone units are generally structureless to massive and form meter-scale bedding and commonly these units will contain stromatactis-like cavities filled with marine cements (Fig. 14A). The dominant allochems are oncoids that nucleate around bivalves, gastropods, *Mizzia*, and brachiopods forming an irregular coating around the grain. Skeletal-oncoid rudstone/grain-dominated packstone units also contains minor amounts of fusulinids and peloids and the primary mineralogy is calcite.

REEF MARGIN

1. Sponge-algal boundstone:

Sponge-algal boundstone units are massive with internal cavities filled with fine-grained geopetal sediment and extensive amounts of botryoidal marine cements upwards of 90 % (Toomey and Babcock 1983; Yurewicz 1976). Dominant allochems consist of calcareous sponges and bryozoans (reef frame builder), *Collenella*, *Tubiphytes*, Bellerophotid gastropods, and brachiopods, as well as binding and encrusting microbial

organism that help with stabilization. Sponge-algal boundstone units are composed predominantly of calcite and are bound above by a crinoid-*Collenella* grain-dominated packstone reef-flat environment and below by upper slope intraclastic-skeletal grain-dominated packstones-to-rudstones.

GULF PDB-04 CORE LITHOFACIES

In total, nine lithofacies were described from the cored interval of the PDB-04 that penetrated the G27 and G28 HFSs, and can be found in (Table 1). There were no lithofacies encountered in the core that were not seen in outcrop. The varying geographic location and burial history of strata within the core resulted in a different diagenetic history than observed from exhumed outcrops in the Guadalupe Mountains. Widespread precipitation of evaporites in the subsurface has occluded the majority of porosity in the Gulf PDB-04 core.

The PDB-04 core is from a position updip from all measured sections within this study. Lithofacies described in the core tend to be more heavily bioturbated and of a finer-grained composition than outcrop. Core lithofacies are also devoid of major skeletal allochems and outer-shelf fauna, and are dominated by peloids. The position of the core on the shelf profile and the peloid mud-rich character of the lithofacies are indicators the dominant facies assemblage is from a restricted, low-energy middle-shelf environment. An added benefit of the PDB-04 core is that it provides the opportunity to observe the character of bedding contact between siliciclastic and carbonate lithologies that cannot be readily observed in the field because of the recessive slope forming tendency of these units. The core revealed that siliciclastic units have a sharp-to-erosional base with a gradational contact with the overlying carbonate sediments.

Facies Tract	Dunham Name	Fabric	Sedimentary Structures	Dominant Grain Type	Bedding Geometry	Outcrop	Core
Restricted middle shelf - low energy	Dolomitic siltstone to UVFSS	Lower very fine to upper very fine sandstone/siltstone	Planar thin bedded, ripple laminated, bioturbated to massive, fenestrae	Quartz, feldspars, peloids, rare skeletal fragments	Recessive, slope-forming	X	X
Restricted middle shelf - low energy	Peloid wackestone to mud-dominated packstone	Wackestone to mud-dominated packstone	Planar laminations, bioturbated, small mm-cm diameter vertical burrows	Peloids, rare skeletal fragments, silt-sized quartz	Planar, submeter scale bedding, flaggy, recessive	X	X
Shelf crest	Fenestral algal laminite	Boundstone	Irregular microbial laminations, fenestrae	Peloids, coated grains, skeletal fragments	Planar, submeter-scale bedding	X	
Shelf crest	Algal laminite	Boundstone	Crenulated and crinkly irregular microbial laminations	Peloids, coated grains, silt-sized quartz, rare skeletal fragments	Planar, submeter-scale bedding	X	X
Shelf crest	Tepees	Rudstone to boundstone	Meter-scale TP-buckle/upwards arching structures, aragonite botryoids, fenestrae, irregular laminations	Pisoids, composite grains, coated grains, peloids, ooids, rare skeletal grains, quartz silt	Concave-upward buckled TP's, cliff-forming	X	X
Shelf crest	Sheet cracks	Rudstone to boundstone	Irregular slightly tilted horizons, aragonite botryoids, fenestrae, irregular laminations	Pisoids, composite grains, coated grains, peloids, ooids, rare skeletal grains	Planar slightly buckled, cliff forming	X	X
Shelf Crest	Pisoid rudstone	Rudstone	Normal and inverse grading, rare minor fenestrae	Pisoids, composite grains, coated grains, superficial ooids, ooids, peloids	Onlaps TP', planar submeter-scale bedding, often recessive	X	X
Shelf crest	Fenestral peloid laminite	Packstone to rudstone	Fenestrae, irregular microbial laminations	Peloids, coated grains, incipient pisoids, superficial ooids, *mizzia* , skeletal fragments	Planar, submeter-scale bedding	X	X
Shelf crest	Peloid-intraclastic grain-dominated packstones to grainstone	Grain-dominated packstone to grainstone	Planar stratified, inclined strata	Intraclast, peloids, rare skeletal fragments	Planar, submeter-scale bedding	X	X
Outer-shelf - high energy	Beachrock conglomerate	Conglomerate/floatstone	Beachrock intraclast, shingled seaward-dipping cross beds, irregular undulose laminations	*Mizzia* , ooids, coated grains, peloids, incipient pisoids, fenestral laminite clast, beachrock clast, gastropod and bivalve fragments	Planar to seaward dipping meter-scale bedding	X	
Outer-shelf - high energy	Ooid grainstone	Grainstone	Shingled seaward-dipping cross beds, multidirectional cross stratified	Ooids after peloids, incipient pisoids, skeletal fragments	Planar meter-scale bedding	X	
Outer-shelf - high energy	Peloid-ooid grain-dominated packstone to grainstone	Grain-dominated packstone to grainstone	Seaward-dipping and planar stratifications	Ooids, peloids, rare skeletal fragments	Planar to seaward dipping submeter-scale bedding	X	
Outer-shelf - high energy	Skeletal-coated-grain-*mizzia g* rain-dominated packstone to grainstone	Grain-dominated packstone to grainstone	Shingled seaward-dipping cross beds, irregular undulose laminations	*Mizzia* , coated grains, ooids, gastropods, bivalves, fusulinids	Planar to seaward dipping meter-scale bedding	X	
Outer-shelf - high energy	Peloid mud-dominated packstone to grain-dominated packstone	Mud-dominated packstone to grain dominated packstone	Planar stratified to structureless	Peloids, rare skeletal fragments	Planar to seaward dipping meter-scale bedding	X	X
Outer-shelf - low energy	Peloid-gastropod-bivalve-packstone to rudstone	Packstone to rudstone	Planar stratified to structureless	Bivalves, gastropods, peloids, *mizzia* , fusulinids, scaphapods, macroporella, rare oncoids	Seaward dipping meter to submeter-scale bedding	X	
Outer-shelf - low energy	Skeletal-fusulinid packstone to fusulinid-coated grain rudstone	Packstone to rudstone	Structureless	Fusulinids, bivalves, gastropods, *mizzia* , forams, coated grains, oncoids, peloids, skeletal fragments	Massive, meter-scale bedding	X	
Outer-shelf - low energy	Skeletal-oncoid rudstone/grain-dominated packstone	Rudstone	Structureless, minor stromatactis cavities	Oncoids, bivalves, gastropods, *mizzia* , brachiopods, fusulinids, peloids	Massive, meter-scale bedding	X	
Shelf margin	Sponge-algal boundstone	Boundstone	Massive with internal cavities filled with aragonite botryoid cement, internal sediment (geopetals)	Sponges, Tubiphytes, internal sediment, brachiopods	Massive	X	

Table 1: Lithofacies from outcrop and core. Table includes facies tracts, constituent lithofacies and lithofacies characteristics. Dominant grain types listed in order of relative abundance. Modified from Harman (2011).

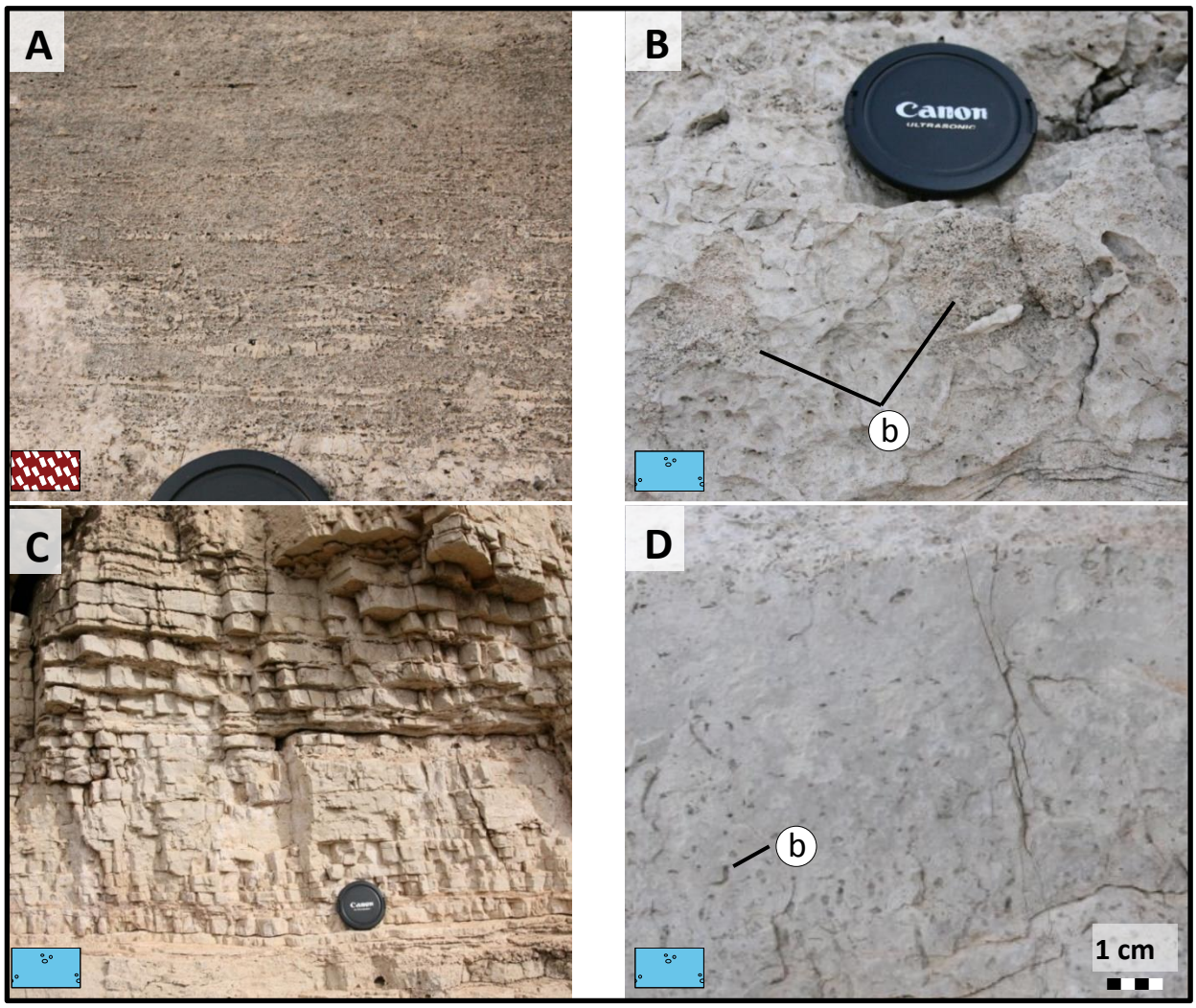

Figure 10: Representative lithofacies photographs of the middle-shelf restricted lagoon outcrop. A) Planar stratified peloid-intraclastic grain-dominated packstone to grainstone. B) Peloid mud-dominated packstone with vertical to subvertical burrowing structures (b) infilled with peloids and minor amounts of small skeletal fragments. C) Thin-bedded flaggy siliciclastic-rich peloidal wackestone. D) Peloid mud-dominated packstone with thin, mm diameter, vertical to subvertical burrow-like structures (b) burrow occluded by cement.

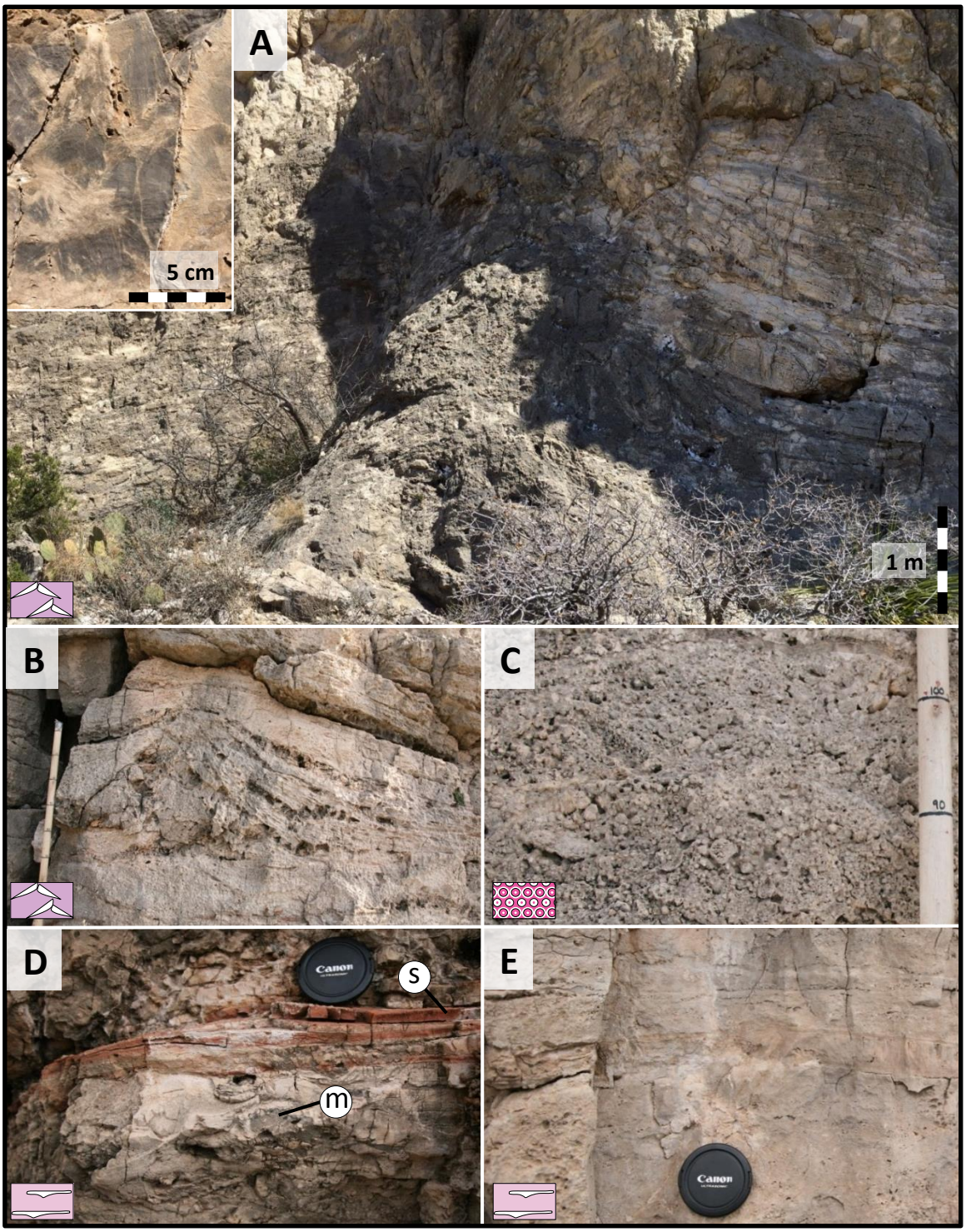

Figure 11

Figure 11: Representative lithofacies photographs of shelf crest outcrop. A) Large, buckled, upwards arching strata of a tepee developed within the G27 highstand formed in a fenestral peloid laminite matrix with incipient pisoids. Inset is photograph of large botryoidal marine cement, calcite after aragonite, infilling depositional voids. B) Small tepee within the G27 TST with pisolite rudstone onlapping the arched strata and filling the tepee along with auto-brecciated fenestral laminite clast. C) Poorly sorted pisoid rudstone composed of singular and composite grains. D) Sheet cracks develop in a pisoid rudstone with multiphase infill. Infill includes reddish silty peloidal mudstone (s) and radial fibrous calcite after aragonite marine cement (m). E) Sheet crack with marine radial fibrous calcite after aragonite cement developed in a fenestral peloid laminite.

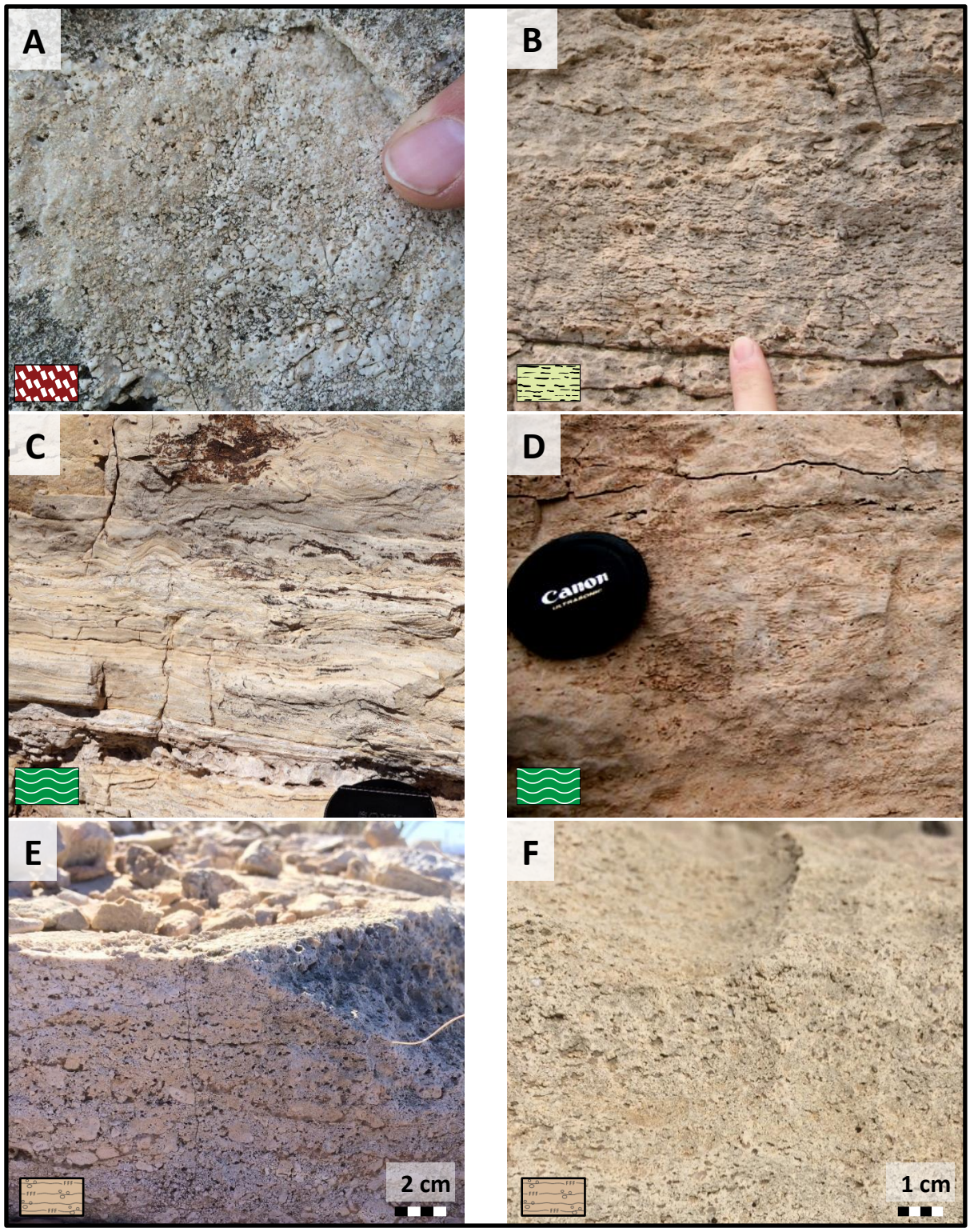

Figure 12

Figure 12: Representative lithofacies photographs of peritidal shelf crest/shelf-crest-flank outcrop. A) Peloid intraclast grain-dominated packstone to grainstone. B) Well developed fenestral algal laminite. C) silt-rich algal laminite with crenulated fabric. D) Crinkly muddy algal laminite. E) Fenestral peloid laminite with peloids, coated grains, and pisoids. F) Fenestral peloid laminite.

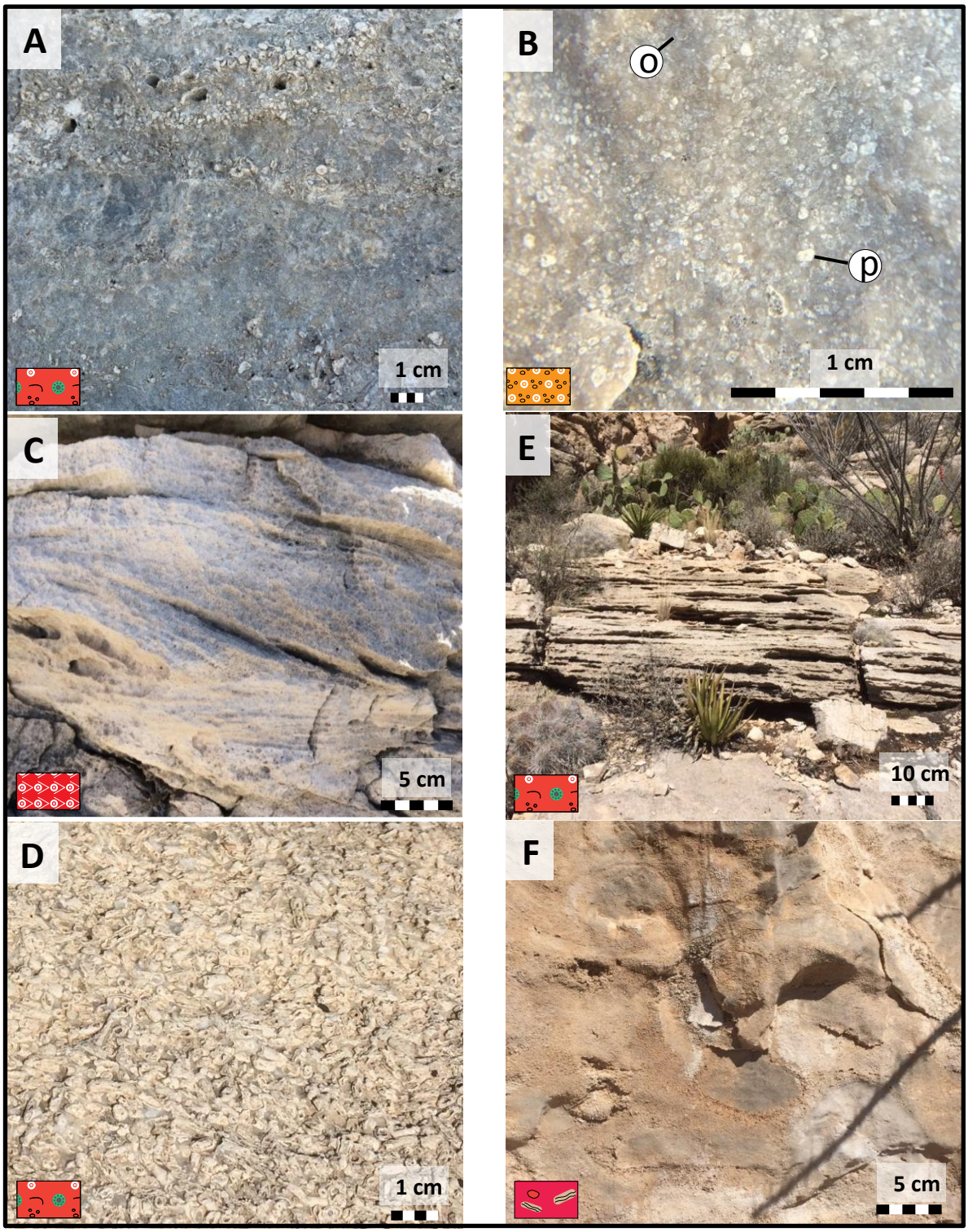

Figure 13

Figure 13: Representative lithofacies photographs of the outer shelf high-energy foreshore/upper shoreface outcrop. A) Skeletal-coated-grain-Mizzia grain-dominated packstone with irregular undulose laminations. B) Photograph taken through a hand lens of an etch surface of an ooid-peloid grain dominated packstone with ooids (o) and peloids (p). C) Cross-bedded ooid grainstone. D) Seaward dipping foreshore coated-grain-Mizzia grainstone striking 75º NW and dipping 8 º. E) Close up of photograph of a coated-grain-Mizzia grainstone. F) Beachrock conglomerate developing on a rocky shoreline in an irregular undulose laminated skeletal-coated-grain-Mizzia grain-dominated packstone to grainstone with clast fenestral laminite and clast of the host rock.

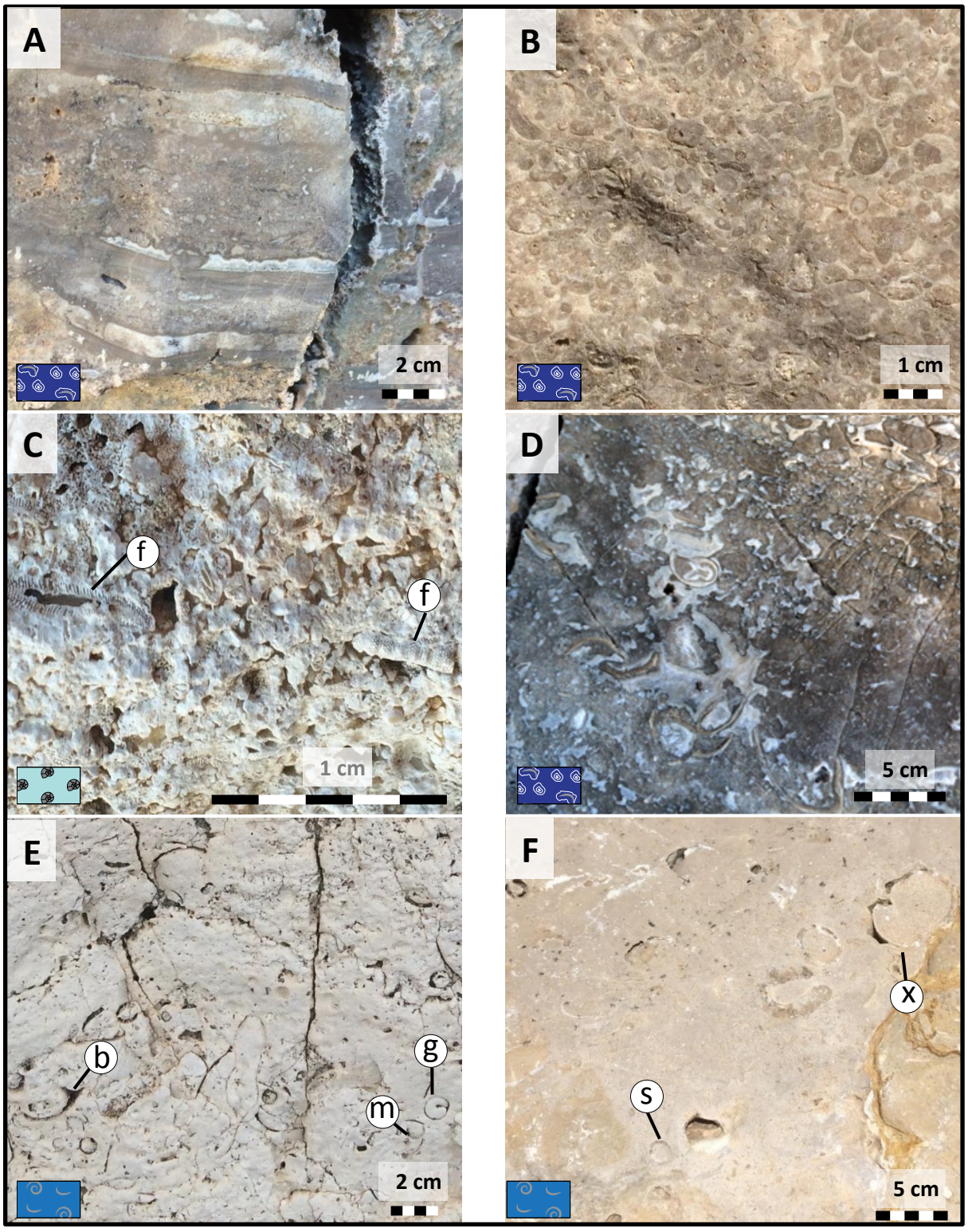

Figure 14

Figure 14: Representative lithofacies photographs of the outer-shelf moderate-to-low energy environment. A) Stromatactis fabric developing in a skeletal-oncoid rudstone limestone host rock. B) Coated-skeletal-oncoid rudstone. C) Fusulinid-coated-grain grain-dominated packstone. This lithofacies contains abundant fusulinids (f). D) Skeletal-oncoid rudstone with large bivalves and abundant marine cement. E) Macroporella-Mizzia gastropod-bivalve mud-dominated packstone. The dominant allochems include bivalves (b), gastropods (g), and Macroporella (m). F) Skeletal rudstone/mud-dominated packstone showing large Bellerophotid gastropods (x) and scaphapods (s).

STRATIGRAPHIC ARCHITECTURE

The depositional profiles of the G27 and G28 HFSs developed for this study were constructed from eight detailed vertical measured sections from Rattlesnake Canyon in the Guadalupe Mountains, New Mexico (Figs. 15 and 16). Diagnostic facies assemblages from well-constrained positions along the shelf profile were used to facilitate 2-dimensional cycle architecture comparisons between measured sections (Fig. 17). Shelf-crest-dominated cycles have an average thickness of 2 – 10 m and record minor signals of flooding events with thin basal peloid and skeletal-*Mizzia*-peloid packstones that transition upwards to tepee/sheet crack/fenestral peloid laminite assemblages. Many of the cycles within this setting have sharp erosional basal contacts with rip-up clasts from the underlying cycle top (Fig. 18). Cycles centered on the high-energy outer-shelf facies tract have an average thickness of between 2 – 4.5 m. They are sensitive proxies for sea level and were the most effective at recording relative sea-level fluctuations. Typically, high-energy outer-shelf cycles shallowed upwards from skeletal grain-dominated packstones to current-stratified to cross-bedded ooid or skeletal grainstones. Outer-shelf-tract-dominated cycles were significantly thicker than HFCs from shallower environments on the profile and have an average thickness of between 7 – 9 m. These cycles are relatively homogenous with skeletal-oncoid rudstones to grain-dominated packstones at the base and fusulinid-gastropod-bivalve mud-dominated to grain-dominated packstones in the upper portions of cycles and cycles caps. The transition of outer-shelf cycles into the reef flat and reef margin occurs over a distance of 25 – 50 m

and is best recognized by the increased abundance of crinoids, the probable calcareous alga *Collinella*, and large gastropods.

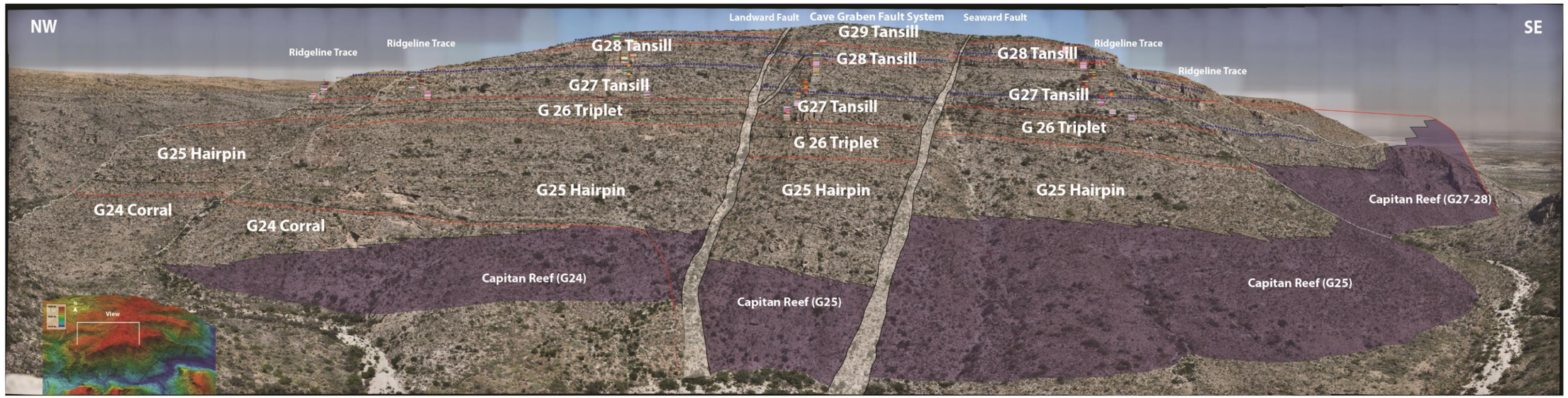

Figure 15: Digitized photomosaic panel of the northern wall in Rattlesnake Canyon with measured section descriptions tied into distinct bedding planes marked in the field. High-frequency sequence boundaries are marked by red lines and maximum flooding surfaces within the G27 and G28 are marked by dotted blue lines. Because of the three-dimensional aspect of the outcrop (see inset of shaded LIDAR digital elevation model), no consistent scale can easily be applied.

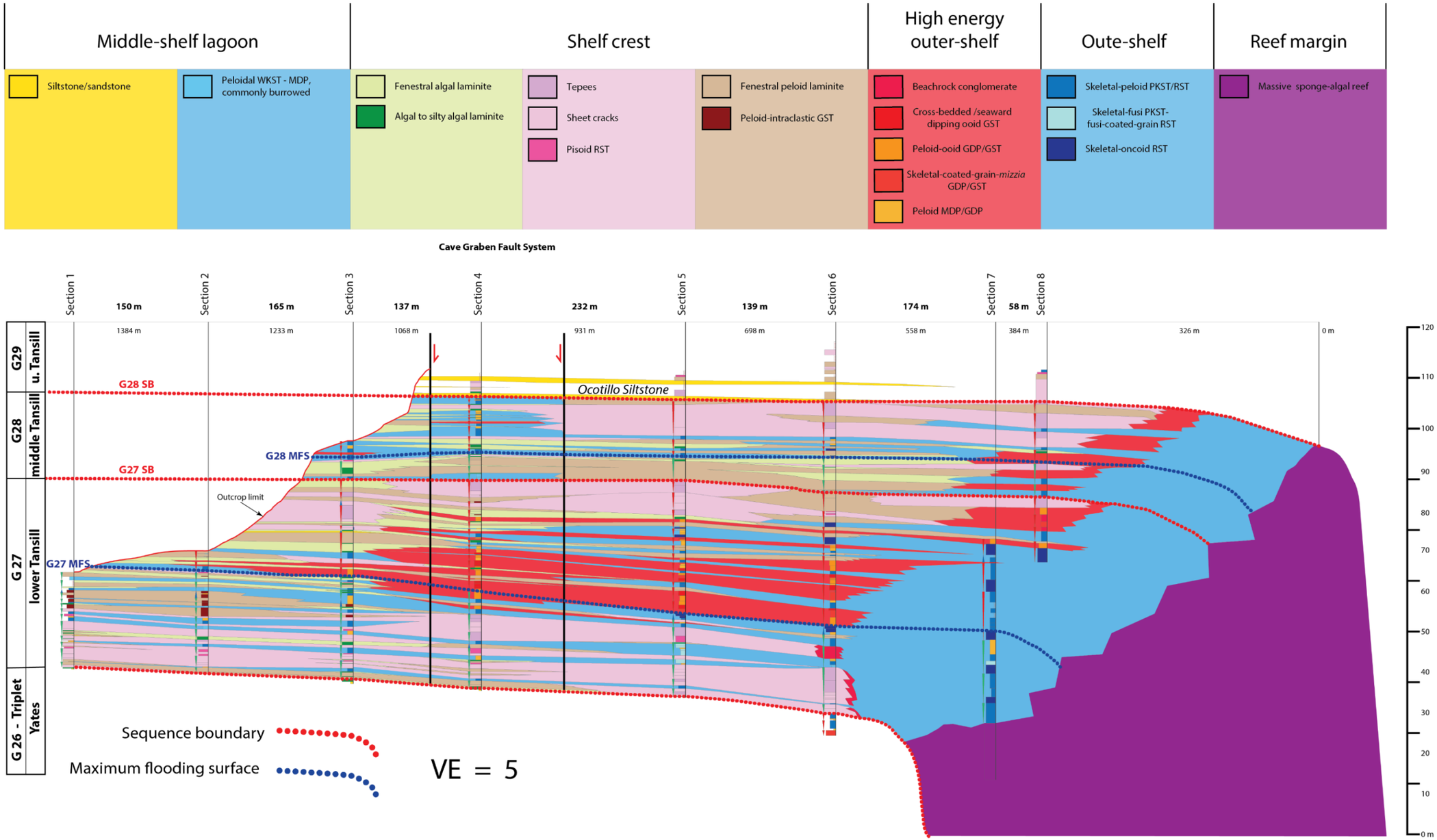

Figure 16: Composite 2-dimensional cycle architecture and sequence stratigraphic framework of the G27 and G28 HFSs in Rattlesnake Canyon. Cross section is aligned parallel to depositional dip.

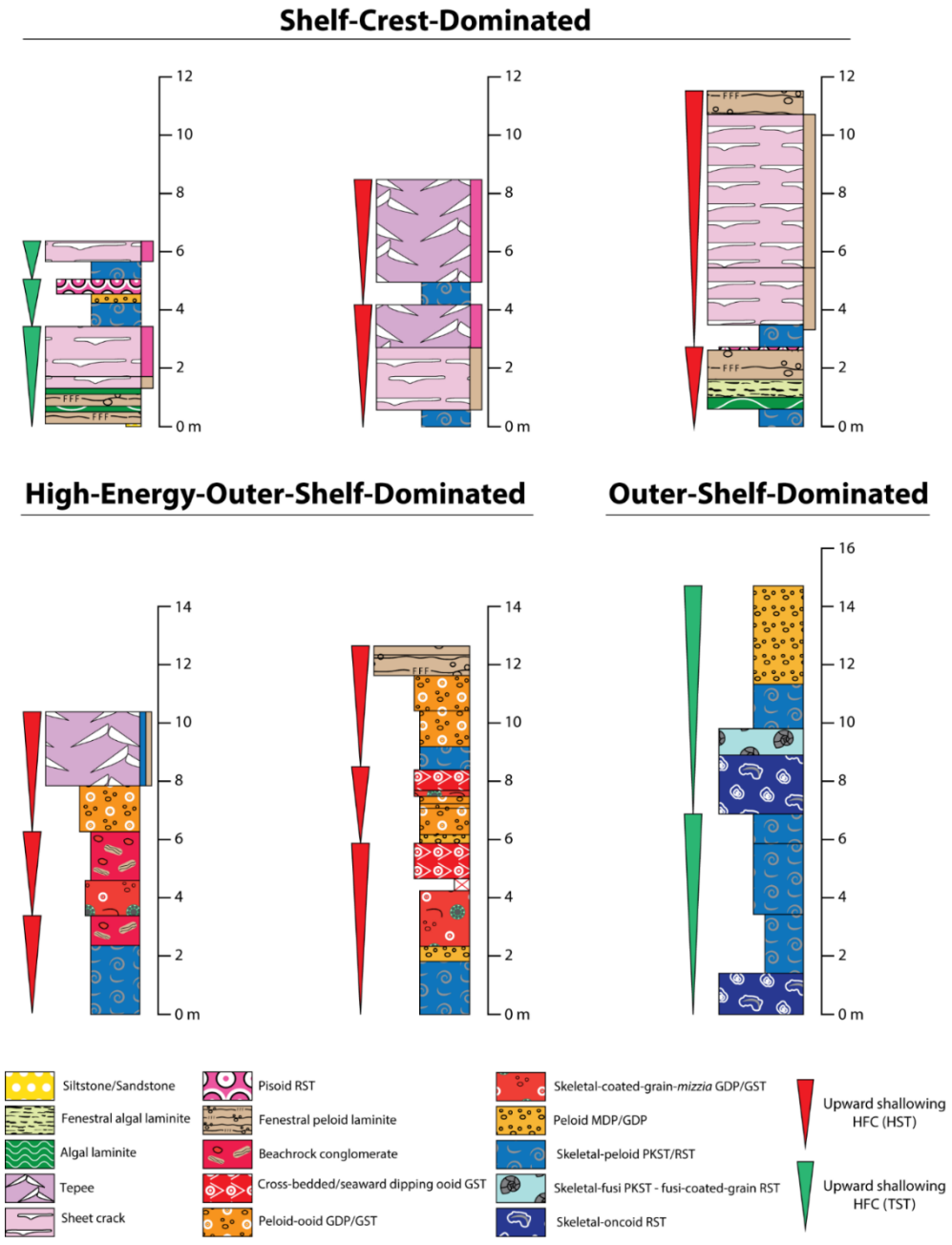

Figure 17: Characteristic 1-dimensional high-frequency cycle stacking architecture of the different dominant facies tract environments of the G27 and G28 HFSs. (A) A cycle stacking pattern from the G27 HFS at section MS 1. (B) A cycle stacking pattern from the G28 HFS at section MS 8. (C) A cycle stacking pattern from the G28 HFS at section MS 5. (D) A cycle stacking pattern from the G27 HFS at section MS 8. (E) A cycle stacking pattern from the G27 HFS at section MS 6. (F) A cycle stacking pattern from the G27 HFS at section MS 7.

Figure 18: Example of a HFC base in the shelf-crest-dominated facies tract. A rip-up clast (R) from the underlying pisoid rudstone was reworked into the overlying Mizzia grain-dominated packstone and is representative of and small-scale flooding event. Note irregular erosional contact between facies.

When constructing the architecture of the G27 – G28 HFSs, the systematic methodology for building a sequence stratigraphic framework outlined in (Kerans and Fitchen 1995) was used when interpreting maximum flooding surfaces and sequence boundaries. High-frequency-sequence-scale maximum flooding surfaces were picked within skeletal-oncoid rudstones and skeletal-packstones that extended the farthest updip on the shelf. Conversely, high-frequency sequence boundaries were picked atop distinctive fenestral-tepee-pisolite dominated shelf-crest cycle sets that could be shown to extend the furthest downdip. The spatial distribution of the current-stratified high-energy, ooid and rocky foreshore capped HFCs were used to track shoreline position and thus to highlight retrogradational to progradational trends within each HFS (Fig. 19).

This study is focused on the G27 HFS that contains the CS 13 MFS and the G28 HFS that forms the first HFS of the CS 13 early HSS. The G27 HFS (Fig. 20) averages 50 m in thickness and initiated with retrograding sets of cycles directly above the upper Triplet sandstones. In the shelf-crest setting retrograding tepee complexes at the base of the sequence initiated 100 m inland of the equivalent shelf margin. High-frequency cycle amalgamation is variable across the shelf profile and commonly occurs in the outer-shelf where minor changes in accommodation play a less significant role in stacking patterns. The G27 TST averages 28 m thick and contains from of 3 – 13 HFCs. Constraints on the CS 13 MFS indicate that cycles within the G27 TST retrograded at least 860 m based on the extent of back-stepping pattern of shelf-crest facies and grainstone geobodies present in Rattlesnake Canyon. The subsequent G27 HST is an average of 22 m thick and

contains between 7 – 13 HFCs. It is characterized by a seaward stepping shelf-crest facies tract with a substantially larger volume of high-energy outer-shelf facies assemblages tracking in front of it relative to the TST. Deposition of the G27 HFS with its distinctive and relatively thick TST reflects a significant long-term change in accommodation, following, as it does, the highly progradational to retrogradational to forced regressive pattern. G 27 cycles are overlain by the thin somewhat asymmetrical G28 HFS (Fig. 21). The G28 TST averages 6.5 m thick and contains between 1 – 4 HFCs. The G28 TST lacks sheet crack and tepee structures and is dominated by algal and fenestral peloid laminites. The maximum flooding surface in the G28 is not well expressed relative to the G27 and does not extend as far landward. The following highstand is an average thickness of 13.5 m and contains 3 – 10 HFCs. The G28 HST is nearly twice as thick as the G28 TST and is characterized by the reappearance of prograding well-developed sheet crack and tepee structures (Figs. 16, 22, and 23).

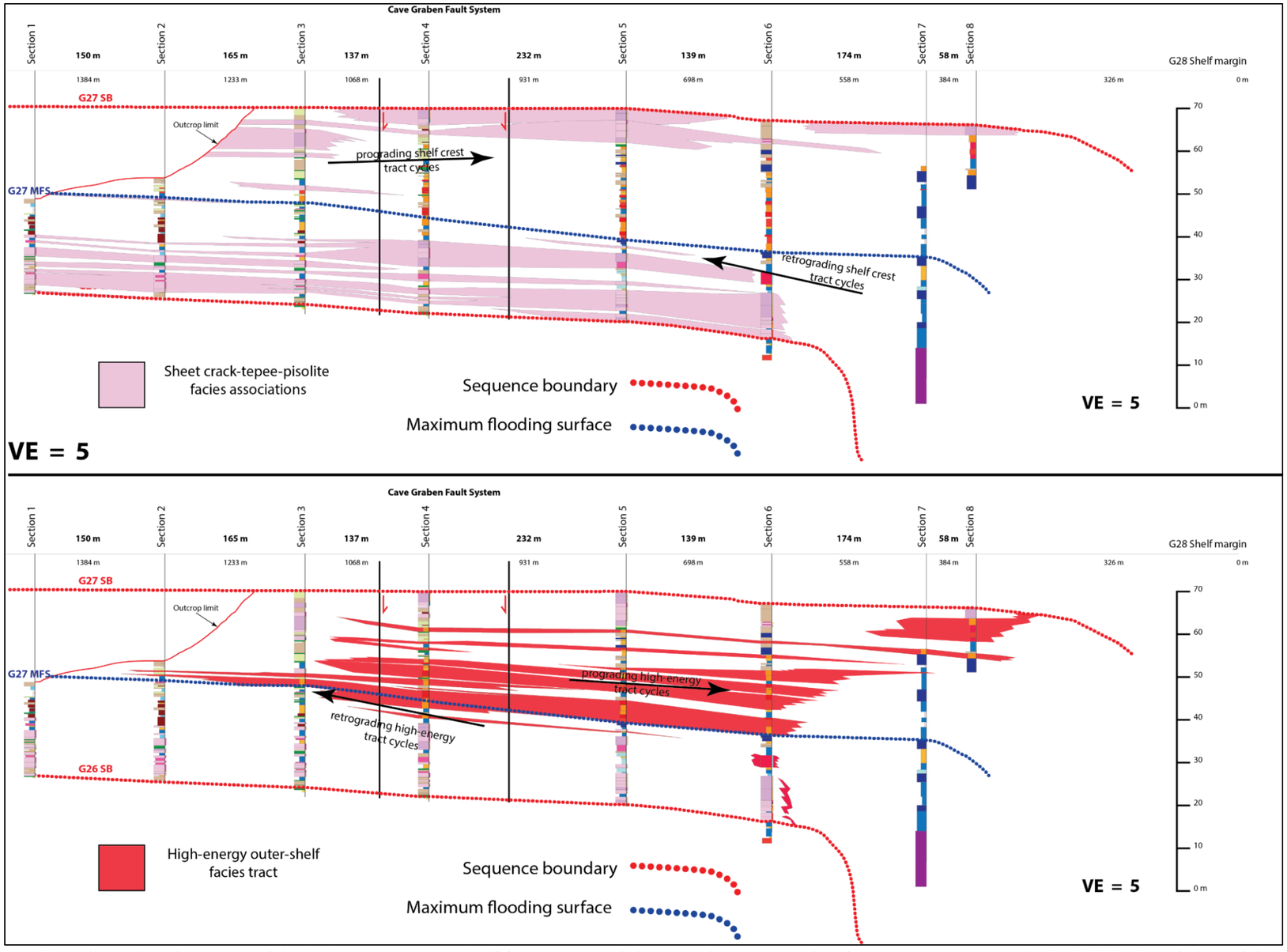

Figure 19: Two-dimensional analysis of the high-energy, outer-shelf facies tract and sheet crack- tepee-pisolite facies associations in the G27 HFS. Correlation of theses facies tracts between measured sections was used to tracking retrogradation and progradation within the G27 and G28 high-frequency sequences, and was also one of the criteria used in picking stratigraphic surfaces.

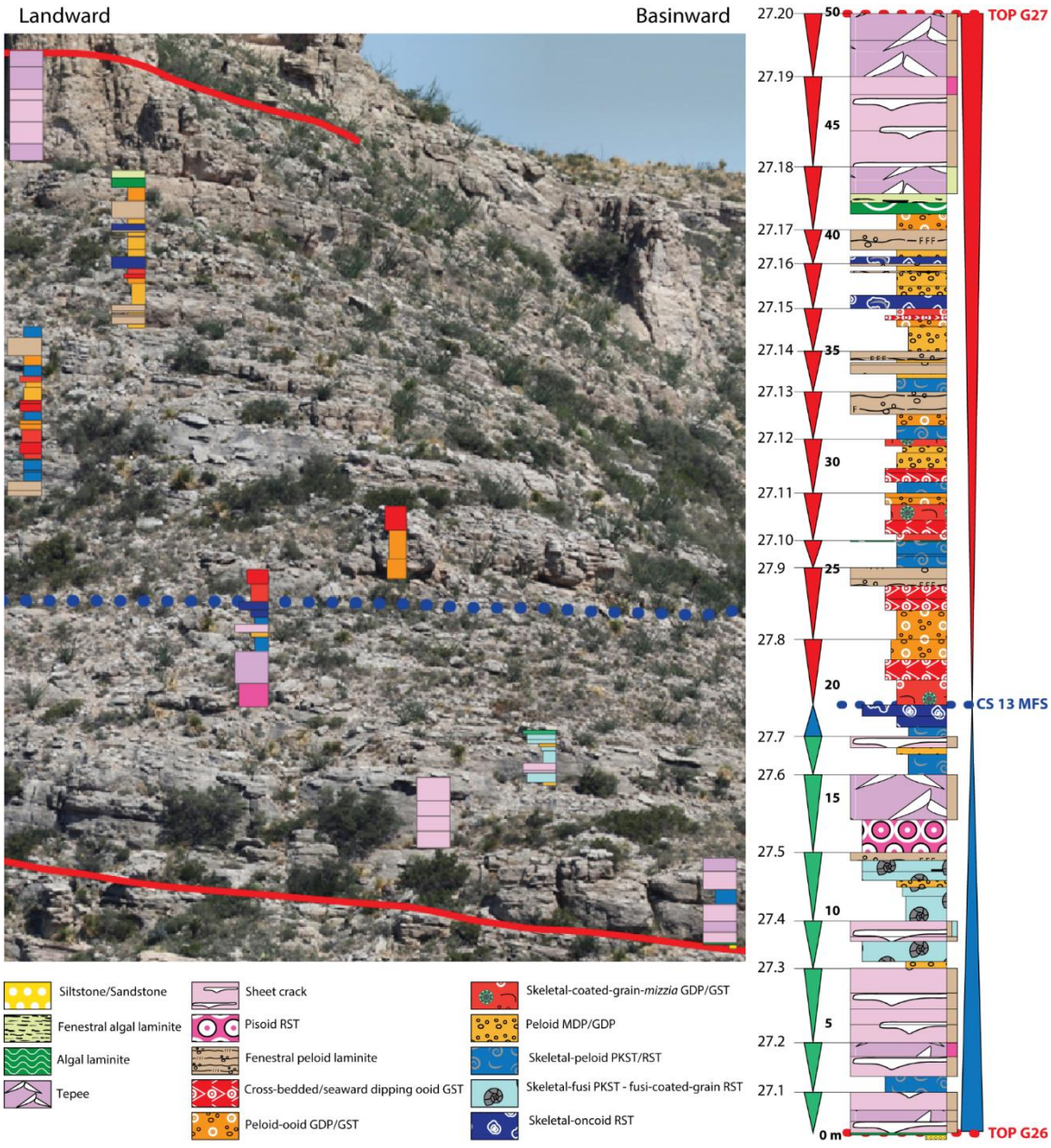

Figure 20: Type section of the G27 HFS taken at MS 5. Key marker beds and distinct outcrop horizons were used to tie the section to a photomosaic panel of the northern wall of Rattlesnake Canyon in the field, and maximum flooding surfaces and sequence boundaries for the G27 and G28 HFS were interpreted on the panel.

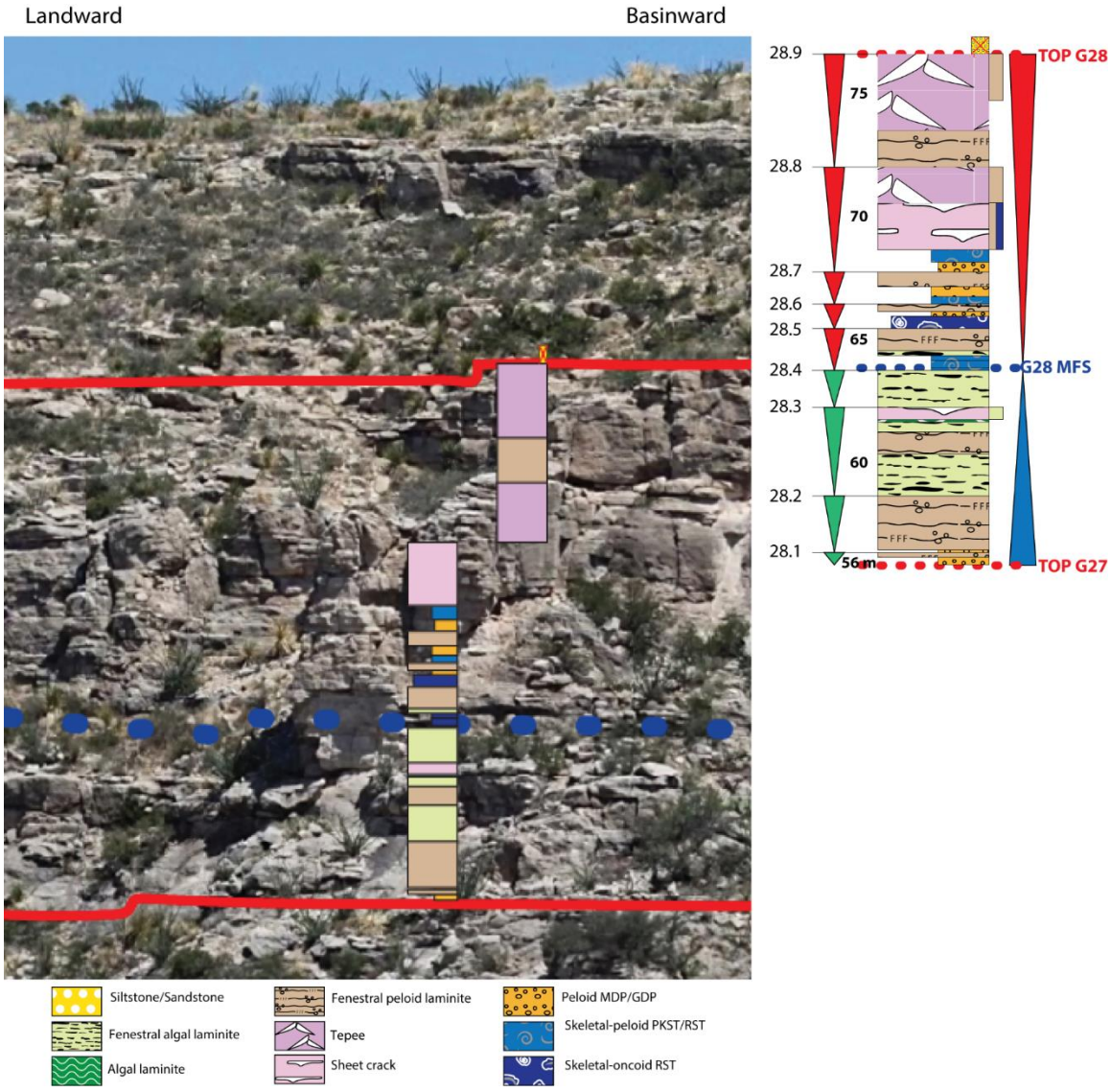

Figure 21: Type section of the G28 HFS taken at MS 6. Key marker beds and distinct outcrop horizons were used to tie the section to a photomosaic panel of the northern wall of Rattlesnake Canyon in the field, and maximum flooding surfaces (dotted blue line) and sequence boundaries (red line) for the G27 and G28 HFSs were interpreted on the panel.

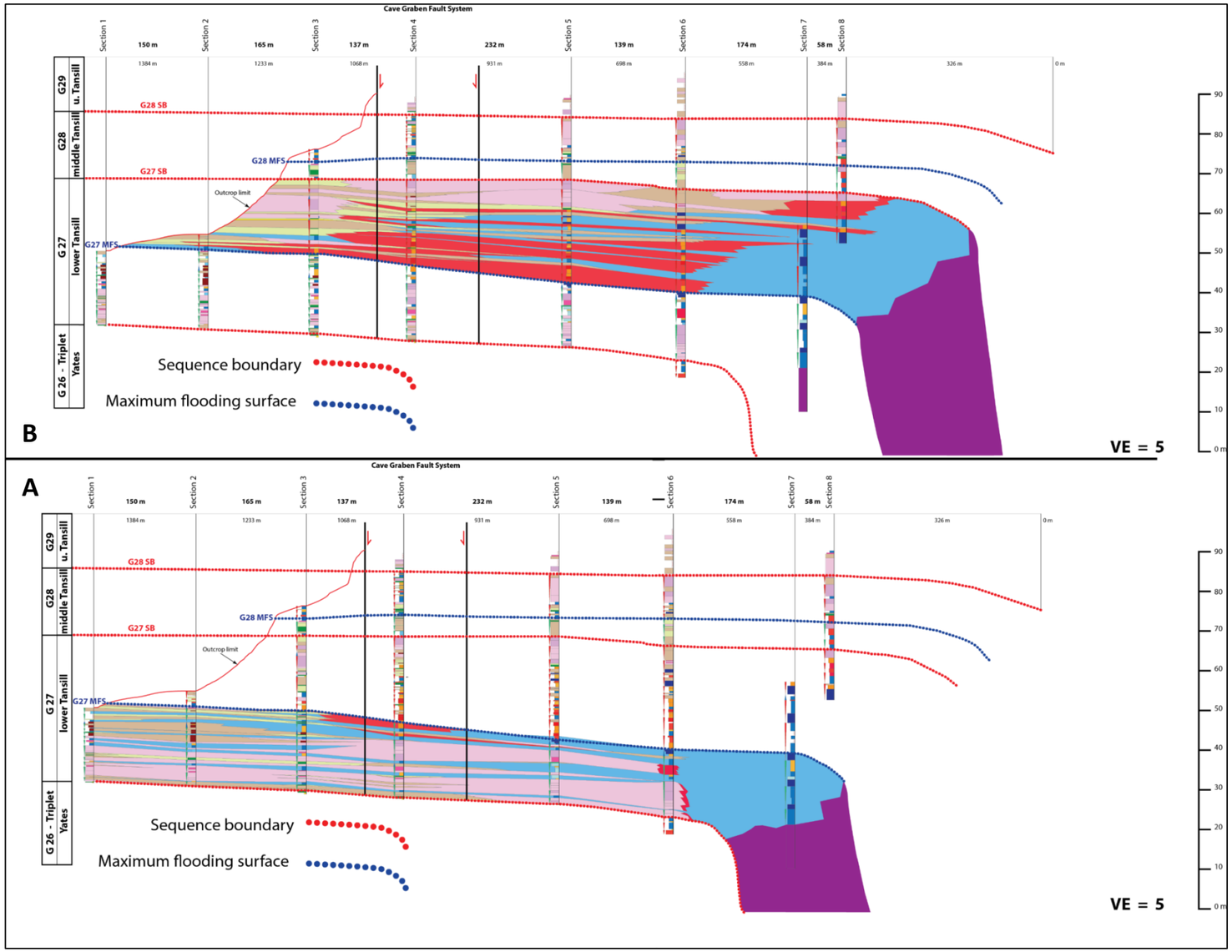

Figure 22: Two-dimensional cycle architecture of the G27 HFS. A) The G27 TST and B) the G27 HST in Rattlesnake Canyon built from correlating high-frequency cycles and high-frequency cycle sets across the depositional profile using 1-dimensional stacking pattern analysis from vertical measured sections.

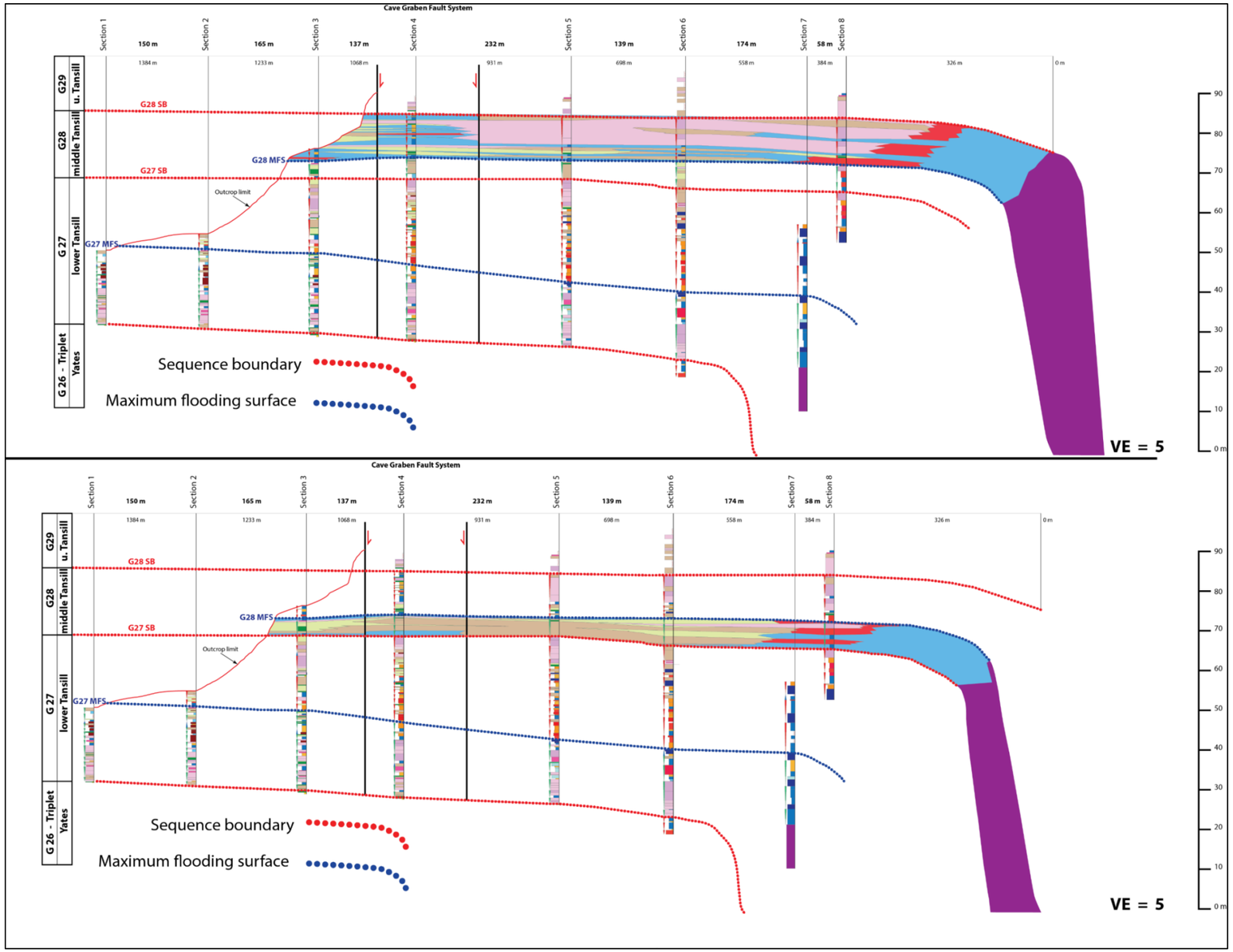

Figure 23: Two-dimensional cycle architecture of the G28 HFS. A) The G28 TST. B) The G28 HST in Rattlesnake Canyon built from correlating high-frequency cycles and high-frequency cycle sets across the depositional profile using 1-dimensional stacking pattern analysis from vertical measured sections.

REGIONAL CORRELATION

LINK TO THE SUBSURFACE

High-resolution core descriptions allowed for detailed facies tracking and the interpretation of the 1-dimensional sequence architecture and stacking patterns in the Gulf PDB-04 core (Figs. 24 and 25). Tying interpretations of the G27 – G28 HFSs from Rattlesnake Canyon into the PDB-04 core allows for: (1) a test of the validity of applying outcrop-derived models to subsurface dataset and (2) the opportunity to gain insights about the complete G27 – G28 HFSs in a more landward position than permitted in outcrop studies because of erosion and truncation of this stratigraphic interval in Rattlesnake Canyon. In core, the G27 HFS TST has 10 HFCs, the HST has 8 HFCs, and the ratio of TST to HST thickness is 1.7. When compared to measured section 3, the most landward vertical section with a complete record of the G27, which had a TST to HST thickness ratio of 1.15, both have a relatively symmetrical record of the transgression and regression with slightly greater accumulation occurring in the TST. Similar to the outcrop area, expression of the G27 in core is marked by shelf-crest tepee associations at the base with peritidal and supratidal cycle caps that transition into peloid-packstone-capped cycles in the early HST and algal laminite capped cycles in the late highstand. In core, G28 HFS had 1 HFC within the TST and 7 within the HST, with a TST to HST thickness ratio of 0.2.

Measured section 5 is the most landward vertical section with a complete record of the G28 that was not affected by growth strata within the Cave Graben Fault System. Measured section 5 has a TST to HST thickness ratio of 0.4, and when compare to the

PDB-04 core, both are highly asymmetrical with little deposition occurring during the TST and substantially thicker accumulation within the HST. In core, the only HFC in the G28 TST is capped by a thin algal laminite, whereas high-frequency cycles in the early highstand are capped by progressively thicker peloid grain-dominated packstone to intraclastic grainstones, and the late highstand cycles are capped by algal laminites that thicken upwards towards the sequence boundary.

OUTCROP TO SUBSURFACE VARIATIONS

Similarities between the G27 HFS were much stronger than between G28 HFS. The significantly more landward position of the G28 HFS within the PDB-04 core relative to Rattlesnake Canyon makes it difficult to draw comparisons between the two areas. The record of G28 strata in the core is interpreted to be from the restricted middle shelf lagoon based on the lack of skeletal allochems and abundance of peloidal mud-dominated packstones and grain-dominated packstones. This highlights the difficulty in making correlations between 1-dimensional stacking patterns separated by significant distances, particularly when in the low-energy, restricted middle shelf there is an inherent lack of diagnostic facies and . In general, HFC patterns between the G27 – G28 tend to be partly incongruous. Subtle variations in sedimentation rate, subsidence, and ocean circulation between the two locations are likely the causes of this variation. However, cycle sets exhibit strong similarities in patterns indicating broad scale mechanisms of accommodation were operating simultaneously across the 42 km area between Rattlesnake Canyon and the core.

A major difference between outcrop analogs in Rattlesnake Canyon and the PDB-04 core area is the landward extent of the tepee and sheet-crack complex at the base of the G27 HFS. It is present at a substantially more landward position (0.5 – 0.7 km farther) within the PDB-04 core. Regardless of disputes over the position of the speculated Hovey channel (King 1942, 1948) or Diablo channel (Hill, 1999) both are located at southern end of the Delaware Basin and acted as an inlet for open-marine waters during the Late Permian. Water circulation would decrease moving north to a more distal positions on the shelf, and ocean current stagnation would give rise increasingly supersaturated seawater with respect to carbonate and sulfate in these areas. A trend towards increased restriction moving north within the Delaware Basin could have led to voluminous precipitation of marine cements and enhancement of tepee development in the Tansill. This offers a potential explanation for why there is a more expansive tepee-pisolite shelf-crest complex in the PDB-04 core, drilled (42 km) northeast of Rattlesnake Canyon at a position 2.1 km inland from the equivalent Tansill shelf margin, than documented in Rattlesnake Canyon.

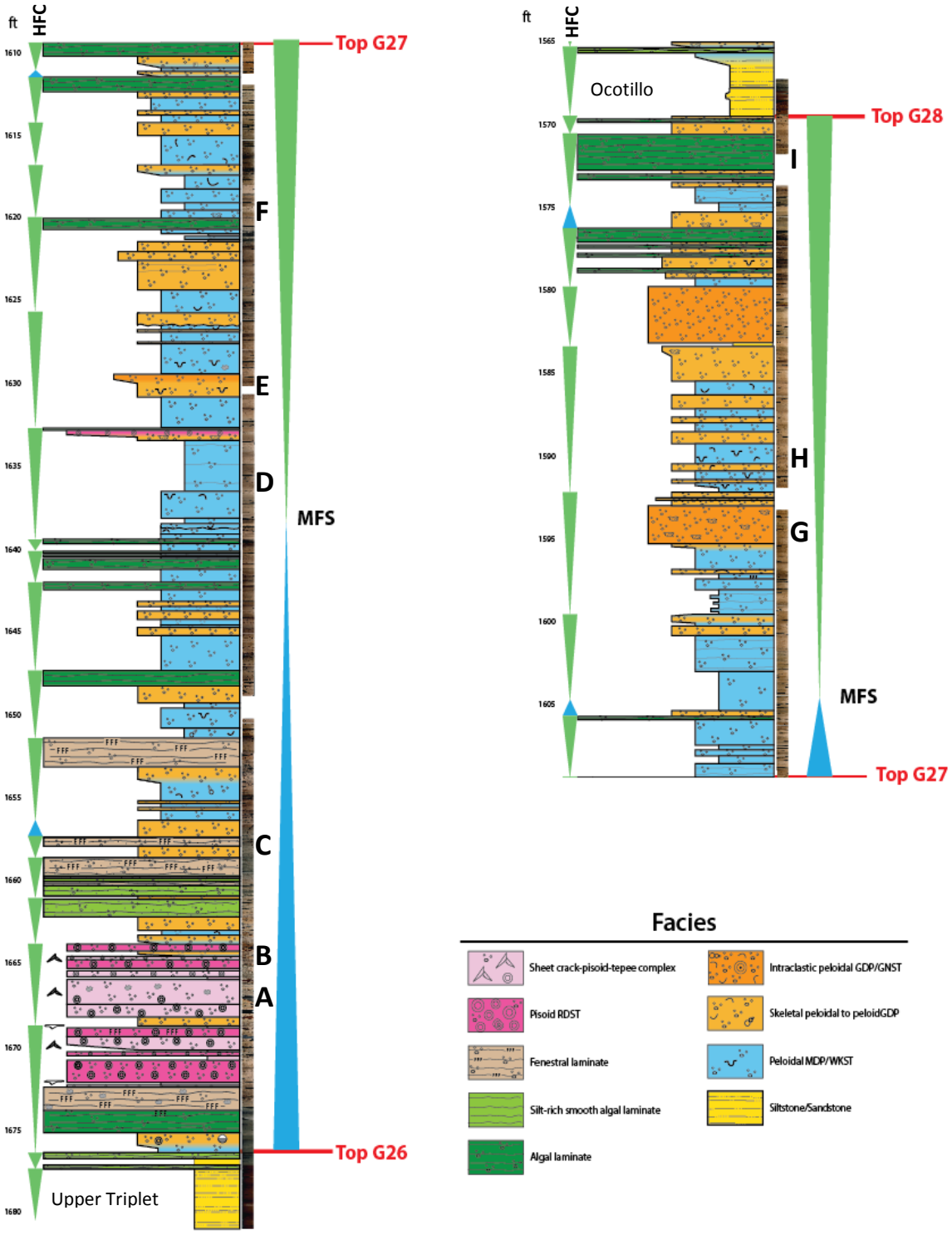

Figure 24: One-dimensional cycle architecture and sequence stratigraphic framework of the G27 and G28 HFSs in the Gulf PDB-04 core.

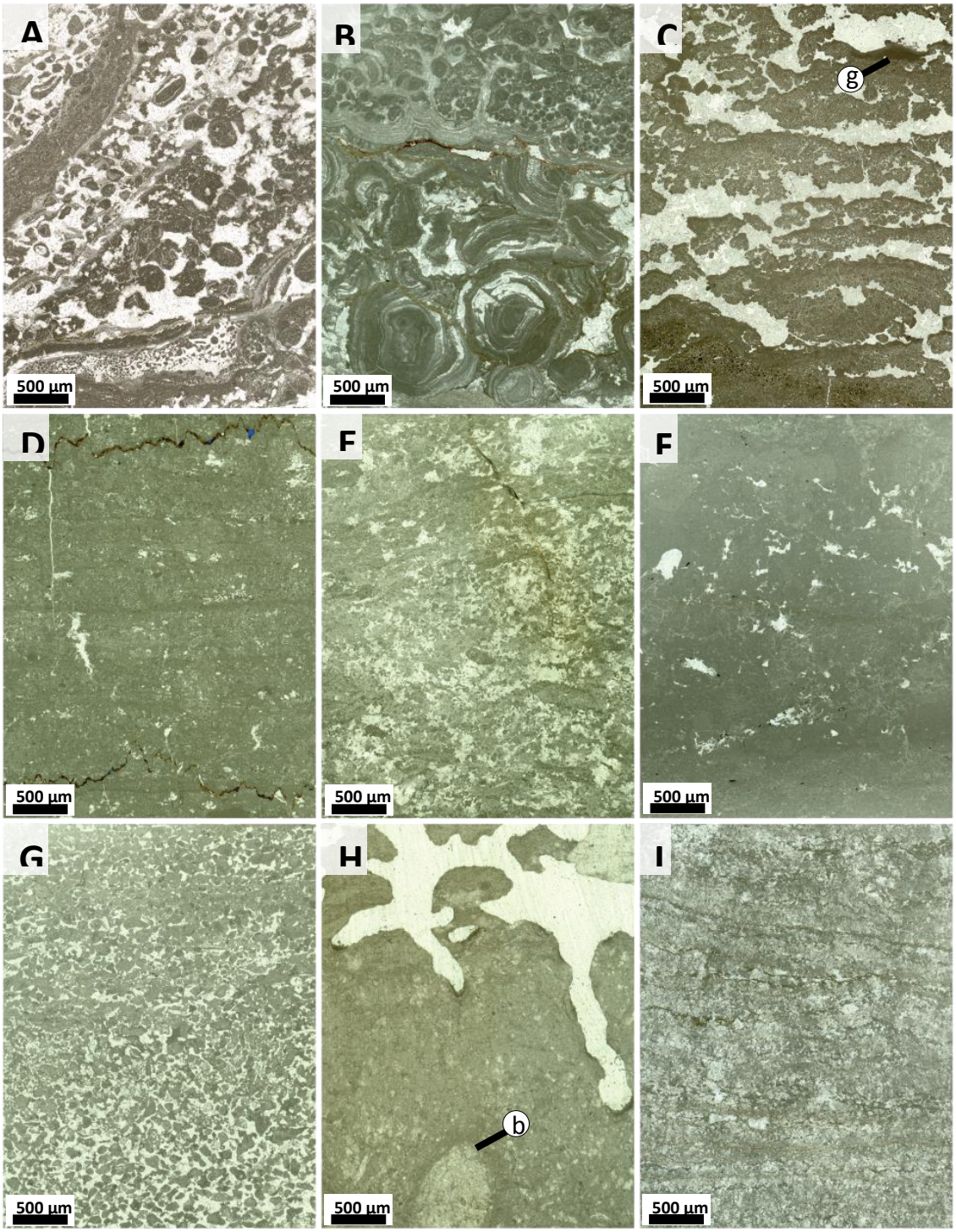
A
500 µm
B
500 µm
C
g
500 µm
D
500 µm
F
500 µm
F
500 µm
G
500 µm
H
b
500 µm
I
500 µm

Figure 25

Figure 25: Representative photomicrographs of the facies present in the PDB-04 core arranged in order form deepest to shallowest. Stratigraphic location of the thin sections are marked on the core description denoted by the corresponding letter in the upper right hand corner of each photomicrograph. **A)** Pisoids, coated grains, and peloids from within a tepee. Note the irregular and steeply inclined strata that is diagnostic of tepees. **B)** Pisoid rudstone. **C)** Fenestral peloid laminite. Not elongate fenestral pores with geopetal infill (g) that were later occluded by anhydrite cement. **D)** Laminated peloid wackestone to grain-dominated packstone. **E)** Bioturbated peloid grain-dominated packstone. **F)** Peloid wackestone. **G)** Laminated peloid intraclastic grainstone with a minor component of skeletal fragments. **H)** Burrowed (b) peloid mud-dominated packstone. Note the irregular white pattern at the top of the photomicrograph is the result of desiccation that caused degradation of the thin section. **I)** Silty algal laminite in a peloid wackestone matrix.

FACIES TRACT DIMENSIONS

Significant exposure of the G27 and G28 HFSs is restricted to the northern reaches of the Guadalupe Mountains. Within this region, Rattlesnake Canyon offers the most complete record of the G27 and G28 (Fig. 26) and presents the best opportunity to constrain facies tract dimensions (Figs. 7 and 27). The seaward limit of the G27 HFS stratal architecture is unconstrained in Dark Canyon (limited exposure) and in Walnut Canyon (margin collapse). Similarly, the seaward limit of the G28 HFS stratal architecture is unconstrained in Dark Canyon (limited exposure) and Walnut Canyon where stratal geometries are distorted related to onlapping wedges of shelfal strata against the antecedent collapsed G27 margin. Documenting shelf-crest facies tract dimensions is critical for understanding the evolution of the system and the encroachment of restricted inner shelf and middle shelf facies tracts on the Capitan Reef.

Transitioning from the Seven Rivers to the Tansill, the shelf crest systematically migrated seawards and became successively more expansive (Tinker 1998; Tinker and Kerans 1999, Kerans and Kempter 2002). Sheet crack and tepee development in the G27 TST extends from 100 – 1385 m updip form the reef margin and was documented as far updip as measured section 1. No measured sections in this study extend beyond measured section 1 in the landward direction, but reconnaissance mapping of the complete G27 – G28 section exposed in the area of Reef Top Circle road showed the absence of tepee structures or extensive sheet cracks. When this outcrop is projected southwest along strike to Rattlesnake Canyon (4 km away), the location of this outcrop tracks to a position 1.6 km updip of the terminal G28 margin. This helps constrains the landward extent of

the shelf crest and agrees with the facies belt trend seen in the measured sections from Rattlesnake Canyon in which the most landward section (1385 m from the terminal G28 margin) had only minor amounts of silt and marine cement filled sheet cracks present. Measured sections from Schwartz (1981) and Kerans et al. (2012) positioned several km inland of the reef margin, also lack tepee and sheet crack structures in the TST of the G27 and confirm the constraint of between 1.3 – 1.8 km inland from the equivalent reef margin for the landward extent of the shelf-crest facies tract during this time with a narrow 100 m outer-shelf.

During the maximum flooding of CS13 the shelf-crest was inundated, the development of tepees ceases, and only algal and fenestral peloid laminites persist. During this time, the outer-shelf extended a minimum distance of 860 m across the shelf. By the G27 sequence boundary the sheet crack-tepee-pisolite complex was reestablished and prograded to within 150 m of the reef margin and associated peritidal fenestral algal laminites extended updip to the limit of outcrop exposure 1.1 km from the margin. In the G28 TST sheet cracks and tepees are poorly developed to nonexistent, but peritidal, shelf crest associated, algal laminites and fenestral peloid laminites dominate the facies tract and extend from the updip outcrop limit at 1.1 km to within 220 m of the equivalent reef margin. In the G28 HST sheet cracks and tepees become well developed once again and the shelf crest prograded to within approximately 200 m of the end-G28 reef margin and extended to beyond the outcrop limit 1.1 km updip form the G28 reef margin.

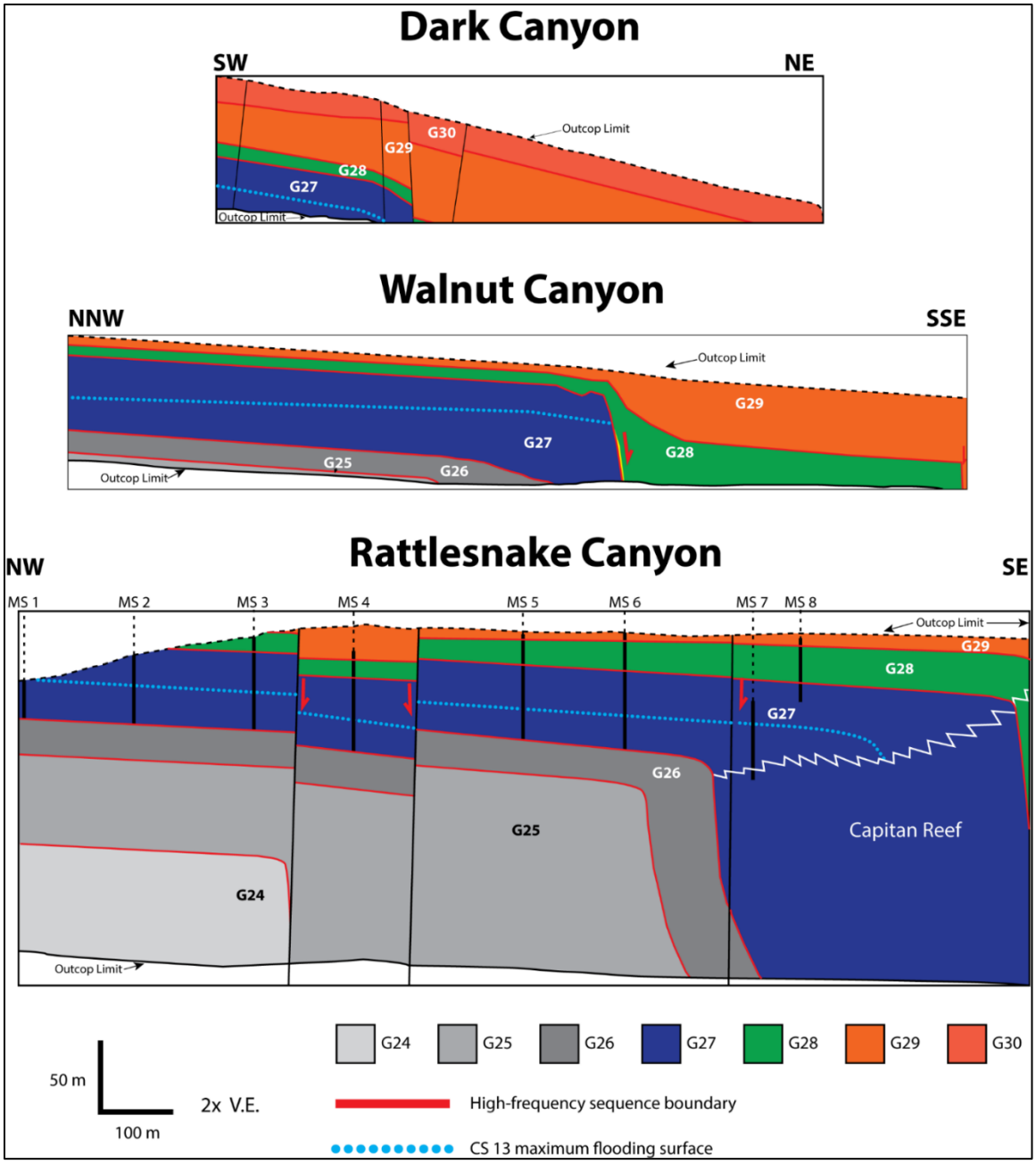

Figure 26: Scaled schematic diagram showing the extent of Tansill (G27 – G30) exposure in the northern Guadalupe Mountains. Dark Canyon represent the range of data used in Frost et al. (2012), Walnut Canyon represent the range of data used in Rush and Kerans (2010), and Rattlesnake Canyon represents the range of data and the eight vertical measured sections used in this study. Note that Rattlesnake Canyon exhibits the best and most continuous exposure the G27 and G28 HFSs.

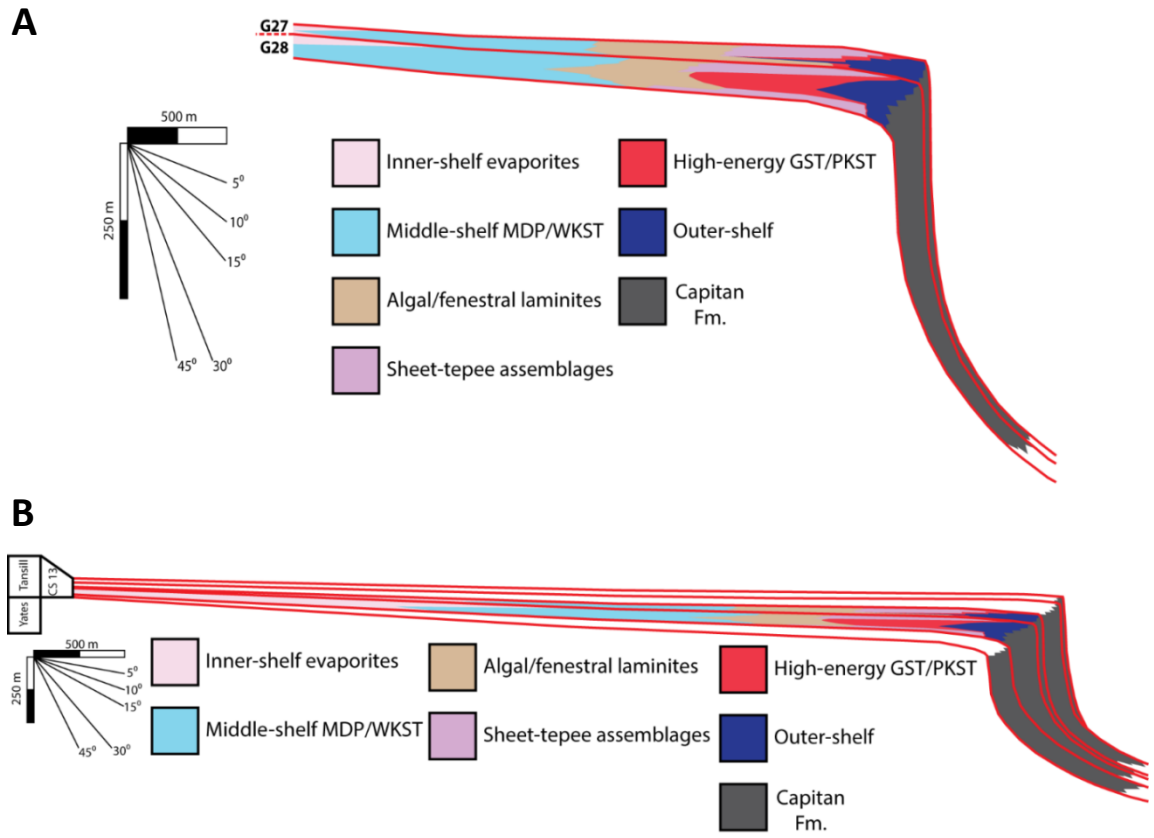

Figure 27: Depositional profile of the Permian Composite Sequence 13. A) Shows the flat platform top and high-relief steep-rimmed reef margin, characteristic geometries of the CS13, modified form Frost et al. (2012). Facies tract dimensions constrained by this study are plotted within the G27 and G28 HFSs. B) Expanded view of the G27 and G28. Facies tract widths were defined by the 2-dimensional cycle architecture built in Rattlesnake Canyon by this study.

The most landward measured section with G28 HST strata is within the downthrown block of the Cave Graben Fault System (CGFS) that overlies the antecedent G24 margin. Within the graben, the G28 displays signs of syndepositional fault displacement and exhibits growth strata with a deeper subtidal facies assemblage within the graben bound on either side of the fault system by shallower subtidal to peritidal facies. Mathisen (2012) found that displacement within the CGFS was muted by the time of G27 and G28 deposition, but there was still at least 3 m of thickening within the Graben. Measured section 4 indicates the majority of growth strata are found within the G28 HST with a minor component of growth in the G28 TST. It is possible that activity within the CGFS during the G28 might be linked with an event that triggered the collapse of the G27 margin documented in Walnut Canyon by Rush and Kerans (2010). Seaward of the antecedent G26 margin in Rattlesnake Canyon are numerous strike-parallel syndepositional open-mode fractures (Fig. 28) that are spatially controlled by the underlying sequence architecture (Frost et al. 2012). Although there was no collapsed margin documented in Rattlesnake Canyon it was likely these syndepositional fractures acted as a plane of weakness that initiated the collapse in Walnut Canyon.

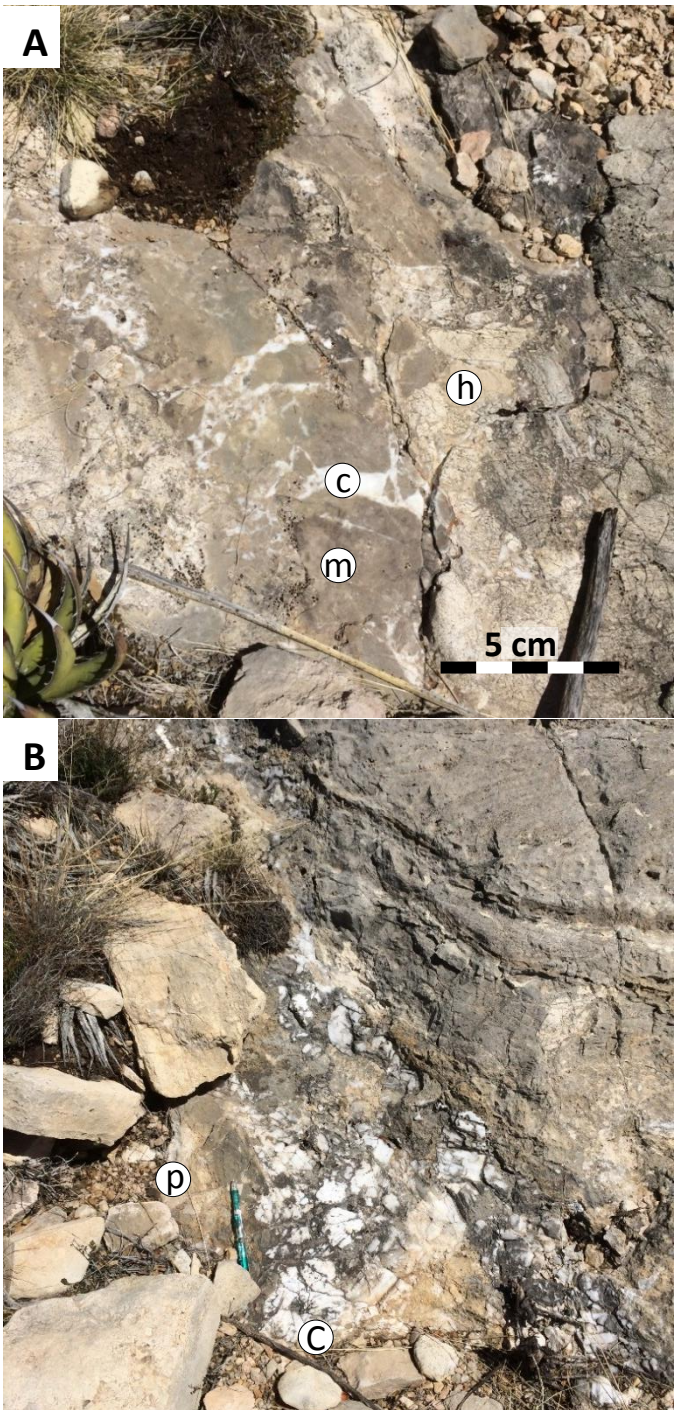

Figure 28: Syndepositional fractures in the G28 HFS seaward of the antecedent G26 margin. A) Syndepositional fracture with a polyphase infill of marine cements (m), brecciated clast of host rock (h) and a later stage fine-crystalline calcite cements (c). (B) Coarse-crystalline calcite cement (C) and brecciated skeletal-peloid packstone (p) infilling a syndepositional fracture.

EVOLUTION OF THE ROCKY SHORELINE SETTING

When evaluating cycle architecture within a HFS the stacking pattern will vary with changing position on the dip profile. The further landward or basinward a 1-dimensional measured section is positioned within the platform depositional profile, the higher the propensity for cycle amalgamation related to the decreasing effects of minor sea-level fluctuations on sediment accumulation and grain type. The ideal location for tracking the high-frequency cycle signal is at the paleoshoreline. Beachrock and beachrock conglomerates formed in the foreshore environment juxtaposed against the flank of the shelf crest during Tansill deposition. Similarly, the tepee-pisolite complex has an affinity for shedding autobrecciated clasts on the seaward flank of the shelf crest that intermix with the beachrock and enhance the character of the conglomeratic beach deposits. Together they form a distinct rocky shoreline and provide a sensitive proxy for tracking mean sea level.

Autobrecciation within tepees occurs when the cemented surfaces undergo expansive crystallization (Kendall and Warren, 1987). This self-breaking force generates blocks of the tepee host rock that most commonly develop in a fenestral laminite fabric, and, invariably, the greater the tepee dimension the greater the internal complexity and more pronounced the brecciation (Smith 1974). The general increase in tepee dimension both in moving seaward on the shelf crest profile and through the Late Guadalupian creates a high probability of abundant brecciated clasts along the lower and middle Tansill shoreline. In addition, the reduced distance between the shelf margin and the

tepee-shelf crest means that greater wave impact along this shoreline are observed associated with the G27 and G28 sequences.

Beachrocks are lithified sediments, irrespective of grain type (Russel 1963), formed in or above the intertidal zone of an active coastline. They are best developed in areas with a minimal tidal range where the direct precipitation of cements from marine and meteoric vadose waters is favored (Vousdoukas et al 2007). The cyclic wetting-drying mechanism of beachrock formation is coincident with proposed mechanisms of tepee formation (Ginsburg 1953; Assereto and Kendall 1977; Klappa 1980). Microbial mediation is also a crucial factor during beachrock cementation processes. The microenvironment created around the microbes enhances the formation of micritic cements and expedites the initial lithification process by altering the seawater chemistry nucleation sources for crystals to precipitate (Neumeirer 1999). Abundant fenestral laminites and microbial-related fabrics developed in the shelf crest during the G27 and G28 HFSs indicating microbial organisms flourished within this peritidal/supratidal environment. Beachrock and tepees also preferentially form in environments with similar ocean-water geochemistry. They both exhibit an affinity for developing in hypersaline carbonate-saturated solutions (Assereto and Kendall 1977; Hanor 1978), and need persistent seawater flushing to precipitate substantial amounts of cements (Gischler and Lomando 1997; Rush and Kerans 2010). The striking similarities between environmental parameters favorable for the formation of both beachrock and tepees indicate they do not form in mutually exclusive environments and developed in concert with one another.

The transgressive systems tract of the G27 HFS shelf crest has a well-developed assemblage of sheet cracks and tepees on its seaward flank with large volumes of marine cements and extensive autobrecciated fabrics (Figs. 29 and 30). During this time, the shelf-crest facies tract was within 100 m of the time-equivalent shelf margin making the tepees vulnerable to high-energy ocean currents. A compressed outer-shelf and such close proximity to the shelf margin resulted in autobrecciated clasts commonly being reworked and onlapping the syndepositional relief produced by tepees (Rush and Kerans 2010) or deposited into a foreshore environments during HFC-scale flooding events. Maximum flooding in the CS13 is coincident with a brief cessation of tepee development as well as the conglomeratic beachrock facies. The beachrock conglomerate only reemerges once the tepees begin to develop again in the late highstand of the G27 and highstand of the G28. These highstand shorelines differ from the one developed during the G27 TST in that they are a combination of intermixed supratidal brecciated laminites and clasts of early cemented beachrock conglomerates developed in the intertidal range and reworked downdip into foreshore and upper shoreface grainstones (Figs. 31 and 32.

The substantially lower P/A of the Tansill, 3.3 (Rush and Kerans 2010), relative to the Seven Rivers and Yates Formation of CS12, 10 and 24 respectively (Kerans and Tinker 1999), and the compressed outer-shelf facies tract, average of 150 m, defined by this study allowed for the establishment of a setting prone to formation of a rocky coastline. The stable shoreline and increased wave energy along the narrow outer-shelf enhanced the development of conglomeratic clasts and aided in reworking them across the coastline. Similar to the facies association described above, work by Frost (2007) on

Famennian steep-rimmed platforms in the Canning Basin of Western Australia also documented beachrock deposits that could be traced updip into tepee-pisolite horizons and basinward into ooid grainstones. This suggests conglomerate-beachrock-shelf-crest facies associations, although insignificant in term of total rock volume, might be a common characteristic of steep-rimmed platforms and can serve as a distinct indicators of the ancient shoreline in these systems.

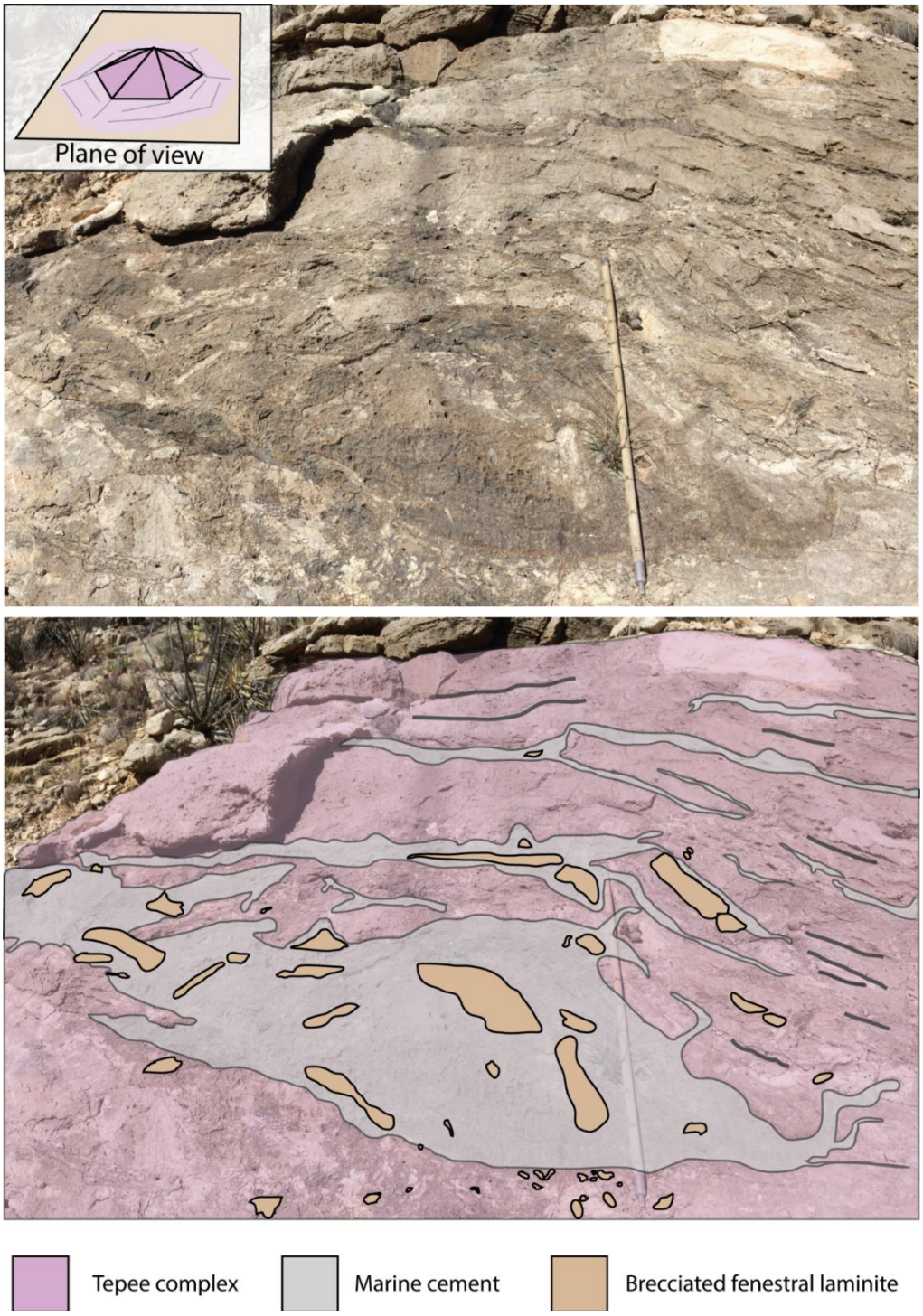

Figure 29: Interpretation of a tepee on the seaward flank of the shelf crest at the base of the G27 HFS near measured section 6. Tepees at such a proximal position to the outer shelf are well developed with extensive marine cements and autobrecciated clasts.

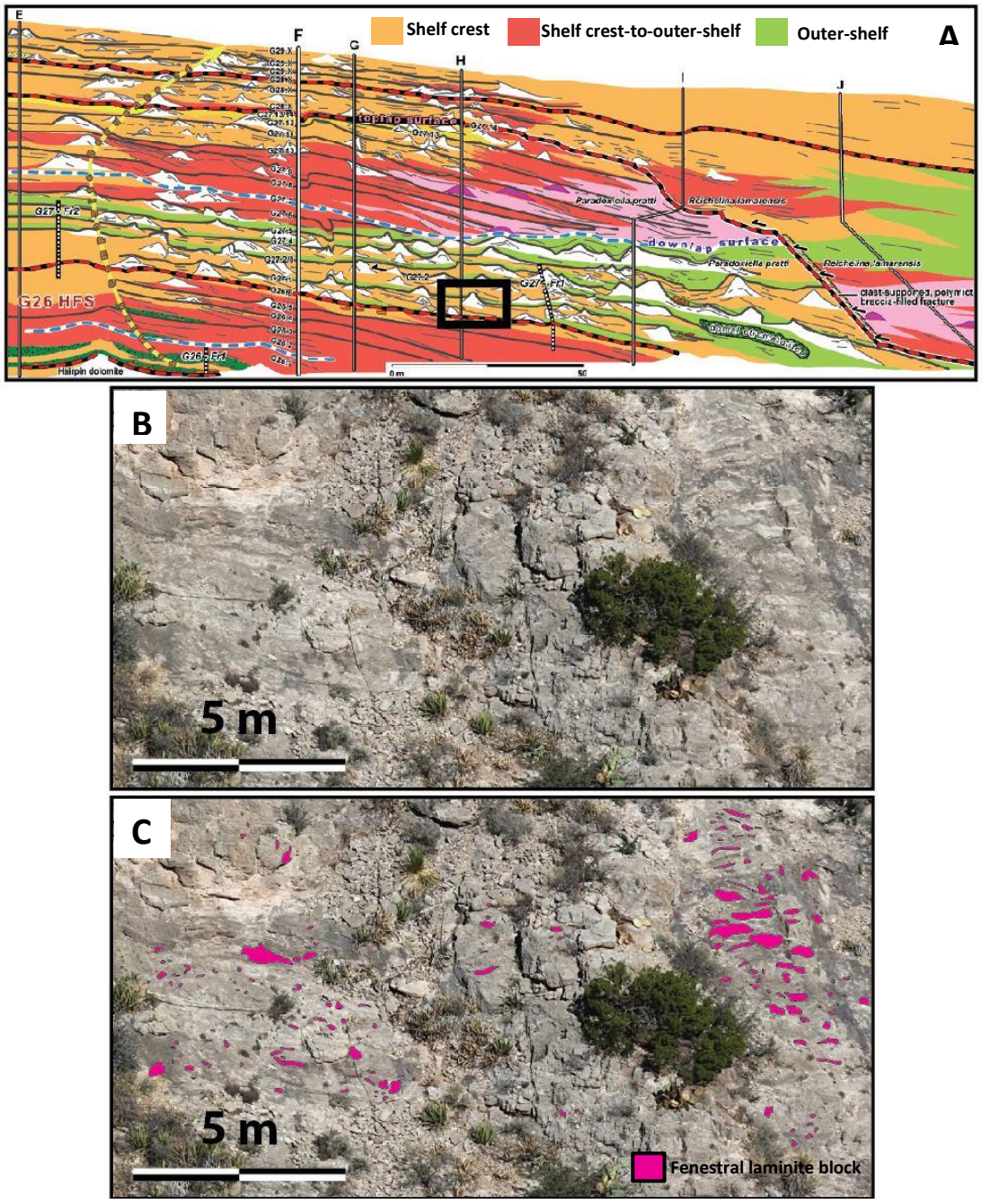

Figure 30: Interpretation of fenestral laminite blocks and tepee breccia from Walnut Canyon. A) Simplified stratigraphic cross section of the northeast wall in Walnut Canyon from Rush and Kerans (2010). Black box indicates the location of the photomosaic panel B). C) Interpretation of brecciated fenestral laminite blocks (pink) near the seaward limit of shelf crest at the base of the G27 HFS. Also, note large size of the clasts and abundance of marine cements (dark gray/brown color).

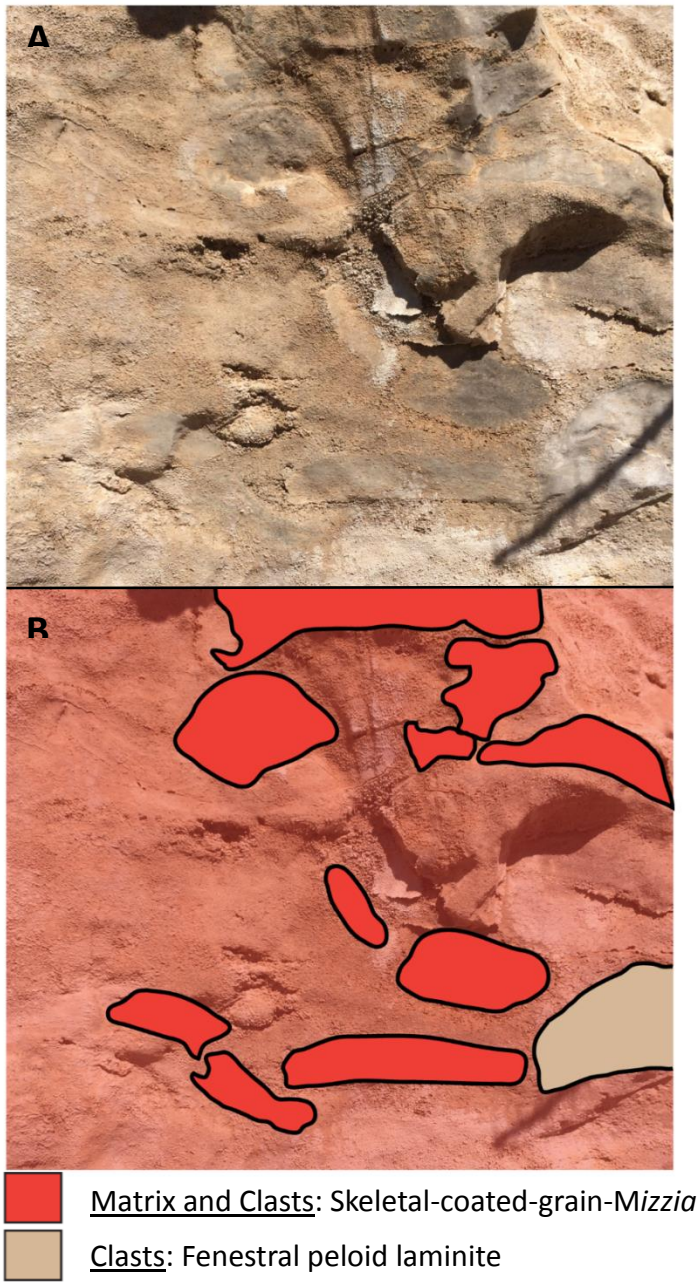

Figure 31: Outcrop photograph of a rocky shoreline environment. A) Clasts of beachrock and fenestral laminite blocks in a skeletal-peloid-coated-grain-Mizzia grain-dominated packstone to grainstone with irregular undulose laminations. Beachrock is the same composition as the matrix they are found within, and fenestral blocks are interpreted to be a product of autobrecciation processes on the shelf crest that were subsequently reworked into the high-energy shoreline deposits. B) Interpreted photograph of the beachrock conglomerate.

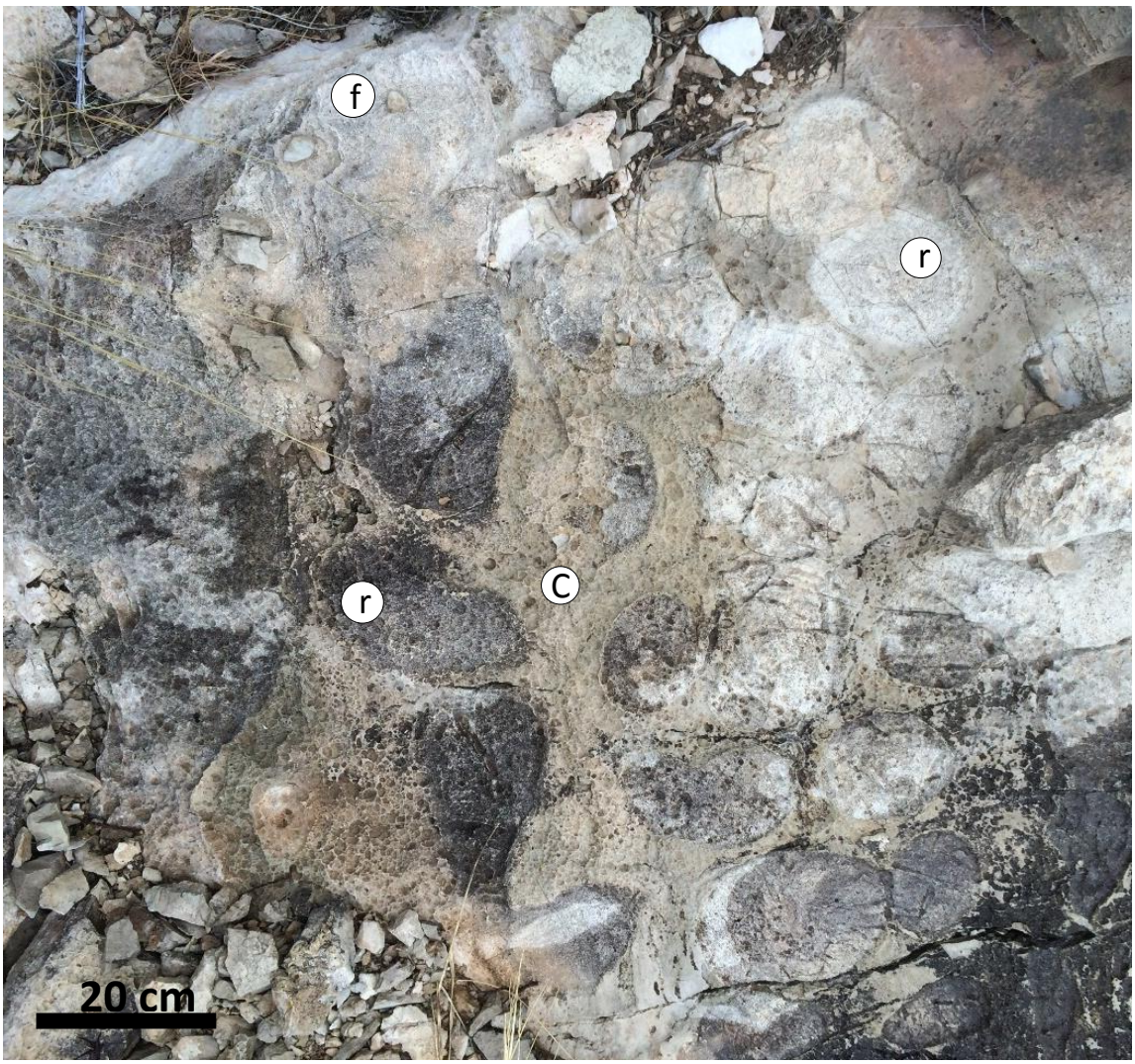

Figure 32: Outcrop photograph of rounded blocks of reworked fenestral laminite (r) in a matrix of marine cements (C) and in-situ fenestral peloidal laminites (f).

CONCLUSION

The Tansill G27 through G28 HFS, represent a major shift in sequence–scale stacking patterns from the low-accommodation, sand-rich, high P/A Yates HFS that preceded it. Although previously noted (Kerans and Tinker, 1999), this study uses optimum outcrops in Rattlesnake Canyon to fully document this high-accumulation phase of Capitan shelf evolution immediately preceding terminal draw-down and initiation of evaporite deposition. The more extensive record of the G27 – G28 HFSs shelf profile captured by this study allowed for the refinement of the sequence stratigraphic framework of CS13 and better constraints on facies tract dimensions. Constraints on the dimensions of the outer-shelf showed that it is significantly compressed relative to the older Seven Rivers and Yates Formation.

The eight measured sections and photopans of Rattlesnake Canyon show a nearly symmetrical G27 HFS with 10 cycle sets and between 10 – 26 HFCs that build a 28 m thick TST followed by a 22 m thick HST. Coincident with this aggradational stacking pattern, facies tracts compress laterally with outer-shelf dimensions between 100-150 m, and a shelf crest width of approximately 1.5 km. The CS13 MFS occurs in the G27 HFS and was constrained by retrograding ooid geobodies that extended as far updip as 860 m from the equivalent margin.

The G28 HFS is documented fully for the first time in Rattlesnake Canyon. The asymmetrical G28 HFS has 4 cycle sets and between 4 – 14 HFC that build a 6.5 m thick TST followed by a 13.5 m thick HST. Lateral compression of facies tracts in the G28

HFS was similar to compression in the G27 HFS, with outer-shelf facies tract dimensions of 200 m in the G28HFS.

Better documentation of outer-shelf tract narrowing through time can be built into our understanding of steep-rimmed platforms and the evolution of the Capitan Reef. Consequently, the narrower outer-shelf and stable shoreline allowed for a distinctive rocky shoreline that produced beachrock conglomerates separating supratidal and subtidal settings. Moving forward, this newly described facies should be incorporated into depositional models. Spatiotemporal documentation of the rocky shoreline across the Northwest Shelf will help in determining if its exhibits a stepwise correlation with the evolving steep-rimmed platform geometries with a compressed outer-shelf in the Late Guadalupian.

The refined framework of this study was also applied to the Gulf PDB-04 core allowing for regional observations between outcrop and the subsurface. High-frequency cycle and high-frequency sequence correlations between the two datasets confirm that outcrop derived models are applicable to subsurface datasets. If there is a dense enough spacing of cores, then 1-dimensional stacking pattern analysis can be used to build a 2-dimensinal framework much like the measured sections were used in constructing the cycle architecture in Rattlesnake Canyon. Similarities between the two datasets have implications that regional accommodation trends operated similarly across the Northwest Shelf and help validate the widespread use of the outcrop derived sequence stratigraphic framework developed in the Guadalupe Mountains.

APPENDIX

The purpose of this appendix is to provide the full description of each measured section to provide supplementary information on the documentation of the G27 and G28 HFS's cycle architecture in Rattlesnake Canyon.

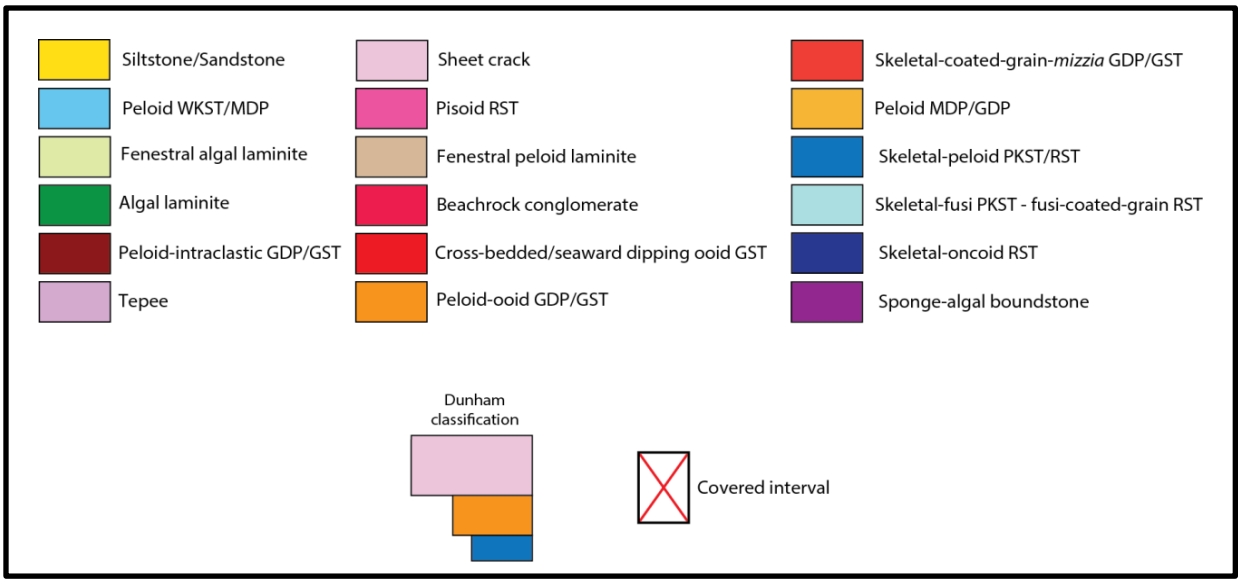

Figure 33: Facies key for the measured sections from Rattlesnake Canyon.

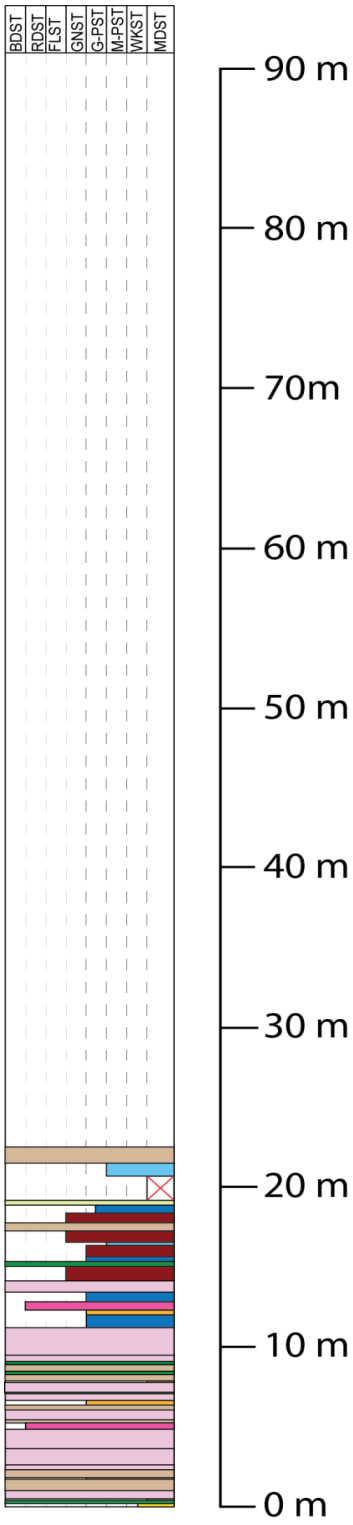

Figure 34: Measured Section 1, Rattlesnake Canyon.

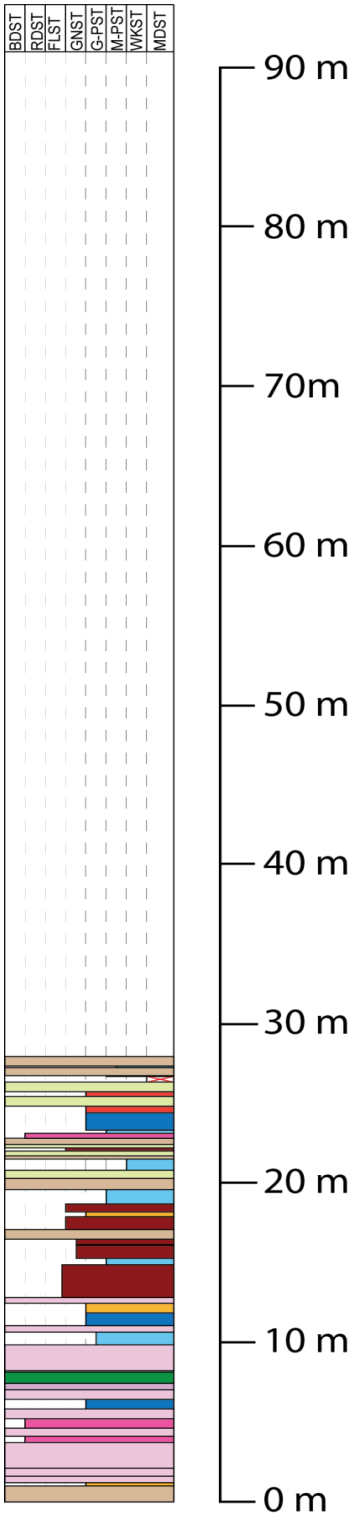

Figure 35: Measured Section 2, Rattlesnake Canyon.

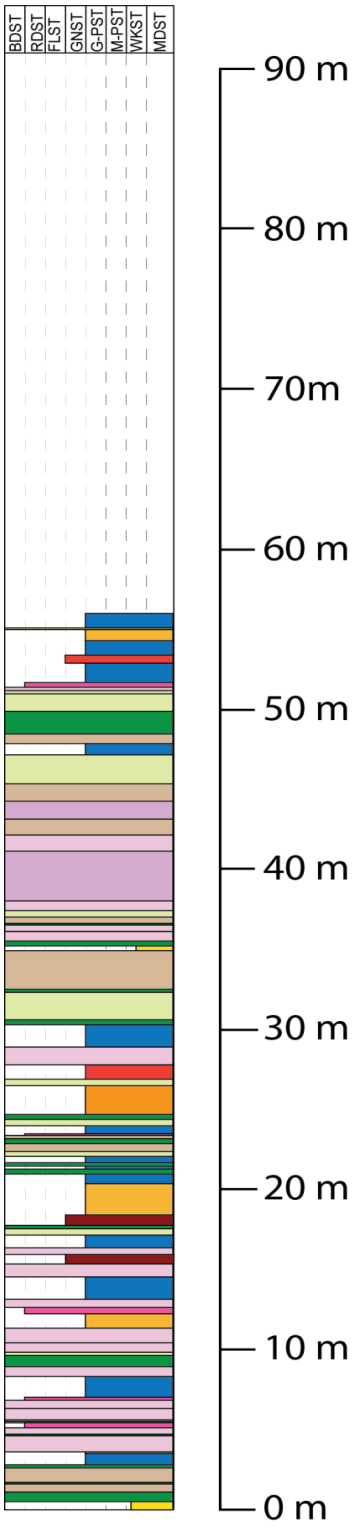

Figure 36: Measured Section 3, Rattlesnake Canyon.

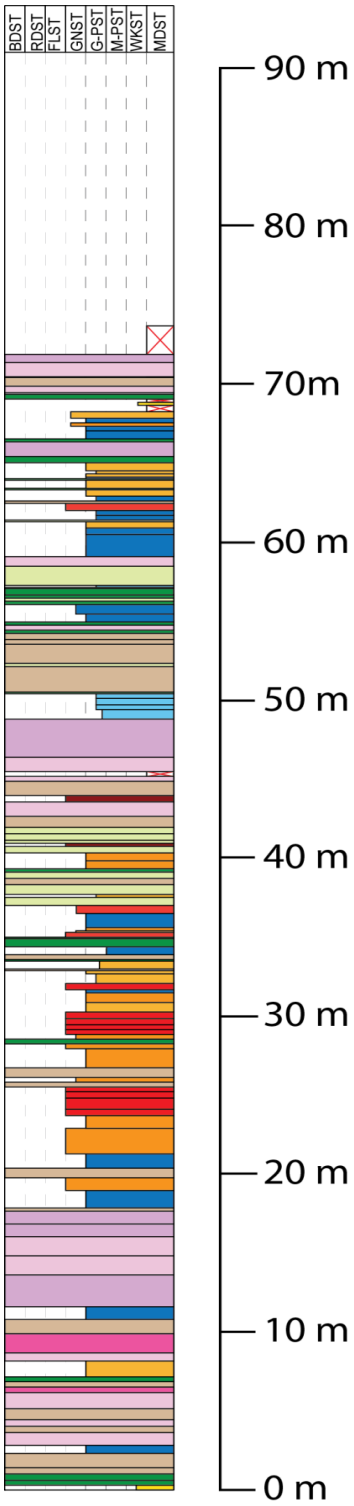

Figure 37: Measured Section 4, Rattlesnake Canyon.

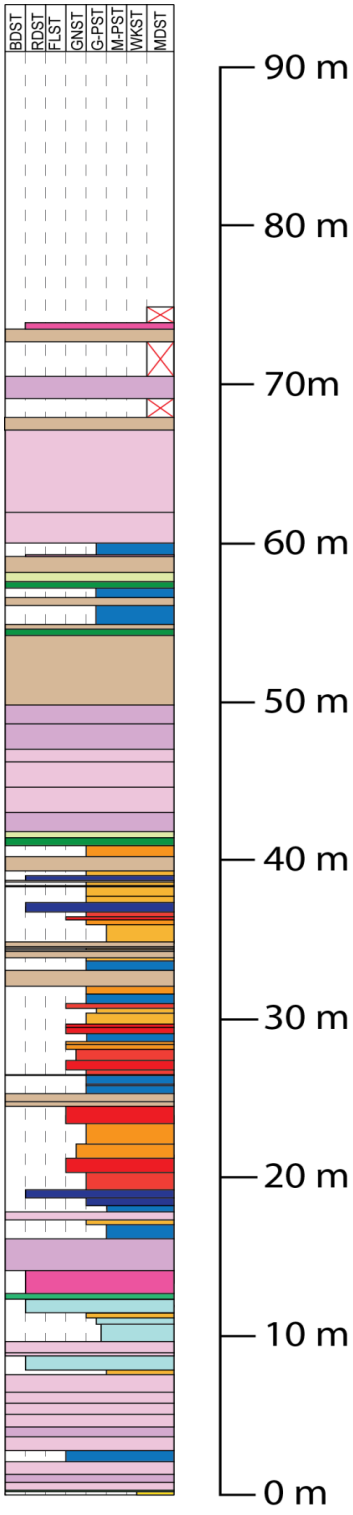

Figure 38: Measured Section 5, Rattlesnake Canyon.

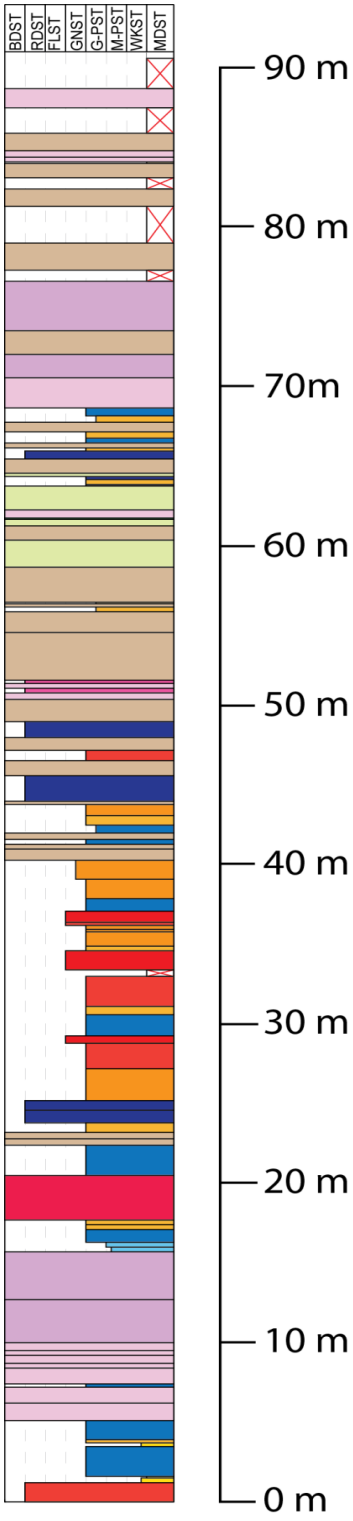

Figure 39: Measured Section 6, Rattlesnake Canyon.

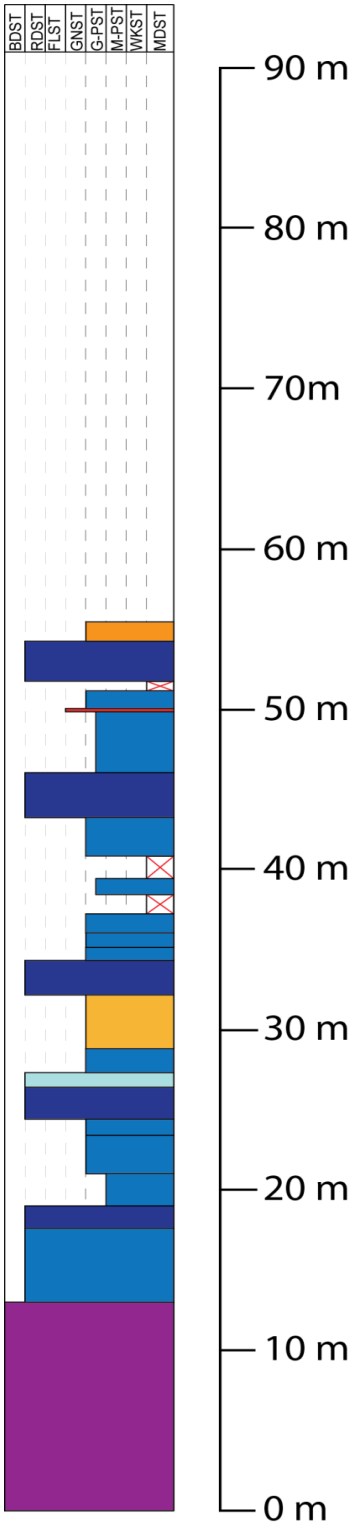

Figure 40: Measured Section 7, Rattlesnake Canyon.

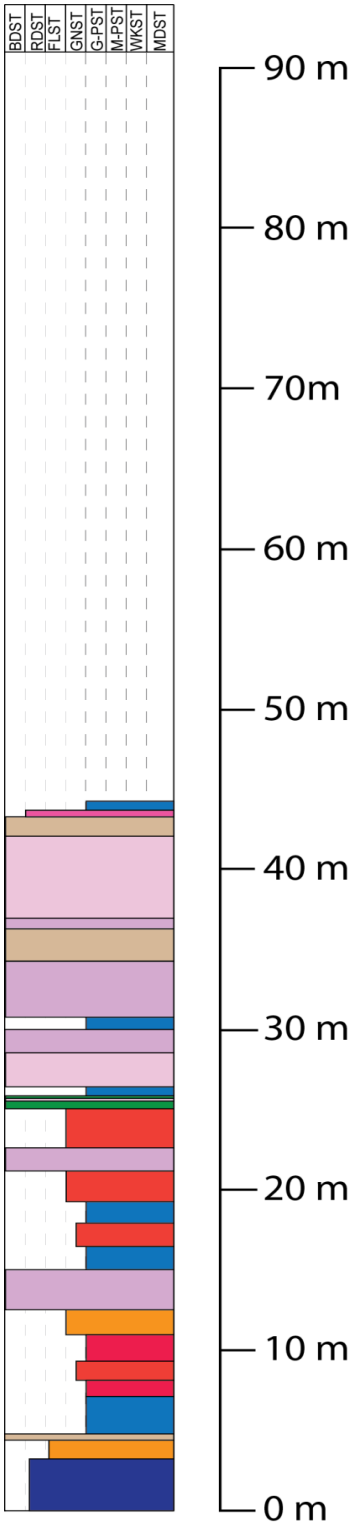

Figure 41: Measured Section 8, Rattlesnake Canyon.

REFERENCES CITED

Assereto, R. L. A. M., Kendall, C. G. ST. C., 1977, Nature, Origin and Classification of Peritidal Teepee Structures and Related Breccias Sedimentology, v. 24, p.153-210.

Bebout, D. G., and C. Kerans, 1993, Guide to the Permian Reef Geology Trail, McKittrick Canyon, Guadalupe Mountains National Park, West Texas, Bureau of Economic Geology, University of Texas at Austin, 50 p.

Borer, J. A., Harris, P. M., 1991, Lithofacies and Cyclicity of the Yates Formation, Permian Basin: Implication for Reservoir Heterogeneity, AAPG Bulletin, v. 75, 9. 726-779.

Boyd, D. W., 1975, Fenestral fabric in Permian carbonates of the Bighorn Basin, Wyoming: Wyoming Geol. Assoc. Guidebook, 27th Annual Field Conference, p. 101-106.

DeFord, D. K., and Riggs, G. D., 1941, Tansill Formation wet Texas and southeast New Mexico, AAPG Bulletin, v. 25, p. 1713-1728.

Dunham, R. J., 1969, Vadose pisolite in the Capitan Reef (Permian), New Mexico and Texas. In: Depositional environments in carbonate rocks (ed. By B. H. Purser), p. 329-341

Dunham, R.J., 1972, Capitan Reef, New Mexico and Texas: Facts and Questions to Aid Interpretation and Group Discussion: Publication (Permian Basin Section): Midland, TX, SEPM (Society of Sedimentary Geology, p. 294.

Esteban, M., 1976, Vadose Pisolite and Caliche: Geologic Note, AAPG, v. 60, p. 2048-2057.

Esteban, C.M. and Pray, L.C., 1977, Origin of the pisolite facies of the shelf crest. In: M.E. Hileman and S.J. Mazzullo (Editors), Upper Guadalupian Facies, Permian Reef Complex, Guadalupe Mountains, New Mexico and Texas. Field Conference Guidebook. Permian Basin Sect., Soc. Econ. Paleontol.Mineral. Publ. 77-16: 479-487.

Frost, E. L., Budd, D. A., Kerans, C., 2012, Syndepositional Deformation in a High-Relief Carbonate Platform and its effect on Early Flow as Revealed by Dolomite Patterns, Journal of Sedimentary Research, v. 82, 913-932.

Frost, E. L. 2007, Facies heterogeneity, platform architecture and fracture patterns of the Devonian reef complexes, Canning Basin, Western Australia: Unpublished Ph.D. Dissertation, The University of Texas at Austin, 156 p.

Garber, R. A., Grover, G. A., Harris, P. A., 1989. Geology of the Capitan Shelf Margin – Subsurface Data from the Northern Delaware Basin: SEPM CW13, p. 1-268.

Garber, R. A., Harris, P. A., 1993. Geology of the Upper Permian Capitan Shelf Margin – A Study from a Continuous Core in the Northern Delaware Basin: Carboniferous to Jurassic: Pangea: Core Workshop Guidebook.

Gardner, M. H., 1992, Sequence stratigraphy of eolian-derived turbidites; deep water sedimentation patterns along an arid carbonate platform and their impact on hydrocarbon recovery in Delaware Mountain Group reservoirs, West Texas: in Mruk, D. H., and Curran, B. C., eds., Permian Basin exploration and production strategies; applications of sequence stratigraphic and reservoir characterization concepts. West Texas Geological Society Publication, v. 92-91, p. 7–11.

Ginsburg, R. N., 1953, Beachrock in south Florida: Journal of Sedimentary Research, v. 23, p. 85-92.

Gischler, E. and Lomando, A.J., 1997. Holocene cemented beach deposits in Belize. Sedimentary Geology, v. 110, no. 3, p.277-297.

Goldhammer, R.K., Lehmann, P.J., and Dunn, P.A., 1993, The origin of high- frequency platform carbonate cycles and third-order sequences (Lower Ordovician El Paso Gp, west Texas): constraints from outcrop data and stratigraphic modeling: Journal of Sedimentary Petrology, v. 63, p. 318–359.

Grotzinger, J.P. 1986, Upward shallowing platform cycles; a response to 2.2 billion years of low-amplitude, high-frequency (Milankovitch band sea level oscillations, in M. A. Arthur and R. E. Garrison, eds., Special section; Milankovitch cycles through geologic time: Cyclic and periodic events in stratigraphy, evolution and the geologic record, v. 10, p. 403-416.

Hanor, J.S., 1978. Precipitation of beachrock cements: mixing of marine and meteoric waters vs. CO2-degassing. Journal of Sedimentary Research, v.48, no.2, p. 489-501.

Harman, C. & Kerans, C. 2011, Quantified Facies Distribution and Sequence Geometry of the Yates Formation, Slaughter Canyon, New Mexico. Department of Geological Sciences, Austin, TX, The University of Texas at Austin, Masters of Science. 137 p.

Harris, P.M., Kerans, C. and Bebout, D.G., 1993. Ancient Outcrop and Modern Examples of Platform Carbonate Cycles--Implications for Subsurface Correlation and Understanding Reservoir Heterogeneity: Chapter 18, p. 475-492.

Harris, P. M., Kerans, Charles, and Bebout, D. G., 1993, Ancient outcrop and modern examples of platform carbonate cycles—implications for subsurface correlation and understanding reservoir heterogeneity, in Loucks, R. G., and Sarg, J. F., eds., Carbonate Sequence Stratigraphy: Recent Developments and Applications: American Association of Petroleum Geologists, Memoir 57, p. 475–492.

Hayes, P.T., 1964, Geology of the Guadalupe Mountains, New Mexico: United States

Geological Survey Professional Paper, 446, 69 p. Carbonate sequence stratigraphy: recent developments and applications: American Association of Petroleum Geologists, Memoir 53, p. 475–492.

Hills, J. M., 1972, Late Paleozoic sedimentation in west Texas Permian basin. AAPG Bulletin, v. 56, p. 2303-2322.

Hill, C.A., 1999. Reevaluation of the Hovey channel in the Delaware basin, West Texas. AAPG bulletin, 83(2), pp.277-294.

Hoark, R. L., 1985. Tectonic and Hydrocarbon Maturation history in the Permian Basin: Oil and Gas Journal, V. May 27, p. 124-129.

Jones, N. B., 2012, Integrated Lidar and Outcrop Study of Syndepositional Faults and Fractures in the Capitan Formation, Guadalupe Mountains, New Mexico, U.S.A. [unpublished MS thess]: The Unuversity of Texas at Austin, 154p.

Kendall, C.G. St. C., 1969, An environmental re-interpretation of the Permian evaporite/carbonate shell' sediments of the Guadalupe Mountains, Geol. Soc. Am. Bull., v. 80, p. 2503 2526.

Kerans, C., and Harris, P.M., 1993, Outer Shelf and Shelf Crest, in D.G. Bebout and C. Kerans, eds., Guide to the Permian Reef Geology Trail, McKittrick Canyon, Guadalupe Mountains National Park, west Texas: The University of Texas, Bureau of Economic Geology, Guidebook 26, p.32-43.

Kerans, C., Lucia, F.J., and Senger, R.K., 1994, Integrated characterization of carbonate ramp reservoirs using Permian San Andres Formation outcrop analogs: American Association of Petroleum Geologists, Bulletin, v. 78, p. 181–216.

Kerans C, Fitchen WM, Gardner MH, Sonnenfeld MD, Tinker SW, Wardlaw, BR. 1992. Styles of sequence development within uppermost Leonardian through Guadalupian strata of the Guadalupe Mountains, Texas and New Mexico. In Mruk DH, Curran BC (Editors). Permian Basin Exploration and Production Strategies: Applications of Sequence Stratigraphic and Reservoir Characterization Concepts, Publication 92-91: West Texas Geological Society, Midland, Texas. p. 1–7.

Kerans, C., and Tinker, S. W., 1997, Sequence stratigraphy and characterization of carbonate reservoirs. SEPM Short Course Notes No. 40.

Kerans, C., Tinker, S. W., 1999, Extrinsic Stratigraphic Controls on Development of the Capitan Reef Complex: SEPM Special Publication No. 65, p. 15-36.

Kerans, C., 1995. Use of one-and two-dimensional cycle analysis in establishing high-frequency sequence frameworks: in Milankovitch Sea-Level Changes, Cycles, and Reservoirs on Carbonate Platforms in Greenhouse and Icehouse Worlds, v. 35, p. 1-20.

Kerans, C. and W. M. Fitchen, 1995, Sequence hierarchy and facies architecture of a carbonate-ramp system: San Andres Formation on the Algerita Escarpment and western Guadalupe Mountains, West Texas and New Mexico, Report of investigation, Austin, TX, The University of Texas at Austin, 86 p.

Kerans, C., and Kempter, K., 2002, Hierarchical stratigraphic analysis of a carbonate platform Permian of the Guadalupian Mountains: American Association of Petroleum Geologist, Datapages Discovery Series No. 5, CD-ROM and color plate.

Kerans, C., Playton, T., Phelps, R., and Scott, S.Z., 2013, Ramp to Rimmed Shelf Transitions in the Guadalupian (Permian) of the Guadalupe Mountains, West Texas and New Mexico: SEPM Special Publication No. 105, p. 26-49.

King, P.B., 1942, Permian of West Texas and Southeastern New Mexico: American Association of petroleum Geology., Bulletin v. 26, no. 4, p. 535-763.

King, P. B., 1948. Geology of the southern Guadalupe Mountains, Texas: U.S. Geol. Survey, Prof Paper, p. 183-215.

Kirkland-George, B., 1992, Distinctions between reefs and bioherms based on studies of fossil algae-*Mizzia*, Permian Capitan reef Complex (Guadalupe Mountains, Texas and New Mexico) and Eugonophyllum , Pennsylvanian Holder Formation (Sacramento Mountains, New Mexico): Unpublished Ph.D. Dissertation, Louisiana State University, 156 p.

Kirkland, B.L., Longacre, S.A., and Stoudt, E.L., 1993, Reef, in D. Bebout, and Kerans, C., eds., Guide to the Permian Reef Geology Trail, McKittrick Canyon, Guadalupe Mountains National Park, west Texas, The University of Texas, Bureau of Economic Geology, Guidebook 26, p. 23–31.

Koša, E. and Hunt, D.W., 2006, The effect of syndepositional deformation within the Upper Permian Capitan Platform of the speleogenesis and geomorphology of the Guadalupe Mountains, New Mexico, USA: Geomorphology, v. 78, p. 279-308.

Lehrmann, D.J., Goldhammer, R.K., 1999. Secular variation in parasequence and facies stacking patterns of platform carbonates: a guide to application of stacking-patterns analysis in strata of diverse ages and settings in advances in Carbonate Sequence Stratigraphy: application to Reservoirs, Outcrops and Models, SEPM Special Publication, No. 63, p. 187-225.

Mitchum, R. M. Jr., Van Wagoner, J. c., 1991 High frequency sequences and their stacking patterns sequence stratigraphic evidence of high frequency eustatic cycles in Biddle KT and Schlager W eds The Record of Sea Level Fluctuations Sedimentary Geology v 70 p 131 160.

Mazzullo, S. J., Mazzullo, Jim, Harris, Paul M., 1985, Significance of Eolian Quartzose Sheet Sands on Emergent Carbonate Shelves: Permian of West Texas-New Mexico. AAPG Bulletin, v. 69, No. 2, p. 284.

Mazzullo, S.J., 1999, Paleoenvironments, cyclicity, and diagenesis in the Outer Shelf Tansill Formation in the Carlsbad Embayment (Dark Canyon), Northern Guadalupian Mountains, New Mexico: in Framework of the Capitan Reef, SEPM Special Publication No. 65, p. 107-128.

Mutti, M. and Simo, J. A. 1994. Distribution, Petrography and Geochemistry of Early Dolomite in Cyclic Shelf Facies, Yates Formation (Guadalupian), Capitan Reef Complex, USA, in Dolomites: A Volume in Honour of Dolomieu (eds B. Purser, M.

Tucker and D. Zenger), Blackwell Publishing Ltd., Oxford, UK. doi: 10.1002/9781444304077.ch7.

Neese, D.A., and Schwartz, A.H., 1977, Facies mosaic of the upper Yates and lower Tansill formations, Walnut and Rattlesnake canyons, Guadalupe Mountain, New Mexico in Hileman, M.E., and Mazzulo, S.J. eds, Upper Guadalupian Facies, Permian Reef Complex, Guadalupe Mountains, New Mexico and West Texas: SEPM, Permian Section Publication 77-16, 1977 Field Conference Guidebook, p. 437-450.

Neumeier, U., 1999. Experimental modelling of beachrock cementation under microbial influence. Sedimentary Geology, v. 126, p.35-46.

Newell, N.D, Rigby, J. K., Fischer, A. G., Whiteman, A. J., Hickox, J. E., Bradley, J.S., 1953, The Permian Reef Complex of the Guadalupe Mountains Region, Texas and New Mexico. Free, San Francisco, Calif., 280 p.

Osleger, D., Read, J.F., 1991, Relation of eustacy to stacking patterns of meter-scale carbonate cycles, Late Cambrian, USA. Journal of Sedimentary Research v. 61, p.1225-1252.

Osleger, D. A., and Tinker, S., 1999, Three-dimensional architecture of upper Permian high-frequency cycles, Yates-Capitan shelf margin, Permian Basin, USA in Harris, P.M., Simo, T., and Handford, R., eds., Advances in Carbonate Sequence Stratigraphy—Applications to Reservoirs, Outcrops, and Models: SEPM, Special Publication.

Parsley, M., 1988, Deposition and Diagenesis of Late Guadalupian Barrier-Island Complex from the Middle and Upper Tansill Formation (Permian), East Dark Canyon, Guadalupe Mountains, New Mexico: [unpublished MS thess]: The Unuversity of Texas at Austin, 247 p.

Read, J.F., 1985, carbonate platform facies models. American Association of Petroleum Geologist, Bulletin 69: p. 1-21.

Ross, C.A., 1978, Late Pennsylvanian and Early Permian sedimentary rocks and tectonic setting of the Marathon Geosyncline, in Mazzullo, S.J., ed., Tectonics and Paleozoic Facies of the Marathon Geosyncline, West Texas, Permian Basin Section, SEPM, Publication 78-17, p. 89–93.

Rush, J., Kerans, C., 2010, Stratigraphic Response Across a Structurally Dynamic Shelf: the Last Guadalupian Composite Sequence at Walnut Canyon, New Mexico, U.S.A.: Journal of Sedimentary Research, v 80, p. 808-828.

Russel, R. J., 1963, Beach Rock: J. Trop. Geogr., v. 17, p. 22-27.

Scholle, P.A. and Kinsman, D. J. J., 1974, Aragonitic and High-Mg calcite caliche from the Persian Gulf – a modern analog for the Permian of Texas and New Mexico, Sedimentology, v. 44, p. 904-916.

Schwartz, A.H., 1981, Facies Mosaic of the Upper Yates and Lower Tansill Formations (Upper Permian), Rattlesnake Canyon, Unpublished Master's Thesis, University of Madison-Wisconsin, 149 p.

Thomas, C., 1968. Vadose pisolites in the Guadalupe and Apache Mountains, West Texas. In: Permian Basin Section. Soc. Econ. Palentol. Mineral. Punl. V. 68, no.11, p.32-35.

Tinker, S. W., 1998, Shelf-to-Basin Facies Distribution and Sequence Stratigraphy of a Steep-Rimmed Carbonate Margin: Capitan Depositional System, McKittrick Canyon, New Mexico and Texas: Journal of Sedimentary Research, v. 68, p. 1146-1174.

Toomey, D.F., Babcock, J. A., 1983, Precambrian and Paleozoic algal carbonates, West Texas–southern New Mexico: field guide to selected localities of late Proterozoic, Ordovician, Pennsylvanian, and Permian ages, including the Permian reef complex: Colorado School of Mines, Professional Contributions, v. 11, 345 p.

Tyrell, W.W., JR, 1962, Petrology and stratigraphy of near-reef Tansill-Lamar strata, Guadalupe mountains, Texas and New Mexico, in Permian of the central Guadalupe Mountains, Eddy County, New Mexico – Field Trip Guidebook and Geologic Discussions, West Texas Geologic Society, p. 59-69.

Tyrrell, W.W., Jr., 1969, Criteria useful in interpreting environments of unlike but time equivalent carbonate units (Tansill–Capitan–Lamar), Capitan reef complex, west Texas and New Mexico, in Friedman, G.M., ed., Depositional Environments in Carbonate Rocks; A Symposium: SEPM, Special Publication 14, p. 80–97.

Ward, R. F., Kendall, C. G. ST. C., Harris P. M., 1986, Upper Permian (Guadalupian) facies and their association with hydrocarbons--Permian basin, west Texas and New Mexico. AAPG Bulletin v.70, p. 239-262.

Vail, P.R., 1987. Seismic stratigraphy interpretation procedure, in Bally, A.W., ed, Atlas of Seismic stratigraphy, v. 1: Tulsa, American Association of Petroleum Geologist Studies in Geology 27, p. 1-10.

Vousdoukas, M.I., Velegrakis, A.F. and Plomaritis, T.A., 2007. Beachrock occurrence, characteristics, formation mechanisms and impacts. Earth-Science Reviews, v. 85, p.23-46.

Yang, K.M., Dorobek, S.L., 1995. The Permian Basin of West Texas and New Mexico: Tectonic history of a "composite foreland basin and its effects on stratigraphic development. In Dorobek, S.L. Ross GM (editors). Stratigraphic Evolution of Foreland Basins, Special Publication 52: SEPM (Society for Sedimentary Geology), Tulsa, Oklahoma. P. 149 – 179.

Ye, H., Royden, L., Burchfiel, S., 1996. Late Paleozoic Deformation of Interior North America: the Greater Ancestral Rocky Mountains: AAPG Bulletin, v. 80, No. 9, p. 1397-1432.

Yurewicz, D. A., 1976, Sedimentology, paleoecology, and diagenesis of the massive facies of the lower and middle Capitan Limestone (Permian), Guadalupe Mountains, New Mexico and West Texas [Unpublished Ph.D. Thesis]: University of Wisconsin, Madison, Wisconsin, 296 p.